Appendix J

MODELING PROTOCOL AND ATTAINMENT DEMONSTRATION

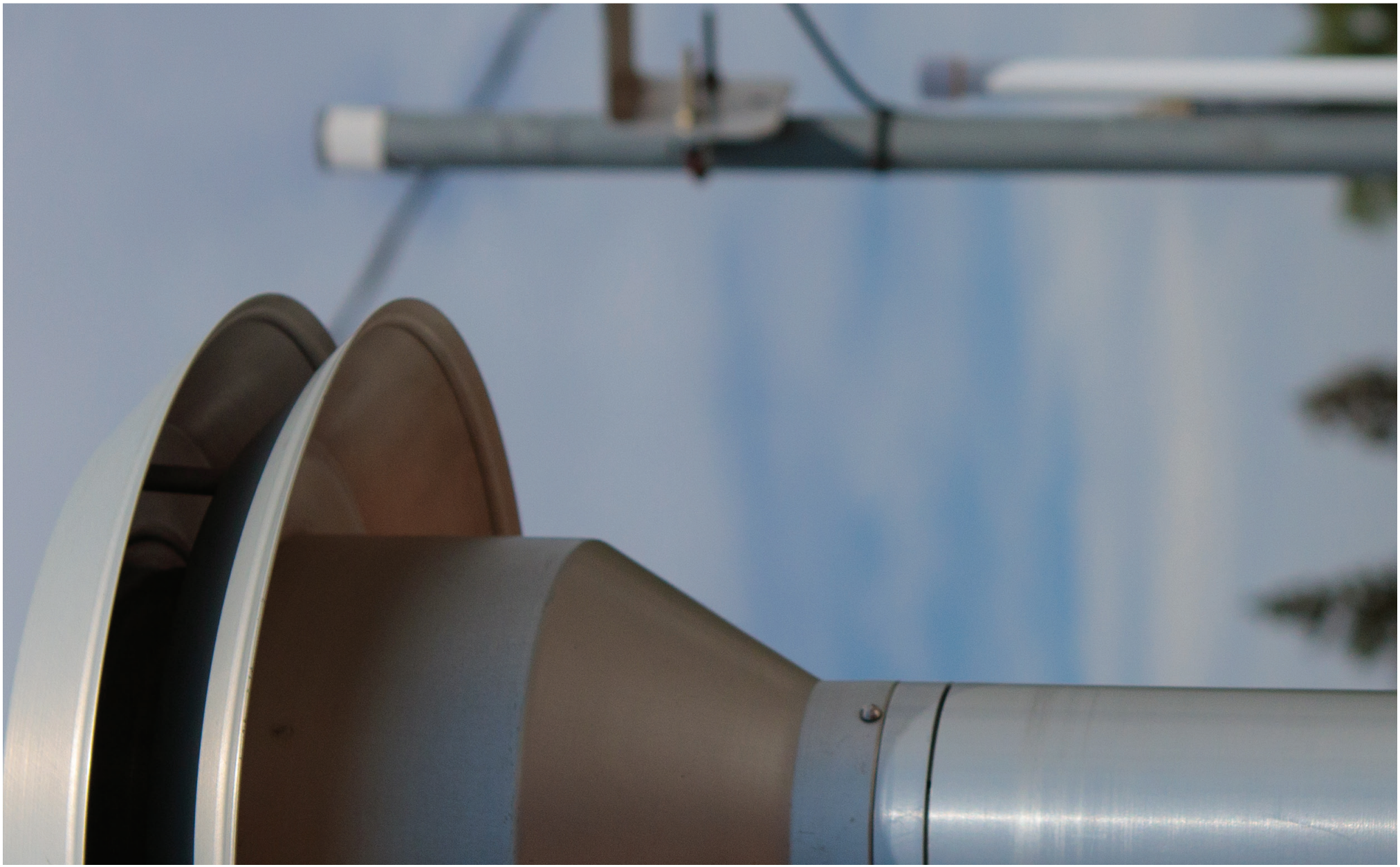

This page intentionally blank.

Appendix J: Modeling Protocol and Attainment Demonstration

[This Appendix provided by the California Air Resources Board]

Modeling Protocol and Attainment Demonstration for the San Joaquin Valley Annual $PM_{2.5}$ State Implementation Plan

Prepared by

California Air Resources Board

San Joaquin Valley Air Pollution Control District

Prepared for

United States Environmental Protection Agency Region IX

May 2024

Table of Contents

List of Figures

List of Tables

Acronyms

BCs – Boundary Conditions

BDSNP – Berkeley-Dalhousie Soil NOx Parameterization

CAPP – Community Air Protection Program

CARB – California Air Resources Board

CMAQ Model – Community Multi-scale Air Quality Model

CRPAQS – California Regional Particulate Air Quality Study

CSN – Chemical Speciation Network

DISCOVER-AQ – Deriving Information on Surface Conditions from Column and Vertically Resolved Observations Relevant to Air Quality

DV – Design Value

EC – Elemental Carbon

FEM – Federal Equivalent Method

FDDA – Four Dimensional Data Assimilation

FRM – Federal Reference Method

GEOS-5 – Goddard Earth Observing System Model, Version 5

ICs – Initial Conditions

IMPROVE - Interagency Monitoring of Protected Visual Environments

IOA – Index Of Agreement

MATS – Model Attainment Test Software

MB – Mean Bias

MCIP – Meteorology-Chemistry Interface Processor

ME – Mean Error

MEGAN – Model of Emissions of Gases and Aerosols from Nature

MFB – Mean Fractional Bias

MFE – Mean Fractional Error

MOZART – Model for Ozone and Related chemical Tracers

NAAQS – National Ambient Air Quality Standard

NARR – North American Regional Reanalysis

NASA – National Aeronautics and Space Administration

NCR – National Center for Atmospheric Research

NMB – Normalized Mean Bias

NME – Normalized Mean Error

NO_x – Nitrogen Oxides

OC – Organic Carbon

OM – Organic Matter

PBL – Planetary Boundary Layer

$PM_{2.5}$ – Particulate Matter of Aerodynamic Diameter less than 2.5 micrometers

RH – Relative Humidity

RMSE – Root Mean Square Error

ROG – Reactive Organic Gases

RRF – Relative Response Factors

RWC – Residential Wood Combustion

SANDWICH – Sulfate, Adjusted Nitrate, Derived Water, Inferred Carbon Hybrid material balance

SAPRC – Statewide Air Pollution Research Center

SASS - Spiral Aerosol Speciation Sampler

SIP – State Implementation Plan

SJV – San Joaquin Valley

SJVAPCD – San Joaquin Valley Air Pollution Control District

SLAMS – State and Local Air Monitoring Stations

SOA – Secondary Organic Aerosol

SO_x – Sulfur oxides

U.S. EPA – United States Environmental Protection Agency

WRF – Weather and Research Forecasting

I. Introduction

The purpose of this document is to demonstrate the attainment of the 2012 National Ambient Air Quality Standard (NAAQS) for annual $PM_{2.5}$ (12 µg/m^3) in the San Joaquin Valley nonattainment area (SJV or the Valley) with an attainment deadline of 2030. It forms the scientific basis for the 2024 SJV $PM_{2.5}$ State Implementation Plan (SIP).

The model demonstration shows that in 2030, the highest projected annual $PM_{2.5}$ design value (DV) in the Valley under the future attainment emission scenario is 12.0 µg/m^3, which demonstrates that SJV will attain the 2012 annual $PM_{2.5}$ standard by 2030.

This document is organized as follows: Section 1 provides background and context to the $PM_{2.5}$ pollution in the SJV. Section 2 describes the general approach for projecting DVs to the future year. Section 3 discusses the meteorological modeling and evaluation. Section 4 describes the emissions inventory used in the modeling. Section 5 shows $PM_{2.5}$ model performance, projected 2030 DVs, $PM_{2.5}$ precursor sensitivities for 2030, and the un-monitored area analysis.

A. Ambient $PM_{2.5}$ Monitors in the SJV

SJV covers an area of 23,490 square miles and is home to approximately 4 million residents. The Valley is bordered on the west by the coastal mountain ranges and on the east by the Sierra Nevada range. These ranges converge at the southern end of the basin at the Tehachapi Mountains. The majority of the population is centered in the urban areas of Bakersfield, Fresno, Modesto, and Stockton. The nonattainment area includes seven full counties (San Joaquin, Stanislaus, Merced, Madera, Fresno, Kings, and Tulare) and one partial county (only the western portion of Kern County, which lies in the jurisdiction of the SJV Air Pollution Control District (SJVAPCD or the District)).

The Valley can be divided into three regions that are characterized by distinct geography, meteorology, and air quality: 1) northern SJV (San Joaquin, Stanislaus, and Merced counties), 2) central SJV (Madera, Fresno, and King counties), and 3) southern SJV (Tulare and Western Kern counties). A third of the Valley's population lives in the northern SJV. This lowland area is bordered by the Sacramento Valley and Delta lowland to the north, the central portion of the SJV to the south, and mountain ranges to the east and west. Because of the marine influence, which extends into this area through gaps in the coastal mountains to the west, the northern SJV experiences a more temperate climate than the rest of the Basin. These more moderate temperatures (cooler in the summer and warmer in the winter) and the predominant air flow patterns generally favor better air quality. Similar to the northern SJV, the central and southern SJV are also low-lying areas, flanked by mountains on their west and east sides. Pollutant concentrations usually reach peak levels in the Valley within these two regions, where the population is primarily clustered around the Fresno and Bakersfield urban areas. In these regions the interaction between geography, climate, and a mix of natural (biogenic) and anthropogenic emissions pose significant challenges to air quality progress. The southern SJV represents the terminus of the Valley and is flanked by mountains on the south. The surrounding mountains in both areas act as barriers to air

flow, combined with recirculation patterns and stable air to trap pollutants near the valley floor. The more extreme temperatures and stagnant conditions in these two regions lead to poorer atmospheric dispersion and a build-up of $PM_{2.5}$. In addition to the urban air quality problems, emissions and pollutants from these areas are transported downwind, resulting in higher pollutant concentrations in downwind areas.

As discussed above, the Valley's regional diversity includes several major metropolitan areas, vast expanses of agricultural land, industrial sources, and major highways, all of which contribute to poor air quality. SJVAPCD and the California Air Resources Board (CARB) work together and operate an extensive network of air quality monitors throughout the Valley to help monitor and protect public health. The data collected from the Valley air monitoring network is used to generate daily air quality forecasts, issue health advisories, support compliance with various ambient air quality standards and serves as the basis for developing long-term attainment strategies and tracking progress towards meeting health-based air quality standards.

Figure 1 shows the spatial distribution of the $PM_{2.5}$ mass and speciation monitors in the Valley (see Table 1 for longitude/latitude information for each monitor). The monitors are located throughout the Valley floor and within the higher population density urban areas. A detailed discussion about the monitoring network and its adequacy can be found in the Valley's 2023 Air Monitoring Network Plan (https://ww2.valleyair.org/media/berdud2a/sjvapcd-2023-air-monitoring-network-plan.pdf).

Figure 1. Map of the ambient $PM_{2.5}$ monitoring network (including monitors for $PM_{2.5}$ mass only or $PM_{2.5}$ mass and speciation) in the San Joaquin Valley.

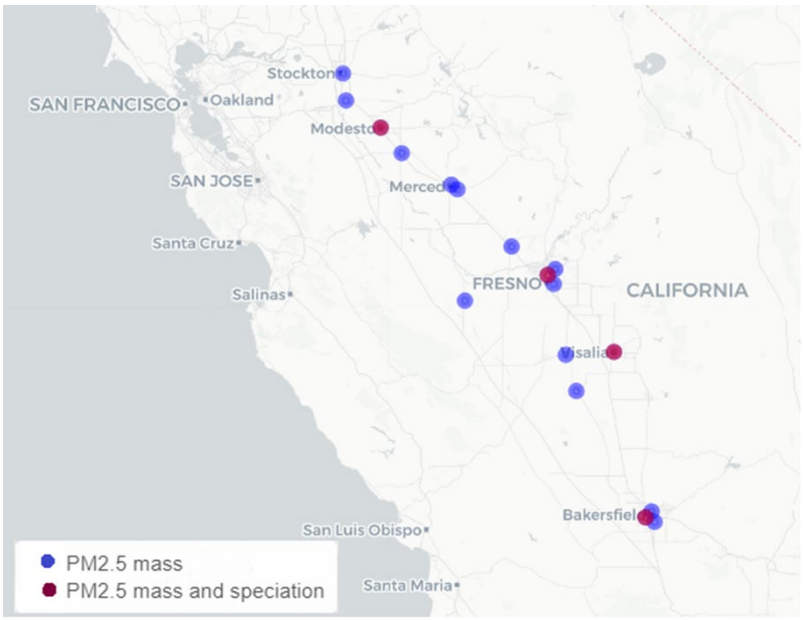

Table 1. 2015-2019 San Joaquin Valley $PM_{2.5}$ Monitoring Sites.*

Site AQS ID	County	Site	FRM $PM_{2.5}$*	FEM $PM_{2.5}$*	Speciation	Latitude	Longitude
060190011	Fresno	Fresno – Garland	X	X	X	36.7854	-119.7732
060195025	Fresno	Fresno - Hamilton & Winery (Pacific)	X			36.7264	-119.7330
060195001	Fresno	Clovis	X	X		36.8194	-119.7164
060192009	Fresno	Tranquillity		X		36.6342	-120.3823
060290016	Kern	Bakersfield - Planz	X			35.3246	-118.9976
060290014	Kern	Bakersfield - California Avenue	X		X	35.3566	-119.0626
060290010	Kern	Bakersfield - Golden	X			35.3856	-119.0150
060311004	Kings	Hanford		X		36.3157	-119.6434
060310004	Kings	Corcoran	X	X		36.1022	-119.5657
061072002	Tulare	Visalia	X		X	36.3322	-119.2912
060392010	Madera	Madera		X		36.9533	-120.0342
060472510	Merced	Merced - M Street	X			37.3083	-120.4805
060470003	Merced	Merced - S. Coffee		X		37.2819	-120.4337

Site AQS ID	County	Site	FRM $PM_{2.5}$*	FEM $PM_{2.5}$*	Speciation	Latitude	Longitude
060990006	Stanislaus	Turlock		X		37.4883	-120.8360
060990005	Stanislaus	Modesto		X	X	37.6422	-120.9942
060772010	San Joaquin	Manteca		X		37.7934	-121.2479
060771002	San Joaquin	Stockton		X		37.9507	-121.2685

*: FRM: Federal Reference Method for $PM_{2.5}$ mass; FEM: Federal Equivalent Method for $PM_{2.5}$ mass.

B. $PM_{2.5}$ Air Quality Trends

Tables 2 and 3 show the annual average $PM_{2.5}$ concentrations and the annual $PM_{2.5}$ design values (i.e., 3-year average), from 1999 to 2019, for sites in the SJV, respectively. Correspondingly, Tables 4 and 5 show the annual 98th percentile and annual 24-hour design values (i.e., 3-year average) over the same time period, respectively. In the most recent years, Bakersfield generally has the highest annual and 24-hour design values in the valley. Figure 2 shows the trend in peak valley-wide annual average $PM_{2.5}$ concentrations and 98th percentile of the 24-hour $PM_{2.5}$ concentrations, as well as the approximate number of days above the 24-hour standard in the valley from 1999 to 2019. While SJV $PM_{2.5}$ concentrations can vary strongly depending on yearly patterns of precipitation or drought conditions, in general, SJV has seen significant improvement in $PM_{2.5}$ concentrations over the last 20 years, with steady decreases in both annual average $PM_{2.5}$ levels and in the number of days above the 24-hour standard, which align with the substantial emission reductions of $PM_{2.5}$, Nitrogen Oxides (NOx) and Reactive Organic Gases (ROG) experienced in the valley (Figure 3).

Table 2. Annual Average $PM_{2.5}$ ($\mu g/m^3$).

SJV Monitoring Site	1999	2000	2001	2002	2003	2004	2005	2006	2007	2008	2009	2010	2011	2012	2013	2014	2015	2016	2017	2018	2019
Stockton	19.7	15.5	13.9	16.7	13.6	13.2	12.5	13.1	12.9	14.4	11.3	11.0	11.3	12.4	17.7	12.1	12.8	11.8	12.0	14.1	9.3
Manteca													10.8	8.3	11.7	9.9	12.6	9.8	10.9	10.3	8.1
Modesto	24.9	18.7	15.6	18.7	14.5	13.6	13.9	14.8	15.0	16.0	13.0	12.3	14.7	11.9	14.3	11.4		11.2	12.6	11.8	7.7
Turlock											16.1	12.7	17.1	14.8	15.1	12.3	14.2	12.7	12.4	13.6	10.6
Merced-Coffee												16.3	15.6	11.0	13.3	10.8	12.8	12.0	13.0	12.9	9.1
Merced-M		16.7	14.5	18.7	15.7	15.2	14.1	14.8	15.2		13.6	11.2	10.4	9.5	13.5	11.2	12.6	11.2	12.4	11.9	9.6
Madera-City													20.4	16.0	17.8	13.5	13.8	12.0	12.3	12.3	9.7
Fresno-First	27.6		19.8	21.5	17.8	16.3	16.7	16.8	18.8	17.4	15.1	13.0	15.5								
Fresno-Garland														14.1	16.8	15.1	14.4	12.7	14.7	14.1	11.1
Fresno-Winery		18.4	18.6	21.3	17.8	17.0	16.9	17.6	16.8	16.5	14.6	13.4	15.4	12.7	15.9	13.8	14.1	13.0	15.0	14.8	11.2
Clovis	19.8	16.3	18.0	16.2	18.5	16.4	16.3	16.4	16.4	16.2	18.3	14.7	17.9	15.4	15.9	16.6	15.0	12.6	13.0	12.6	10.2
Tranquility												7.0	8.2	7.1	8.4	7.7	10.0	7.9	8.1	9.0	5.8
Corcoran		16.4	19.2	21.5	16.2	17.4	17.5	16.9	18.4	15.8	17.7	17.9			15.6	15.4		14.8	15.9	14.9	12.1
Hanford												14.5	18.0	14.8	18.2	17.5	16.5	15.5	17.0	15.4	12.2
Visalia	27.6	23.9	22.5	23.2	18.2	17.0	18.8	18.8	20.4	19.8	16.0	13.6	16.1	14.8	18.9	17.9	16.1	14.7	16.3	16.2	12.9
Bakersfield-California	27.4	22.5	21.2	22.7	17.1	18.9	18.0	18.7	22.0	21.9	19.0	14.2	16.2	13.0	20.0	18.6	16.3	14.8	15.7	15.9	11.8
Bakersfield-Planz		20.3	20.8	23.5	17.8	17.4	19.8	19.3	21.8	23.5	22.5	16.8	14.4	14.7	21.7	21.6	17.9	15.9	18.2	18.0	13.0

Table 3. Annual $PM_{2.5}$ Design Value (three-year average, $\mu g/m^3$).

SJV Monitoring Site	2001	2002	2003	2004	2005	2006	2007	2008	2009	2010	2011	2012	2013	2014	2015	2016	2017	2018	2019
Stockton	16.4	15.3	14.7	14.5	13.1	12.9	12.8	13.5	12.9.	12.2	11.2	11.6	13.8	14.1	14.2	12.2	12.1	12.7	11.8
Manteca													10.2	9.9	11.4	10.8	11.0	10.3	9.8
Modesto	19.7	17.7	16.2	15.6	14.0	14.1	14.6	15.3	14.7	13.8	13.3	12.9	13.6	12.5			10.9	11.8	10.7
Turlock											15.3	14.9	15.7	14.1	13.9	13.1	13.0	12.9	12.2
Merced-Coffee												14.3	13.3	11.7	12.3	11.9	12.5	12.6	11.7
Merced-M		16.6	16.3	16.5	15.0	14.7	14.7				11.7	10.4	11.1	11.4	12.5	11.7	12.1	11.8	11.3
Madera-City													18.1	15.8	15.0	13.1	12.7	12.2	11.4
Fresno -First			19.7	18.6	16.9	16.6	17.4	17.7	17.1	15.2	14.5								
Fresno -Garland													15.4	15.3	15.4	14.1	13.9	13.9	13.3
Fresno -Winery		19.4	19.2	18.7	17.2	17.2	17.1	17.0	16.0	14.9	14.5	13.9	14.7	14.1	14.6	13.6	14.0	14.3	13.7
Clovis	18.0	16.8	17.6	17.0	17.1	16.4	16.4	16.4	17.0	16.4	17.0	16.0	16.4	16.0	15.8	14.7	13.4	12.7	11.9
Tranquility												7.5	7.9	7.7	8.7	8.5	8.6	8.3	7.7
Corcoran		19.0	19.0	18.4	17.0	17.2	17.6	17.0	17.3	17.1								15.2	14.3
Hanford												15.8	17.0	16.8	17.4	16.5	16.3	16.0	14.9
Visalia	24.7	23.2	21.3	19.5	18.0	18.2	19.3	19.7	18.8	16.5	15.2	14.8	16.6	17.2	17.6	16.2	15.5	15.7	15.1
Bakersfield-California	23.7	22.1	20.3	19.6	18.0	18.5	19.6	20.9	21.0	18.4	16.5	14.5	16.4	17.2	18.3	16.6	15.5	15.4	14.5
Bakersfield-Planz		21.5	20.7	19.6	18.4	18.9	20.3	21.5	22.6	20.9	17.9	15.3	16.9	19.3	20.4	18.5	17.2	17.3	16.4

Table 4. Annual 98th percentile of the 24-hour $PM_{2.5}$ ($\mu g/m^3$).

SJV Monitoring Site	1999	2000	2001	2002	2003	2004	2005	2006	2007	2008	2009	2010	2011	2012	2013	2014	2015	2016	2017	2018	2019
Stockton	79.0	55.0	58.0	50.0	41.0	36.0	44.0	42.0	48.0	61.6	40.4	29.7	44.8	33.9	56.3	44.5	39.1	32.4	44.2	42.1	32.9
Manteca													38.9	30.9	40.2	40.0	42.7	29.3	34.5	32.9	26.8
Modesto	100	71.0	69.0	69.0	47.0	45.0	55.0	52.0	57.4	53.9	54.5	37.3	54.7	40.8	56.4	49.5	30.8	36.2	51.1	36	28.4
Turlock										67.4	53.1	43.5	57.4	45.4	55.4	51.2	47.3	38.5	48	37.7	36
Merced-Coffee											41.4	39.9	47.4	35.6	42.3	43.8	40.3	32.8	43.7	34.5	23.4
Merced-M	91.9	60.0	49.3	55.1	44.2	43.0	48.3	43.8	52.7	54.0	45.2	39.1	38.5	41.8	67.3	45.9	39.0	34.6	40.3	35.6	29.5
Madera-City												50.6	59.1	43.2	54.6	51.0	43.7	35.7	45.8	36.5	23.9
Fresno-First	120	90.0	75.0	75.0	56.0	52.0	71.0	51.0	67.0	57.4	55.8	48.8	69.5								
Fresno-Garland														52.6	63.8	66.7	52.0	43.7	68	43.8	36.9
Fresno-Winery		64.8	61.5	71.9	49.7	49.4	71.2	55.0	57.4	44.5	48.2	40.2	67.5	51.3	71.6	61.8	42.0	40.0	73.2	54.5	37.1
Clovis	59.2	72.5	71.5	53.2	48.1	52.4	63.0	51.3	60.9	49.0	49.0	44.3	68.5	48.0	56.2	64.6	45.7	36.1	50	38.4	28
Tranquility											35.8	27.0	27.5	26.9	35.7	31.2	35.8	27.0	34.4	29.5	17.1
Corcoran	53.0	55.1	89.5	65.1	42.2	49.4	74.5	50.1	57.9	47.9	53.4	47.2			66.0	71.0		45.9	69.7	42.3	45.1
Hanford												48.5	64.6	48.3	67.6	81.9	51.4	43.3	68.7	45.1	41.1
Visalia	114	103.0	96.0	70.0	47.0	54.0	65.0	50.0	59.7	62.1	53.9	36.3	50.7	53.8	62.5	75.4	45.8	40.7	74.6	46.8	45.5
Bakersfield-California	98.0	92.7	94.9	73.0	48.3	61.5	63.2	60.5	73.0	64.5	66.7	53.3	65.5	56.4	71.8	79.9	57.2	47.0	71.8	56.7	43.4
Bakersfield-Planz		76.5	90.6	66.8	47.5	47.6	66.4	64.7	72.2	72.3	65.5	47.2	43.2	40.6	83.6	76.7	56.5	50.7	69.7	56.6	46.7

Table 5. 24-hour $PM_{2.5}$ Design Values (three-year average, $\mu g/m^3$).

SJV Monitoring site	2001	2002	2003	2004	2005	2006	2007	2008	2009	2010	2011	2012	2013	2014	2015	2016	2017	2018	2019
Stockton	64	54	50	42	40	41	45	51	50	44	38	36	45	45	47	39	38	40	40
Manteca													37	37	41	37	36	32	31
Modesto	80	70	62	54	49	51	55	54	55	49	49	44	51	49	46	39	39	41	39
Turlock										55	51	49	53	51	51	46	45	41	41
Merced-Coffee											43	41	42	41	42	39	38	37	34
Merced-M	67	55	50	47	45	45	48	50	51	46	41	40	49	52	47	40	38	37	35
Madera-City												51	52	50	50	43	42	39	35
Fresno-First	95	80	69	61	60	58	63	58	60	54	58								
Fresno-Garland														61	61	54	54	52	50
Fresno-Winery		66	61	57	57	59	61	52	50	44	52	53	64	62	54	48	52	56	55
Clovis	68	66	58	51	55	56	58	54	53	47	54	54	58	56	56	49	44	42	39
Tranquility												27	30	31			32	30	27
Corcoran	66	70	66	52	55	58	61	52	53	49	47				75		72	53	52
Hanford												54	60	66	67	59	54	52	52
Visalia	104	90	71	57	55	56	58	57	59	51	47	47	56	64	61	54	54	54	56
Bakersfield-California	95	87	72	61	58	62	66	66	68	62	62	58	65	69	70	61	59	59	57
Bakersfield-Planz		78	68	54	54	60	68	70	70	62	52	44	56	67	72	61	59	59	58

Figure 2. Trends in valley-wide annual average, 24-hour 98th percentile $PM_{2.5}$, and approximate number of days above the 24-hour standard.

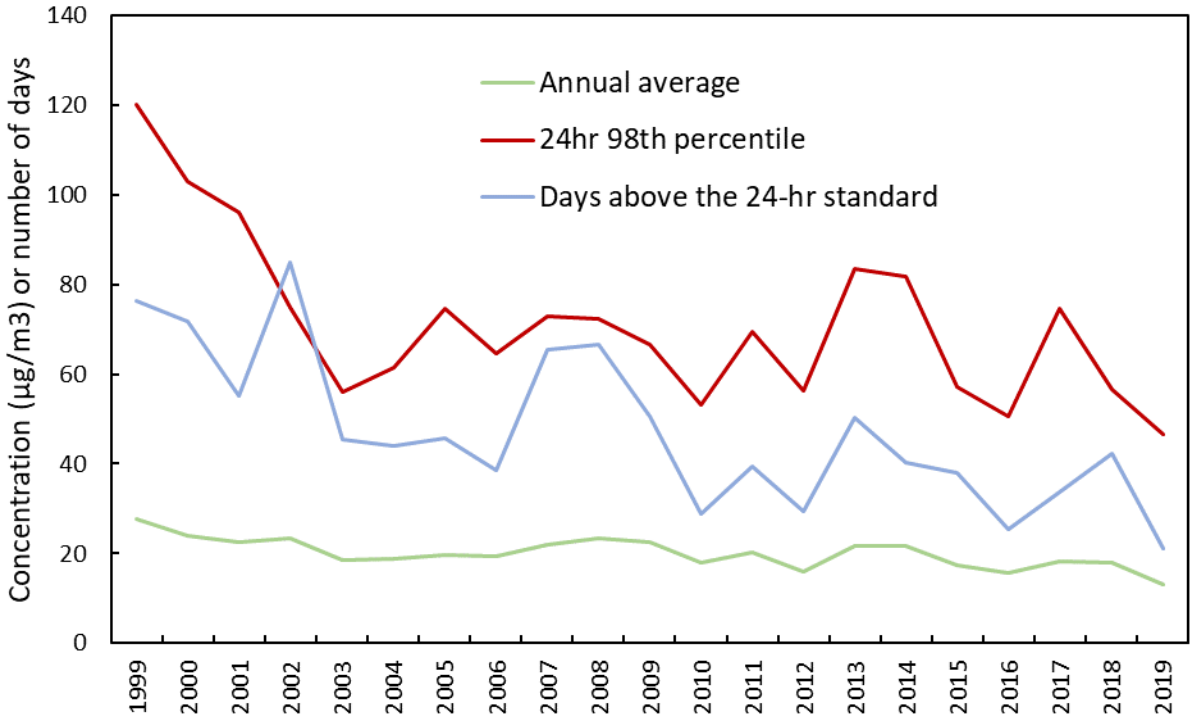

Figure 3. San Joaquin Valley trends in $PM_{2.5}$, NOx, and ROG emissions.

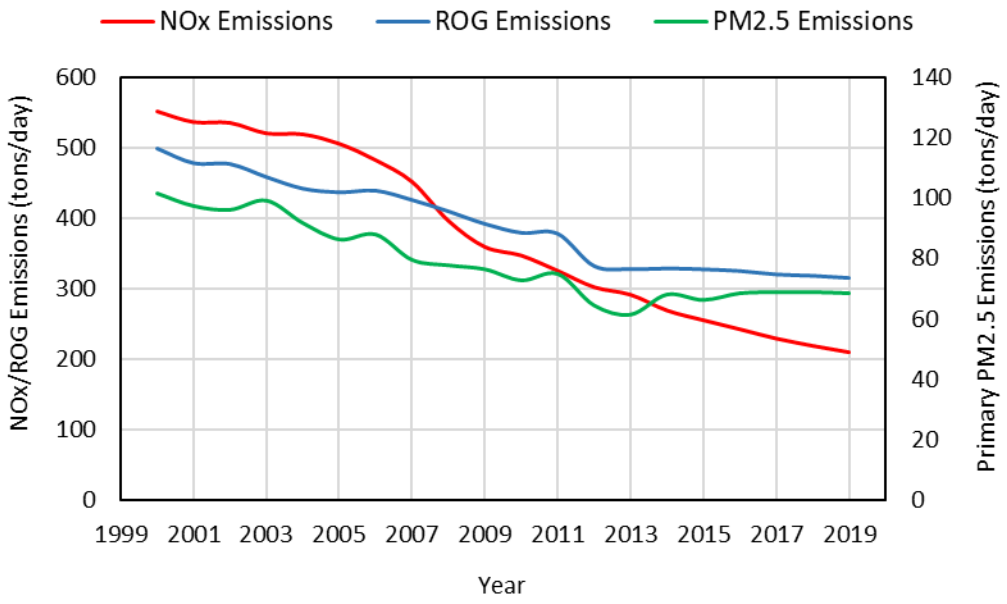

C. Major $PM_{2.5}$ Chemical Components

Four monitoring sites collect $PM_{2.5}$ chemical composition data in the San Joaquin Valley: Bakersfield-California, Fresno-Garland, Modesto, and Visalia. The Bakersfield and Fresno speciation monitors are part of the national Chemical Speciation Network (CSN) while Modesto and Visalia are part of the State and Local Air Monitoring Stations (SLAMS) network. All four sites use Spiral Aerosol Speciation Sampler (SASS) samplers from Met One Instruments for data collection. Since deployment of the speciation sampling, changes were made to the carbon sampling and analysis method. The collection method changed from the Met One SASS to the URG3000N sampler, which is very similar to the Interagency Monitoring of Protected Visual Environments (IMPROVE) module C sampler. The analytical method was changed from the National Institute of Occupational Safety and Health (NIOSH)-like thermal optical transmittance method to IMPROVE_A thermal optical reflectance. At Bakersfield, Modesto, and Visalia these changes were implemented in May 2007, while the Fresno site switched to the new carbon system in April 2009.

Figure 4 illustrates the average of the 2015-2019 annual average $PM_{2.5}$ compositions, as well as the average of the top 10 percent of days at Bakersfield, Fresno, and Modesto over the same period. (Note that this composition can be somewhat different from those used in the DV calculation since there is difference between FRM and CSN filter measurement and analysis methods. More detail can be found in the U.S. EPA modeling guidance (U.S. EPA 2018)). Organic matter (OM) was calculated by multiplying measured OC by 1.5 according to the OM/OC ratio measured at Fresno (Ge et al., 2012). Ammonium nitrate and OM are the largest contributors to $PM_{2.5}$ on an annual basis, accounting for approximately 70-75% of the $PM_{2.5}$ mass. Their contributions are even higher on peak $PM_{2.5}$ days, accounting for 80-85% of $PM_{2.5}$ mass. Formation mechanisms for ammonium nitrate are discussed in Section D. OM sources typically include residential wood combustion, cooking, biomass burning, and mobile sources. In addition, OM can also be formed in the atmosphere from oxidation of ROG. Ammonium sulfate contributes approximately 10% of the $PM_{2.5}$ on an annual basis. Its contribution is half that on peak days, at approximately 6%. Elemental carbon and crustal materials typically contribute less than 10% to $PM_{2.5}$ levels in these cities, except at Bakersfield, where crustal materials contributed more than 10% on an annual basis.

Figure 4. Five-year average (2015-2019) and average peak day (top 10 percent over the same five years) $PM_{2.5}$ compositions at Bakersfield, Fresno, and Modesto.

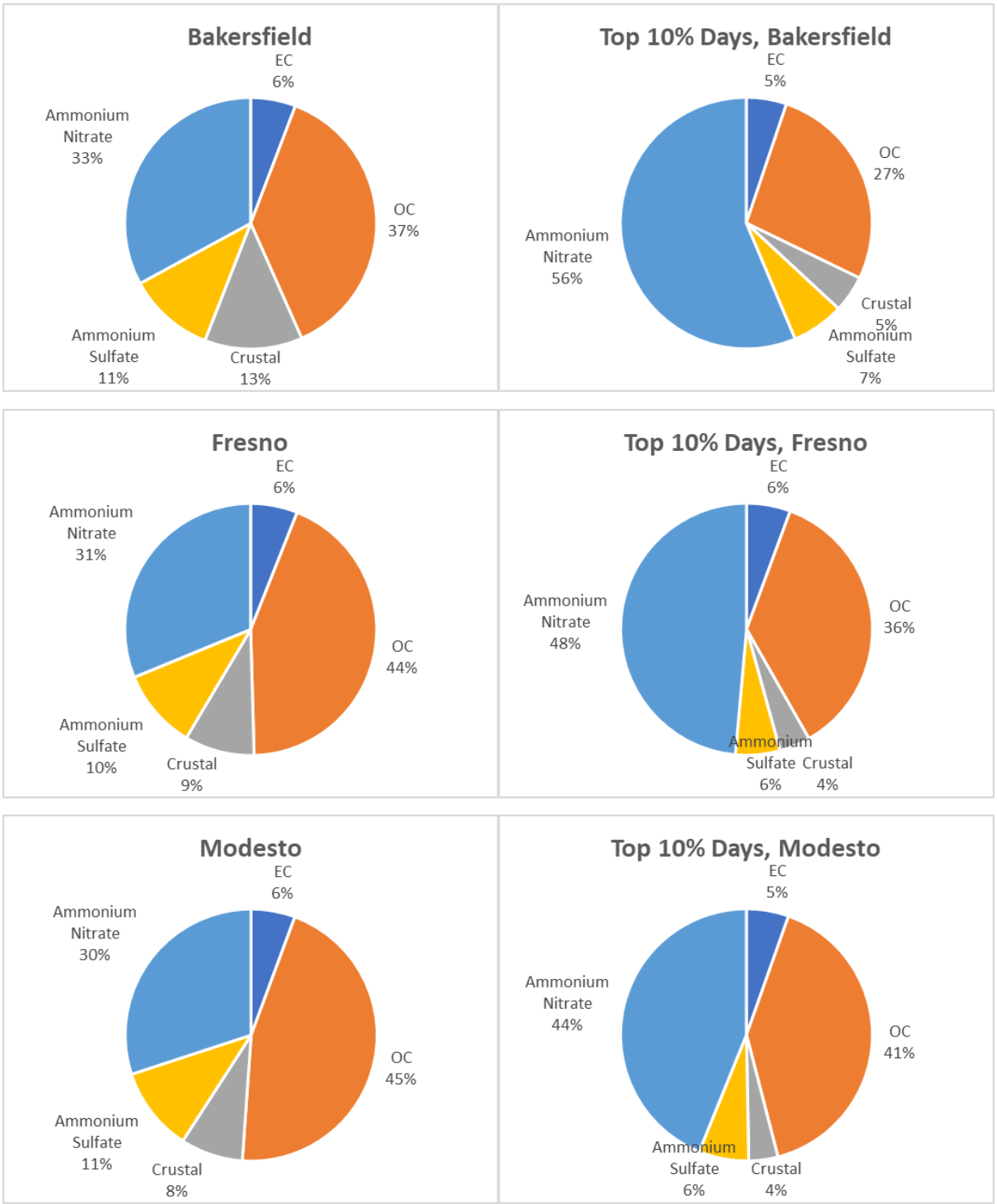

D. Seasonality of $PM_{2.5}$ and Meteorological Conditions Leading to Elevated $PM_{2.5}$

$PM_{2.5}$ concentrations in the SJV exhibit a strong seasonal variability, with the highest concentrations occurring during the months of November through February. For example, Figure 5 represents the time series of 24-hour $PM_{2.5}$ concentrations at Bakersfield - California Avenue in 2017, which shows elevated $PM_{2.5}$ episodes occurred in the first few and last few months of the year. The predominance of elevated $PM_{2.5}$ episodes during winter months results from a confluence of meteorological conditions conducive to the formation and buildup of $PM_{2.5}$, as well as wintertime sources of directly emitted $PM_{2.5}$.

Figure 5. 24-hour $PM_{2.5}$ concentrations at Bakersfield-California Avenue in 2017.

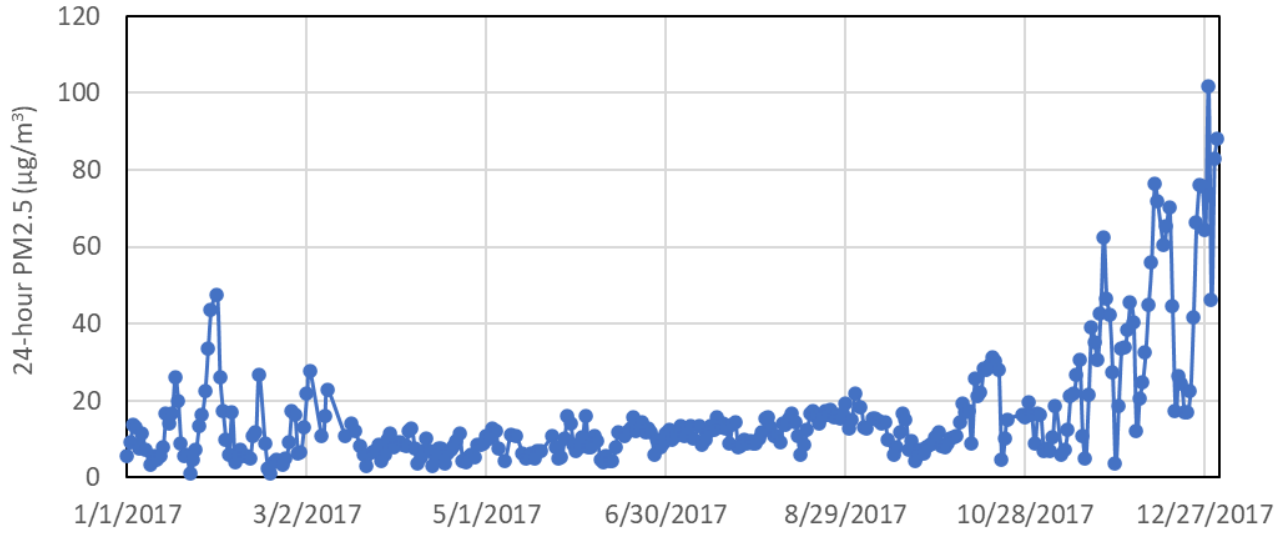

High $PM_{2.5}$ concentrations typically build up during multiday episodes under stagnant winter weather when a high-pressure system (the Great Basin High) reduces the ventilation in the Valley (Ferreria et al., 2005). These stagnation events, sandwiched between two weather systems, are characterized by low wind speeds, moderate temperatures, vertical atmospheric stability, and high relative humidity. This stable atmosphere prevents precursor gases and primary (or directly emitted) $PM_{2.5}$ released at the surface in the Valley from rapidly dispersing. The moderate temperatures and high relative humidity also enhance the formation of secondary particulate matter, especially ammonium nitrate and sulfate. In contrast, hotter and drier weather conditions in summer favor the evaporation of semi-volatile species from particles. Greater mixing heights in the summer can also help the ventilation of air pollutants. As a result, summertime $PM_{2.5}$ concentrations in the SJV are typically much lower compared to wintertime.

Wintertime $PM_{2.5}$ episodes can last for many days. At the beginning of an episode, concentrations are low but increase daily because of both the accumulation of primary pollutants and formation of secondary pollutants (Watson et al, 2002). Concentrations

continue to build until there is a change in the weather significant enough to wash out particles through rainfall or increased ventilation of the Valley. For example, the two main episodes captured during the CRPAQS (i.e., California Regional Particulate Matter Air Quality Study) field study (starting in late 1999) had up to 18 days with $PM_{2.5}$ concentrations exceeding 65 $\mu g/m^3$ (Turkiewicz et al., 2006). In December 2017, Bakersfield experienced 20 days with $PM_{2.5}$ concentrations greater than 35 $\mu g/m^3$. During such episodes, urban sites typically record elevated concentrations earlier than rural sites, and consequently, have a greater number of days with high concentrations. However, due to the buildup of $PM_{2.5}$ concentrations, rural sites can achieve concentrations with similar magnitude as urban sites by the end of an episode.

The elevated wintertime $PM_{2.5}$ concentrations observed during pollution episodes are the result of both directly emitted particulates (known as primary particulate matter) and particulate matter formed via chemical and physical processes in the atmosphere (known as secondary particulate matter). Ammonium nitrate, the dominant $PM_{2.5}$ component throughout the Valley in winter, is formed in the atmosphere from chemical reactions between precursor pollutants such as NO_x, ROG, and ammonia. Carbonaceous aerosol, the second most abundant component, is primarily directly emitted, and is the result of contributions from wood combustion (e.g., wood burning for heating), charbroiling, and mobile sources (Ge et al., 2012; Young et al., 2016).

Ammonium nitrate can be formed both at the surface and aloft and can be fairly uniform across urban and rural sites. The spatial homogeneity of ammonium nitrate is influenced by higher wind speeds aloft (which allow for more efficient transport), and the diurnal variation in mixing heights (which allow entrainment of ammonium nitrate down to the surface). Ammonium nitrate is also formed via both daytime and nighttime chemistry pathways. The amount of ammonium nitrate produced will be limited by the relative abundance of its precursors in the atmosphere. In the San Joaquin Valley, nighttime formation is considered to be the most important pathway (Lurmann et al., 2006; Prabhakar et al., 2017). The nighttime pathway involves oxidation of NO_2, followed by reaction with ammonia to form ammonium nitrate. Since ammonia is abundant in the Valley in the winter, NO_x is considered to be the limiting precursor (Chen, et al., 2014, 2020; Kleeman, et al., 2005; Parworth, et al., 2017; Prabhakar et al., 2017). In contrast, the daytime pathway also involves ROG. Modeling studies that investigated winter episodes in the Valley estimated that reductions in ROG emissions have a small impact on nitrate concentrations only at very high $PM_{2.5}$ concentrations (Pun, et al., 2009). However, at current $PM_{2.5}$ levels the impact is very limited, and in some cases ROG reductions can lead to an increase in $PM_{2.5}$ concentrations (Chen et al., 2014; Kleeman, et al., 2005).

II. Approaches

This section briefly describes CARB's procedures, based on U.S. EPA guidance (U.S. EPA, 2018), for projecting future year annual and 24-hour $PM_{2.5}$ Design Values (DVs) using model output and a Relative Response Factor (RRF) approach.

A. Methodology

The U.S. EPA modeling guidance (U.S. EPA, 2018) outlines the approach for using models to predict future year annual $PM_{2.5}$ DVs. The guidance recommends using model predictions in a "relative" rather than "absolute" sense. In this relative approach, the fractional change (or ratio) in $PM_{2.5}$ concentration between the model future year and model baseline year are calculated for all valid monitors. These ratios are called relative response factors (RRFs). Since $PM_{2.5}$ is comprised of different chemical species, which respond differently to changes in emissions of various pollutants, separate RRFs are calculated for the individual $PM_{2.5}$ species. Baseline DVs are then projected to the future on a species-by-species basis, where the DV is separated into individual $PM_{2.5}$ species and each species is multiplied by its corresponding RRF. The individual species are then summed to obtain the future year $PM_{2.5}$ DV.

A brief summary of the modeling procedures utilized in this attainment analysis, as prescribed by the U.S. EPA modeling guidance (U.S. EPA, 2018), is provided below.

B. Modeling Period

Based on analysis of recent years' ambient $PM_{2.5}$ levels and meteorological conditions leading to elevated $PM_{2.5}$ concentrations, the year 2017 was selected for baseline modeling calculations.

C. Baseline Design Values

Specifying the baseline DV is a key consideration in the model attainment test because this value is projected forward to the future and used to test for future attainment of the standard at each monitor. U.S. EPA guidance (2018) defines the annual $PM_{2.5}$ DV for a given year as the 3-year average (ending in that year) of the annual average $PM_{2.5}$ concentrations, where the annual average is calculated as the average of the quarterly averages for each calendar quarter (e.g., January-March, April-June, July-September, October-December). For example, the 2017 $PM_{2.5}$ DV is the average of the annual $PM_{2.5}$ concentrations from 2015, 2016, and 2017.

To minimize the influence of year-to-year variability in demonstrating attainment, the U.S. EPA (2018) allows the averaging of three DVs, where one of the years is the baseline emissions inventory and modeling year. This average DV is referred to as the baseline DV. Since each DV represents an average over three years, observational data from 2015, 2016, 2017, 2018, and 2019 will influence the average DV, with each year receiving a different weighting. Table 6 illustrates the observational data from each year that goes into the baseline DV.

Table 6. Illustrates the data from each year that is utilized in the baseline DV calculation.

DV Year	Years averaged for the DV				
2017	2015	2016	2017		
2018		2016	2017	2018	
2019			2017	2018	2019

Yearly weighting for the baseline DV calculation is calculated as:

$$\mathbf{2017-2019}\ \boldsymbol{Average} = \frac{\boldsymbol{PM2.5_{2015}+2\times PM2.5_{2016}+3\times PM2.5_{2017}+2\times PM2.5_{2018}+PM2.5_{2019}}}{\mathbf{9}} \quad (1)$$

Table 7 shows the 2017-2019 average annual DVs (or annual baseline DVs) for each Federal Reference Method (FRM) and Federal Equivalent Method (FEM) site in the SJV, which had sufficient data to calculate a DV. For one site with incomplete data, assumptions were made to calculate the baseline DV and the assumptions were annotated following Table 7. The highest DV occurred at the Bakersfield - Planz site with a baseline DV of 16.97 µg/m^3.

Table 7. Average baseline DV for each monitoring site in the SJV, as well as the yearly annual DVs from 2017-2019 utilized in calculating the baseline DVs.*

AQS site ID	Monitoring Site Name	2017	2018	2019	2017-2019 Average Baseline
060290016	Bakersfield - Planz	17.18	17.32	16.41	16.97
060311004	Hanford	16.33	15.99	14.87	15.73
060290010	Bakersfield - Golden	15.83	15.77	14.95	15.52
061072002	Visalia	15.49	15.69	15.12	15.43
060290014	Bakersfield - California Ave.	15.47	15.42	14.48	15.12
060310004	Corcoran *	15.35	15.20	14.31	14.95
060195025	Fresno - Hamilton & Winery	14.05	14.26	13.68	13.99
060190011	Fresno - Garland	13.92	13.86	13.30	13.69
060990006	Turlock	13.00	12.89	12.23	12.70
060195001	Clovis	13.42	12.69	11.94	12.69
060470003	Merced - S Coffee	12.52	12.61	11.69	12.28
060771002	Stockton	12.14	12.65	11.83	12.21
060392010	Madera	12.71	12.19	11.41	12.11
060472510	Merced-M Street	12.07	11.83	11.31	11.73
060990005	Modesto	10.90	11.85	10.71	11.16
060772010	Manteca	11.03	10.31	9.76	10.37
060192009	Tranquillity	8.62	8.29	7.66	8.19

*: Because of incomplete data at Corcoran in 2015, annual 2015 $PM_{2.5}$ concentration was assumed to be average of annual 2016 and 2017 $PM_{2.5}$ concentrations.

D. Base, Reference, and Future Years

The modeling assessment consists of the following three primary model simulations, which all utilized the same model inputs for meteorology, chemical boundary conditions, and biogenic emissions. The only difference between the simulations was the year

represented by the anthropogenic emissions (2017 versus 2030) and certain day-specific emissions.

1. *Base Year (or Base Case) Simulation*

   The base year simulation for 2017 was used to assess model performance and includes as much day-specific detail as possible in the emissions inventory such as hourly adjustments to the motor vehicle and biogenic inventories based on observed local meteorological conditions, as well as known wildfire and agricultural burning events.

2. *Reference (or Baseline) Year Simulation*

   The reference year simulation was identical to the base year simulation, except that certain emissions events which are either random and/or cannot be projected to the future were removed from the emissions inventory, such as wildfires.

3. *Future Year Simulations*

   The future year simulations are identical to the reference year simulation, except that projected future year 2030 anthropogenic emission levels were used rather than 2017 emission levels. All other model inputs (e.g., meteorology, chemical boundary conditions, biogenic emissions, and calendar for day-of-week specifications in the inventory) were the same as those used in the reference year simulation.

To summarize (Table 8), the base year 2017 simulation was used for evaluating model performance, while the reference (or baseline) 2017 and future year 2030 simulations were used to project the average DVs to the future year.

Table 8. Description of CMAQ model simulations used to evaluate model performance and project baseline design values to the future years.

Simulation	Anthropogenic Emissions	Biogenic Emissions	Meteorology	Chemical Boundary Conditions
Base year (2017)	2017 w/ wildfires	2017 MEGAN	2017 WRF	2017 Geos-Chem
Reference year (2017)	2017 w/o wildfires	2017 MEGAN	2017 WRF	2017 Geos-Chem
Future year (2030)	2030 w/o wildfires	2017 MEGAN	2017 WRF	2017 Geos-Chem

E. $PM_{2.5}$ Species Calculations

Since $PM_{2.5}$ consists of different chemical components, it is necessary to assess how each individual component will respond to emission reductions. As a first step in this process, the measured total $PM_{2.5}$ must be separated into its various components. In

the SJV, the primary components on the filter based $PM_{2.5}$ measurements include sulfates, nitrates, ammonium, organic carbon (OC), elemental carbon (EC), particle-bound water, other primary inorganic particulate matter, and passively collected mass (blank mass). Species concentrations were obtained from the four chemical speciation sites in the SJV. These four sites are located at: Bakersfield - California Avenue, Fresno - Garland, Visalia - North Church, and Modesto - 14th Street. Chemical species were measured once every three or six days at those sites. Since not all of the 17 FRM/FEM $PM_{2.5}$ sites in the Valley have collocated speciation monitors, it was necessary to utilize the speciated $PM_{2.5}$ measurements at one of the four speciation sites to represent the speciation profile at each of the FRM/FEM sites. The choice of which speciation site to represent the speciation profile at a given FRM monitor (Table 9) was determined based on geographic proximity, analysis of local emission sources, and measurements from previous field studies (e.g., CRPAQS, DISCOVER-AQ), and is consistent with previous $PM_{2.5}$ SIPs in the Valley.

Table 9. $PM_{2.5}$ speciation data used for each $PM_{2.5}$ design site.

AQS Site ID	$PM_{2.5}$ Design Site (FRM/FEM Monitor)	$PM_{2.5}$ Speciation Site
060290016	Bakersfield - Planz	Bakersfield - California
060311004	Hanford	Visalia - Church
060290010	Bakersfield - Golden	Bakersfield - California
061072002	Visalia	Visalia - Church
060290014	Bakersfield - California Ave.	Bakersfield - California
060310004	Corcoran	Visalia - Church
060195025	Fresno - Hamilton & Winery	Fresno - Garland
060190011	Fresno - Garland	Fresno - Garland
060990006	Turlock	Modesto - 14th
060195001	Clovis	Fresno - Garland
060470003	Merced - S Coffee	Modesto - 14th
060771002	Stockton	Modesto - 14th
060392010	Madera	Fresno - Garland
060472510	Merced - M Street	Modesto - 14th
060990005	Modesto	Modesto - 14th

AQS Site ID	$PM_{2.5}$ Design Site (FRM/FEM Monitor)	$PM_{2.5}$ Speciation Site
060772010	Manteca	Modesto - 14th
060192009	Tranquillity	Fresno - Garland

The FRM $PM_{2.5}$ monitors and speciation samplers utilize different filter media (Teflon vs. nylon, respectively), which can lead to differences in the amount of $PM_{2.5}$ nitrate retained on the filters. When direct measurements of the retained nitrate on the FRM filter are not available, the U.S. EPA (2018) recommends using the SANDWICH approach (Sulfate, Adjusted Nitrate, Derived Water, Inferred Carbon Hybrid material balance) described by Frank (2006) to apportion the FRM $PM_{2.5}$ mass to individual $PM_{2.5}$ species based on nearby CSN speciation data. A key component of the SANDWICH method is to estimate the amount of nitrate evaporated from the FRM filters. Frank (2006) followed Hering and Cass (1999) to estimate the volatized nitrate from the FRM filter which is described below. To estimate volatized nitrate, necessary inputs include 24-hour average nitrate measurements and hourly temperature and relative humidity data. For each hour *i* of the day, calculate the dissociation constant, K_i from ambient temperature and relative humidity (RH).

For RH < 61%:

$$\ln(K_i) = 118.87 - (24084/\mathrm{T}_i) - 6.025 \times \ln(T_i) \qquad (2)$$

where T_i is the hourly temperature in Kelvins and K_i is in nanobars.

For RH ≥ 61%, K_i is replaced by:

$$K_i' = [P_1 - P_2(1 - a_i) + P_3(1 - a_i)^2] \times (1 - a_i)^{1.75} \times K_i, \qquad (3)$$

where, $a_i$is “fractional” relative humidity and

$$\ln(P_1) = -135.94 + 8763/\mathrm{T}_i + 19.12 \times \ln(T_i),$$

$$\ln(P_2) = -122.65 + 9969/\mathrm{T}_i + 16.22 \times \ln(T_i),$$

$$\ln(P_3) = -182.61 + 13875/\mathrm{T}_i + 24.46 \times \ln(T_i).$$

Using this information, calculate the nitrate retained on the filter as:

$$\text{Retained Nitrate} = \text{STN nitrate} - 745.7/\mathrm{T}_R \times (\kappa - \gamma) \times \frac{1}{24}\sum_{i=1}^{24}\sqrt{K_i} \qquad (4)$$

where T_R is the daily average temperature for the sampled air volume in Kelvin, K_i is the dissociation constant for NH_4NO_3 at ambient temperature for hour *i*, and $(\kappa - \gamma)$ relates to the temperature rise of the filter and vapor depletion from the inlet surface and is assumed to have a value equal to one (Hering and Cass, 1999).

During the CRPAQS field study in the SJV, Chow et al. (2005) performed a series of experimental studies to study loss of $PM_{2.5}$ nitrate from FRM samples and found that the Hering and Cass (1999) methodology overestimated nitrate loss from the FRM filter for every sample during warm months and most of samples during cold months. The possible reasons for these differences include the presence of ammonia in the sampling system, which suppresses volatilization of ammonium nitrate from the filter, or the presence of non-volatilized nitrate associated with sea salt and mineral dust. Chow et al. (2005) reported that the amount of nitrate lost to evaporation during sampling at the Angiola, Fresno, and Bakersfield sites ranged from 3.5 to 6.5% during cold months and from 61 to 84%, during warm months. Based on the nitrate evaporation range in Chow et al. (2005), we assume that 20% of nitrate is evaporated from the FRM filter (or 80% nitrate is retained on FRM filter) during the colder months (quarters 1 and 4) and 90% of nitrate is evaporated from the FRM filter (or 10% nitrate is retained on FRM filter) during the warmer months (quarters 2 and 3). It is important to note that the calculation of nitrate loss from FRM filters only impacts the relative percentage of nitrate and OM in the filter, but it does not change the baseline DVs.

Once the retained nitrate is calculated along with sulfate, ammonium, elemental carbon, and sea salt, particle bound water is calculated using the Aerosol Inorganics Model (AIM, or http://www.aim.env.uea.ac.uk/aim/aim.php). Organic Matter (OM) mass is calculated as the difference between FRM $PM_{2.5}$ mass and all other species (i.e., retained nitrate, sulfate, ammonium, elemental carbon, crustal material, and blank mass which is 0.2 $\mu g/m^3$) as suggested in U.S. EPA's SANDWICH approach (U.S. EPA 2018).

To apportion the FRM $PM_{2.5}$ mass to specific species, $PM_{2.5}$ speciation data from 2015-2019 were utilized. For the annual DV calculation, for each quarter, percent contributions from individual chemical species to FRM $PM_{2.5}$ mass were calculated as the average of the corresponding quarters from 2015-2019.

F. Future Year Design Values

The approach taken for projecting future year annual $PM_{2.5}$ DVs is described briefly below. See U.S. EPA (2018) for additional details. Projecting baseline annual $PM_{2.5}$ DVs to the future involves the following steps:

Step 1: Compute observed quarterly weighted average concentrations (consistent with the weighted average DV calculation) at each monitor for the following species: ammonium, nitrate, sulfate, organic carbon, elemental carbon, sea salt, and other primary PM. This is done by multiplying quarterly weighted average FRM $PM_{2.5}$ concentrations by the fractional composition of $PM_{2.5}$ species for each quarter.

Step 2: Compute the component-specific RRF for each quarter and each species at each monitor based on the reference and future year modeling. The RRF for a specific component *j* is calculated using the following expression:

$$RRF_j = \frac{[C]_{j,\ future}}{[C]_{j,\ reference}} \quad (5)$$

Where $[C]_{j,\ future}$ is the modeled quarterly mean concentration for component *j* predicted for the future year averaged over the 3x3 array of grid cells surrounding the monitor, and $[C]_{j,reference}$ is the same, but for the reference year simulation. An RRF was calculated for each species in Step 1 and at each monitor and for each quarter.

Step 3: Apply the component specific RRF from Step 2 to the observed quarterly weighted average concentrations from Step 1 to obtain projected quarterly species concentrations.

Step 4: Use the online E-AIM model (http://www.aim.env.uea.ac.uk/aim/aim.php) to calculate future year particle-bound water for each quarter at each monitor based on projected ammonium sulfate and ammonium nitrate concentrations.

Step 5: The projected concentration for each quarter is summed over all species, including particle bound water from Step 4, as well as a blank mass of 0.2 μg/m^3 to obtain the future quarterly average $PM_{2.5}$ concentration. Finally, the future annual $PM_{2.5}$ DVs are calculated as the average of the projected $PM_{2.5}$ concentrations from the four quarters. If the projected annual DV is ≤ NAAQS, then the attainment test is passed.

III. Meteorological Modeling

California's proximity to the ocean, complex terrain, and diverse climate pose unique challenges for developing meteorological fields. These fields must adequately represent the synoptic and mesoscale features of the regional meteorology. In summertime, the majority of the storm tracks are far to the north of the state and a semi-permanent Pacific high typically sits off the California coast. Interactions between this eastern Pacific subtropical high pressure system and the thermal low pressure further inland over the Central Valley or South Coast lead to conditions conducive to pollution buildup (Fosberg and Schroeder, 1966; Bao et al., 2008). In wintertime, periods of high atmospheric pressure bring light winds and, sometimes, low solar insolation (Daly et al. 2009) to the Central Valley. Because of the topographical features surrounding San Joaquin Valley, under such conditions, a layer of cold and wet air can be overlaid by warm air aloft creating strong and long-lasting stagnation in the area (Whiteman et al. 2001). It is under such conditions that high surface particulate matter concentrations typically occur (Gillies et al. 2010; Baker et al. 2011).

In the past, CARB has utilized both prognostic and diagnostic meteorological models, as well as hybrid approaches in an effort to develop meteorological fields for use in air quality modeling that most accurately represent the meteorological processes which are important to air quality (e.g., Jackson et al., 2006). In this work, the state-of-the-science Weather Research and Forecasting (WRF) prognostic model (Skamarock, et al. 2021)

4.2.1 was utilized to develop the meteorological fields used in the subsequent photochemical model simulations.

A. WRF Model Setup

The WRF modeling domain consisted of three nested Lambert projection grids of 36 km (D01), 12 km (D02), and 4 km (D03) uniform horizontal grid spacing as shown in Figure 6. The 4 km innermost domain has 427x427 grid points and spans 1748 km in the east-west and the north-south directions. All three domains utilized 30 vertical sigma layers with the lowest layer extending to 30 m above the surface (Table 10). The North America Regional Reanalysis (NARR) fields, enhanced with surface and upper-air observations, were used for initial and boundary conditions as well as Four Dimension Data Assimilation (FDDA) on the outermost (36 km) domain. The horizontal spatial resolution of the NARR data is 32 km. The major physics options for each domain are listed in Table 11, which include the Yon-Sei University (YSU) planetary boundary layer (PBL) scheme, Kain-Fritsch cumulus parameterization for the outer two domains, and 5-layer thermal diffusion land-surface option.

Figure 6. WRF modeling domains (D01 36 km; D02 12 km; and D03 4 km).

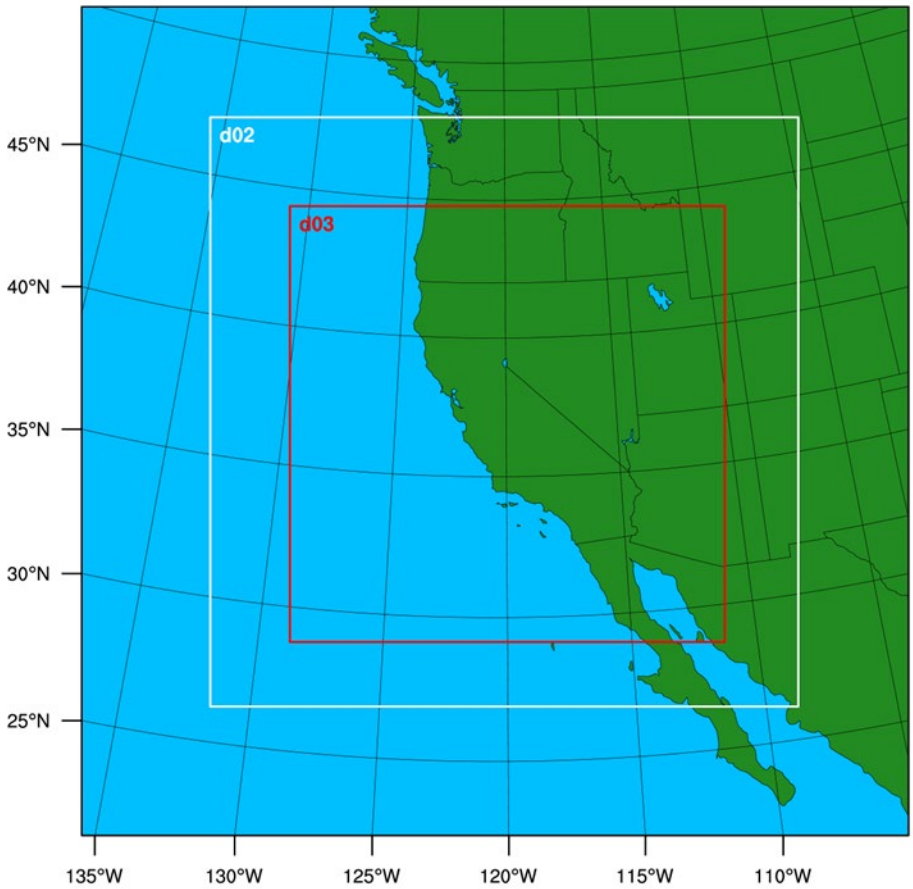

Table 10. WRF vertical layer structure.

Layer Number	Height (m)	Layer Thickness (m)	Layer Number	Height (m)	Layer Thickness (m)
30	16082	1192	15	2262	403
29	14890	1134	14	1859	334
28	13756	1081	13	1525	279
27	12675	1032	12	1246	233
26	11643	996	11	1013	194
25	10647	970	10	819	162
24	9677	959	9	657	135
23	8719	961	8	522	113
22	7757	978	7	409	94
21	6779	993	6	315	79
20	5786	967	5	236	66
19	4819	815	4	170	55
18	4004	685	3	115	46
17	3319	575	2	69	38
16	2744	482	1	31	31

To prevent any large deviations from the reanalysis data, analysis nudging was applied to the outermost domain (D01) above the planetary boundary layer (PBL) for moisture and above 2 km for wind and temperature. No nudging was used on the two inner domains to allow the model physics to work fully without externally imposed forcing. Boundary conditions on the outermost domain were updated every 6 hours, while WRF was reinitialized every 6 days with one day overlap, where the first day after being reinitialized was discarded as model spin-up. The Meteorology-Chemistry Interface

Processor (MCIP) version 5.3.3 was used to process the 4 km (D03) WRF output for use in the CTM simulations.

Table 11. WRF Physics options.

Physics Option	D01 (36 km)	D02 (12 km)	D03 (4 km)
Microphysics	WSM 6-class	WSM 6-class	WSM 6-class
Longwave Radiation	RRTM	RRTM	RRTM
Shortwave Radiation	Dudhia	Dudhia	Dudhia
Surface Layer	Revised MM5 Monin-Obukhov	Revised MM5 Monin-Obukhov	Revised MM5 Monin-Obukhov
Land Surface	5-layer Thermal Diffusion	5-layer Thermal Diffusion	5-layer Thermal Diffusion
Planetary Boundary Layer	YSU	YSU	YSU
Cumulus Parameterization	Kain-Fritsch Scheme	Kain-Fritsch Scheme	No

B. WRF Model Results and Evaluation

WRF simulated surface wind speed, temperature, and relative humidity from the 4 km domain were validated against hourly observations at 78 surface stations in the SJV. Observational data for the surface stations were obtained from CARB's archived meteorological database http://www.arb.ca.gov/aqmis2/aqmis2.php). Table 12 lists the observational stations and the parameters measured at each station, including wind speed and direction (wind), temperature (T) and relative humidity (RH). The location of each of these sites is shown in Figure 7. Quarterly and annual quantitative performance metrics for 2017 were used to compare hourly surface observations and modeled estimates: mean bias (MB), mean error (ME) and index of agreement (IOA) based on recommendations from Simon et al. (2012). A summary of these statistics by performance region is shown in Table 13 through Table 17. The performance regions cover roughly the Modesto, Fresno, Visalia, and Bakersfield regions, as well as one for the entire San Joaquin Valley (SJV), respectively. The region around Modesto includes

sites 5737, 2833, and 2080. The region surrounding Fresno encompasses sites 5741, 2449, 2013, and 2844. The region around Visalia includes sites 2032, 5386, and 3250, while the region covering Bakersfield includes sites 5287 and 3146 (note that no wind data available at these two sites for the 4th quarter in 2017). Model performance statistical metrics were calculated using all available data. All the sites in the valley are included in the SJV performance region (in addition to the sites mentioned above). The distribution of daily mean bias and mean error are shown in Figure 8 and Figure 9. Figure 10 and Figure 11 show observed vs. modeled scatter plots.

The wind speed biases were positive in each quarter of 2017 from a valley-wide perspective, as well as over the four performance regions. The wind speed mean biases are mostly less than 0.7 m/s in all performance regions. The annual temperature biases are within -1.5 K over the entire SJV and in three of the four performance regions (i.e., Modesto, Fresno and Visalia); whereas the annual temperature bias is -2.09 K in Bakersfield. Temperature biases show seasonal patterns in all performance regions, with higher biases during the second and third quarter of 2017 and lower biases during the first and fourth quarter. The higher temperature biases during spring and summer are likely related to the difficulty in accurately representing irrigation in the WRF model. Irrigation in SJV is most likely to occur during the spring and summer (i.e. the growing season) due to the fact that the maximum precipitation occurs in winter and the minimum precipitation occurs in summer. Simulated temperature is generally in good agreement with the observations in almost all regions with the index of agreement (IOA) above 0.90 (1.0 represents perfect agreement). Relative humidity biases are positive in all performance regions. The annual bias values range from 8.19% to 19.63%, with the largest bias occurring in Bakersfield. These results are comparable to other recent WRF modeling efforts in California investigating ozone formation in Central California (e.g., Hu et al., 2012) and modeling analysis for the CalNex and CARES field studies (e.g., Fast et al., 2012; Baker et al., 2013; Kelly et al., 2014; Angevine et al., 2012). Detailed hourly time-series of surface temperature, relative humidity, wind speed, and wind direction for SJV for each month of 2017 can be found in the supplementary material. Spatial distribution of 2017 quarterly mean bias and mean error of these parameters are also shown in the supplementary material. In addition, model simulated hourly precipitation are compared to observations. Stations with precipitation data are limited during this period, therefore, comparison results at Modesto, Fresno and Belridge are shown here to represent northern, central and southern part of SJV, respectively. Time series plots at these three sites for wetter months (i.e., January to March and November to December) are shown in the supplementary material. Model comparison to observations suggests that both the timing and amount of precipitation are simulated reasonably well by WRF over SJV.

Figure 7. Meteorological observation sites in San Joaquin Valley. The numbers correspond to the sites listed in Table 12.

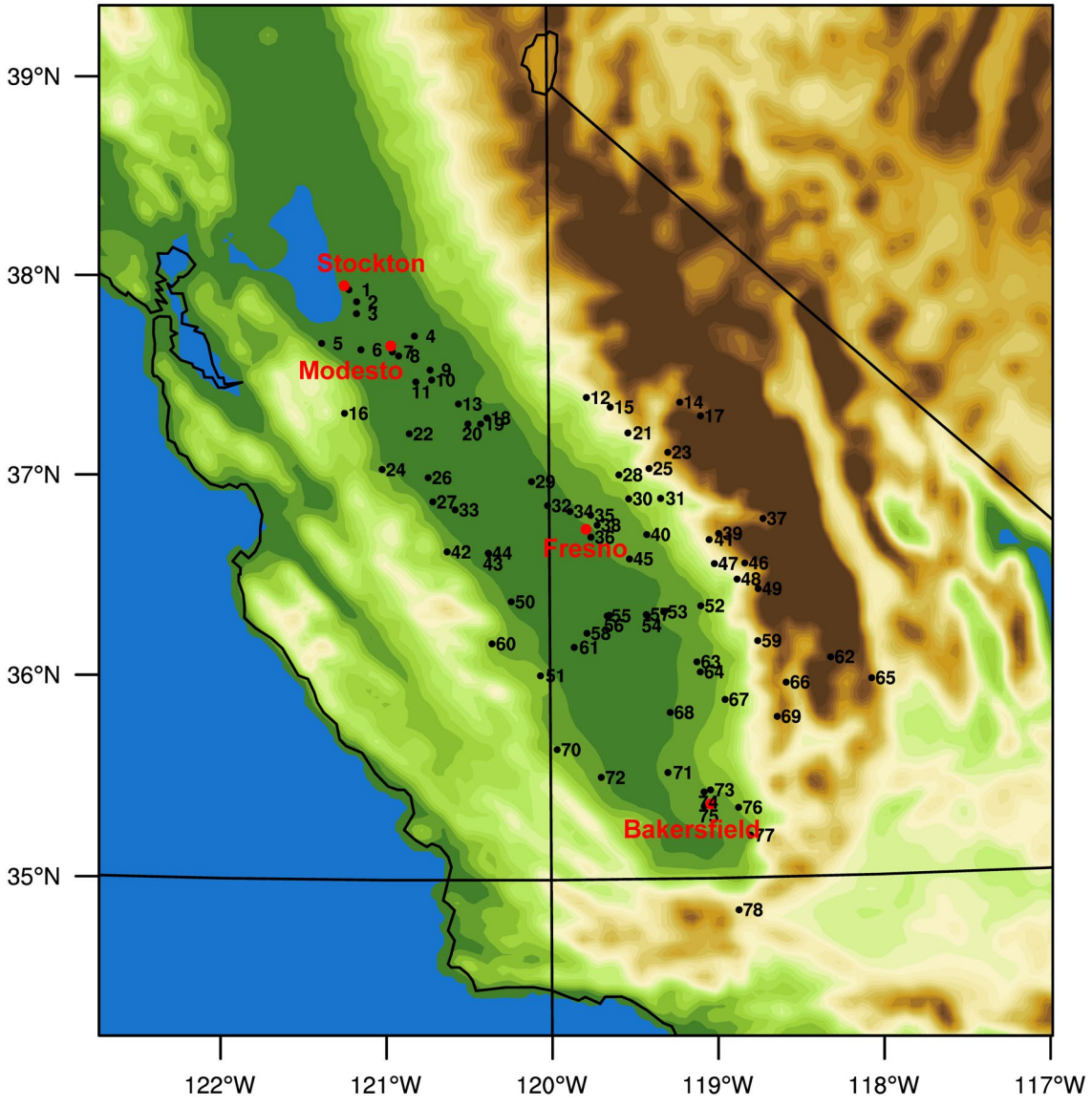

Table 12. Meteorological monitor location and parameter(s) measured. Sites are shown in Figure 7.

Site Number	Site ID	Site Name	Parameter(s) Measured
1	2094	Stockton-Hazelton Street	Wind, T, RH
2	5362	Stockton Metropolitan Airport	T, RH
3	5736	Manteca	Wind, T, RH
4	5831	Oakdale #2	Wind, T, RH
5	3696	Tracy-Airport	Wind, T
6	5737	Modesto #3	Wind, T, RH
7	2833	Modesto-14th Street	Wind, T, RH
8	2080	Modesto City - County Airport-Sham Field	T, RH
9	7233	Denair II	Wind, T, RH
10	3303	Rose Peak	Wind, T, RH
11	2996	Turlock-S Minaret Street	Wind, T
12	3344	Metcalf Gap	Wind, T, RH
13	2814	Merced-Castle Air Force Base	T, RH
14	3570	Mount Tom (FTS)	Wind, T, RH
15	3582	Batterson	Wind, T, RH
16	3526	Diablo Grande	Wind, T, RH
17	3510	High Sierra	Wind, T, RH
18	5793	Merced	Wind, T, RH
19	3022	Merced-S Coffee Avenue	Wind, T

Site Number	Site ID	Site Name	Parameter(s) Measured
20	5318	Merced Municipal Airport	T, RH
21	3455	North Fork	Wind, T, RH
22	5752	Kesterson	Wind, T, RH
23	3649	Shaver #2	Wind, T, RH
24	3307	Los Banos	Wind, T, RH
25	3638	Mountain Rest (FTS)	Wind, T, RH
26	5730	Los Banos #2	Wind, T, RH
27	5770	Panoche	Wind, T, RH
28	3522	Hurley 1	Wind, T, RH
29	5317	Madera Municipal Airport	T, RH
30	3346	Fancher Creek	Wind, T, RH
31	3535	Trimmer (FTS)	Wind, T, RH
32	3211	Madera-Pump Yard	Wind, T, RH
33	5711	Firebaugh - Telles	Wind, T, RH
34	2844	Fresno-Sierra Skypark #2	Wind, T
35	5741	Fresno State #2	Wind, T, RH
36	2013	Fresno-Drummond Street	Wind, T
37	3550	Cedar Grove	Wind, T, RH
38	2449	Fresno-Fresno Air Terminal	T, RH
39	3534	Park Ridge	Wind, T, RH
40	5787	Orange Cove	Wind, T, RH

Site Number	Site ID	Site Name	Parameter(s) Measured
41	3523	Pinehurst	Wind, T, RH
42	3309	Panoche Road	Wind, T, RH
43	3759	Tranquillity-32650 West Adams Avenue	Wind, T
44	5757	Westlands	Wind, T, RH
45	5723	Parlier #2	Wind, T, RH
46	3036	Sequoia Natl Park-Lower Kaweah	Wind, T, RH
47	3349	Shadequarter	Wind, T, RH
48	3484	Sequoia and Kings Canyon Natl Park	Wind, T, RH
49	3533	Wolverton	Wind, T, RH
50	5828	Five Points SW	Wind, T, RH
51	3330	Kettleman Hills	Wind, T, RH
52	5746	Lindcove	Wind, T, RH
53	2032	Visalia-N Church Street	Wind, T, RH
54	3250	Visalia-Airport	Wind, T, RH
55	3129	Hanford-S Irwin Street	Wind, T
56	5308	Hanford Municipal Airport	T, RH
57	5386	Visalia Municipal Airport	T, RH
58	3712	Santa Rosa Rancheria-17225 Jersey	Wind, T
59	3457	Oak Opening	Wind, T, RH
60	6028	Coalinga-CIMIS	Wind, T, RH

Site Number	Site ID	Site Name	Parameter(s) Measured
61	5715	Stratford #2	Wind, T, RH
62	3519	Blackrock	Wind, T, RH
63	5812	Porterville #3	Wind, T, RH
64	5351	Porterville Municipal Airport	T, RH
65	3543	Whittier Hills	Wind, T, RH
66	3554	Johnsondale	Wind, T, RH
67	3350	Fountain Springs	Wind, T, RH
68	5823	Delano #2	Wind, T, RH
69	3476	UHL	Wind, T, RH
70	5729	Blackwells Corner	Wind, T, RH
71	5709	Shafter - USDA	Wind, T, RH
72	5791	Belridge	Wind, T, RH
73	2772	Oildale-3311 Manor Street	Wind, T, RH
74	5287	Meadows Field Airport	T, RH
75	3146	Bakersfield-5558 California Avenue	Wind, T, RH
76	2312	Edison	Wind, T, RH
77	5771	Arvin-Edison	Wind, T, RH
78	5414	Lebec	Wind, T

Table 13. Hourly surface wind speed (m/s), temperature (K) and relative humidity statistics (%) in Modesto.

Variable	Quarter	Observed Mean	Modeled Mean	Mean Bias	Mean Error	IOA
Wind Speed	Q1	2.32	3.06	0.74	1.08	0.82
Wind Speed	Q2	2.64	3.33	0.68	1.17	1.00
Wind Speed	Q3	2.07	2.51	0.44	0.89	0.77
Wind Speed	Q4	1.91	2.41	0.50	0.97	1.00
Wind Speed	Annual	2.23	2.82	0.59	1.02	1.00
Temperature	Q1	284.79	283.87	-0.92	1.55	0.95
Temperature	Q2	293.28	291.51	-1.77	2.22	0.96
Temperature	Q3	298.08	296.70	-1.38	2.34	0.94
Temperature	Q4	285.48	286.21	0.74	2.43	1.00
Temperature	Annual	290.43	289.60	-0.83	2.14	0.99
Relative Humidity	Q1	76.84	79.45	2.62	7.85	0.91
Relative Humidity	Q2	55.15	63.64	8.49	12.10	0.85
Relative Humidity	Q3	50.07	63.91	13.85	14.37	0.79
Relative Humidity	Q4	68.87	76.56	7.69	9.98	0.89
Relative Humidity	Annual	62.67	70.86	8.19	11.09	0.88

Table 14. Hourly surface wind speed (m/s), temperature (K) and relative humidity (%) statistics in Fresno.

Variable	Quarter	Observed Mean	Modeled Mean	Mean Bias	Mean Error	IOA
Wind Speed	Q1	1.60	2.24	0.64	0.92	0.74
Wind Speed	Q2	1.92	2.67	0.75	0.98	0.70
Wind Speed	Q3	1.85	2.02	0.16	0.82	0.99
Wind Speed	Q4	1.36	1.56	0.20	0.73	0.99
Wind Speed	Annual	1.68	2.12	0.44	0.86	0.99
Temperature	Q1	284.95	284.17	-0.79	1.52	0.96
Temperature	Q2	294.42	292.55	-1.86	2.11	0.97
Temperature	Q3	300.64	298.55	-2.1	2.53	0.93
Temperature	Q4	286.26	286.42	0.15	1.74	0.97
Temperature	Annual	291.60	290.45	-1.15	1.98	0.98
Relative Humidity	Q1	75.53	78.28	2.75	9.36	0.88
Relative Humidity	Q2	50.14	64.42	14.27	16.27	0.79
Relative Humidity	Q3	41.72	63.42	21.70	21.90	0.68
Relative Humidity	Q4	64.44	77.08	12.63	14.40	0.92
Relative Humidity	Annual	57.88	70.77	12.89	15.52	0.86

Table 15. Hourly surface wind speed (m/s), temperature (K) and relative humidity (%) statistics in Visalia.

Variable	Quarter	Observed Mean	Modeled Mean	Mean Bias	Mean Error	IOA
Wind Speed	Q1	1.38	2.03	0.65	0.91	0.65
Wind Speed	Q2	1.45	2.23	0.79	0.98	0.60
Wind Speed	Q3	1.23	1.85	0.62	0.89	0.47
Wind Speed	Q4	1.35	1.64	0.29	0.84	0.99
Wind Speed	Annual	1.35	2.00	0.64	0.92	0.99
Temperature	Q1	285.07	284.23	-0.84	1.62	0.95
Temperature	Q2	294.76	292.23	-2.52	2.68	0.95
Temperature	Q3	300.34	298.23	-2.10	2.73	0.90
Temperature	Q4	285.93	286.23	0.29	2.50	0.99
Temperature	Annual	291.58	290.28	-1.30	2.39	0.99
Relative Humidity	Q1	77.74	81.43	3.69	9.90	0.82
Relative Humidity	Q2	53.07	72.79	19.71	20.33	0.71
Relative Humidity	Q3	49.73	73.41	23.68	23.69	0.64
Relative Humidity	Q4	65.92	82.94	17.02	17.52	0.73
Relative Humidity	Annual	61.55	77.64	16.09	17.90	0.74

Table 16. Hourly surface wind speed (m/s), temperature (K) and relative humidity (%) statistics in Bakersfield (No wind data available for the 4th quarter).

Variable	Quarter	Observed Mean	Modeled Mean	Mean Bias	Mean Error	IOA
Wind Speed	Q1	1.17	1.70	0.53	0.89	0.99
Wind Speed	Q2	1.55	2.04	0.49	0.88	0.71
Wind Speed	Q3	1.29	1.58	0.29	0.67	0.78
Wind Speed	Q4	--	--	--	--	--
Wind Speed	Annual	1.34	1.80	0.45	0.83	0.99
Temperature	Q1	286.07	285.07	-1.00	1.88	0.94
Temperature	Q2	296.23	293.31	-2.91	3.07	0.94
Temperature	Q3	302.75	299.28	-3.47	3.58	0.86
Temperature	Q4	288.22	287.27	-0.95	1.97	0.96
Temperature	Annual	293.35	291.26	-2.09	2.63	0.96
Relative Humidity	Q1	68.86	74.76	5.90	11.81	0.79
Relative Humidity	Q2	42.06	64.45	22.39	22.83	0.62
Relative Humidity	Q3	36.02	65.70	29.68	29.72	0.74
Relative Humidity	Q4	54.58	74.85	20.27	21.21	0.68
Relative Humidity	Annual	50.30	69.93	19.63	21.44	0.75

Table 17. Hourly surface wind speed (m/s), temperature (K) and relative humidity (%) statistics in the San Joaquin Valley.

Variable	Quarter	Observed Mean	Modeled Mean	Mean Bias	Mean Error	IOA
Wind Speed	Q1	1.98	2.60	0.61	0.66	0.84
Wind Speed	Q2	2.15	2.77	0.62	0.66	0.79
Wind Speed	Q3	1.84	2.29	0.44	0.47	0.80
Wind Speed	Q4	1.53	1.97	0.45	0.50	0.81
Wind Speed	Annual	1.87	2.40	0.53	0.57	0.83
Temperature	Q1	283.16	282.63	-0.53	1.12	0.98
Temperature	Q2	292.39	290.37	-2.02	2.16	0.96
Temperature	Q3	298.35	296.01	-2.34	2.78	0.91
Temperature	Q4	285.33	285.35	0.02	1.91	0.96
Temperature	Annual	289.84	288.62	-1.22	2.00	0.97
Relative Humidity	Q1	76.57	73.82	-2.74	6.67	0.91
Relative Humidity	Q2	53.70	64.07	10.37	12.01	0.82
Relative Humidity	Q3	44.20	64.44	20.23	20.27	0.64
Relative Humidity	Q4	56.88	66.97	10.09	11.32	0.80
Relative Humidity	Annual	57.75	67.30	9.55	12.6	0.81

Figure 8. Distribution of model daily mean bias for Modesto, Fresno, Visalia, Bakersfield and SJV. Results are shown for wind speed (top), temperature (middle), and Relative Humidity (bottom).

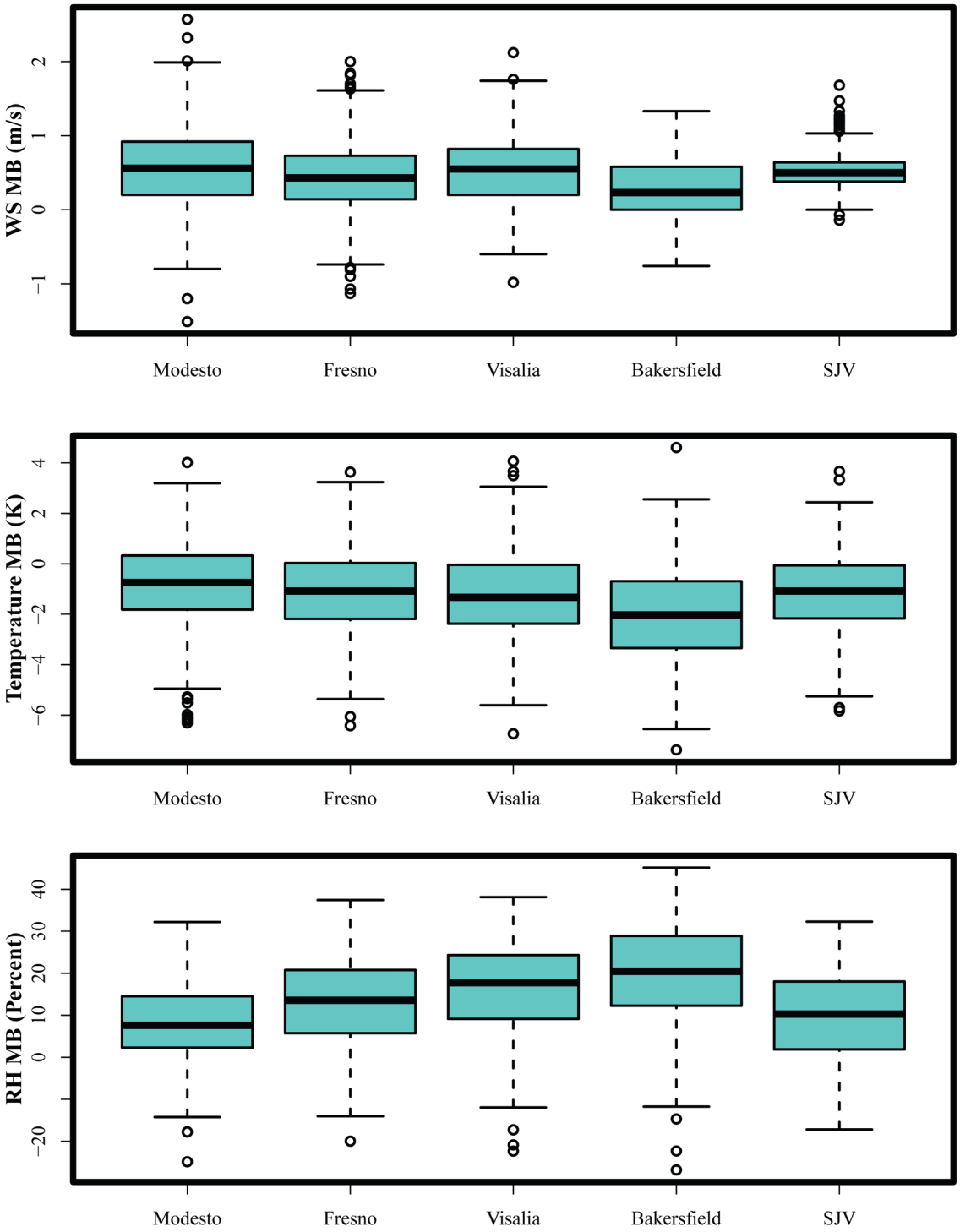

Figure 9. Distribution of model daily mean error for Modesto, Fresno, Visalia, Bakersfield and SJV. Results are shown for wind speed (top), temperature (middle), and Relative Humidity (bottom)

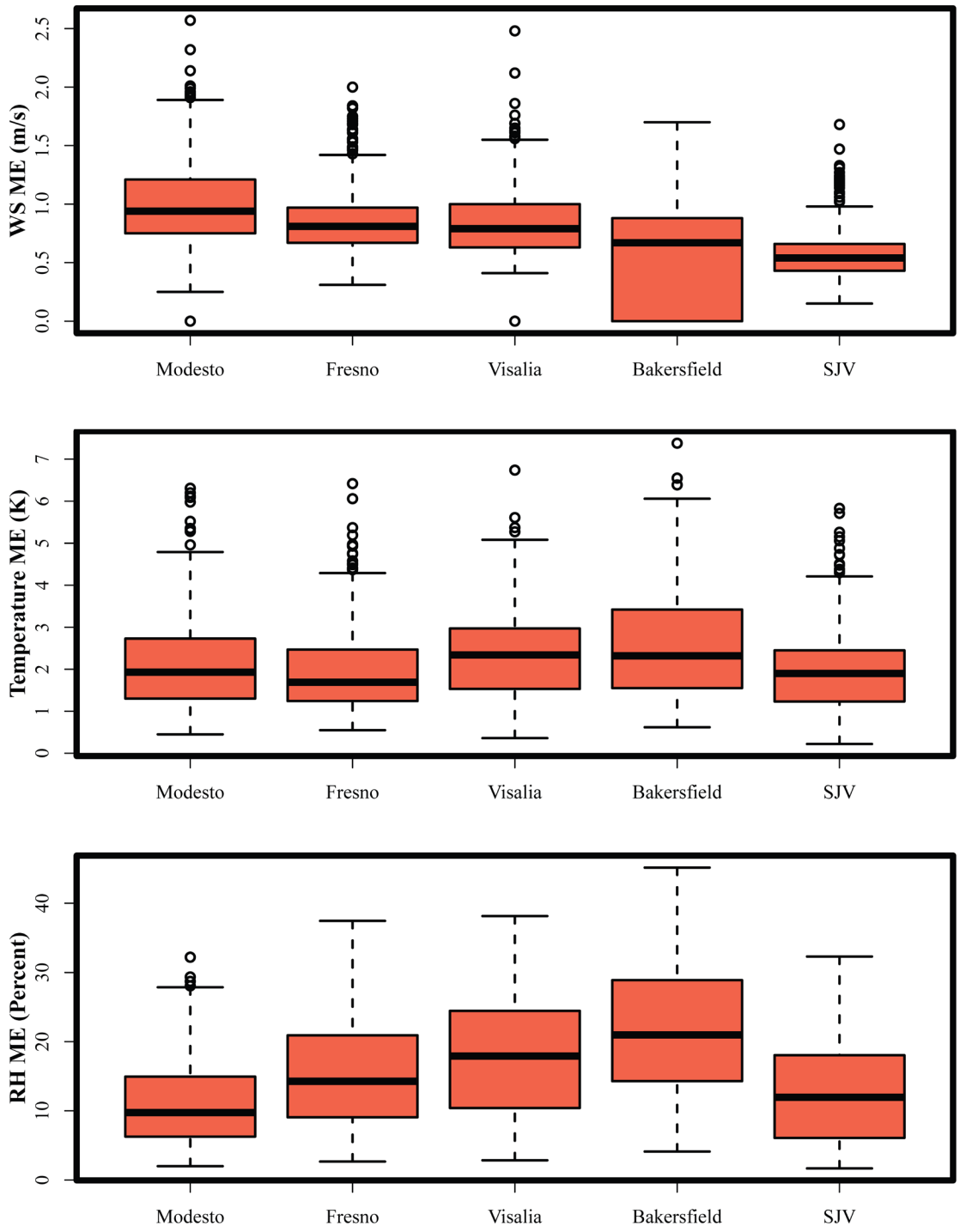

Figure 10. Comparison of modeled and observed hourly wind speed (left column), 2-meter temperature (middle column), and relative humidity (right column). Results for Modesto are shown in the top row, Fresno in the middle row, and Visalia in the bottom row.

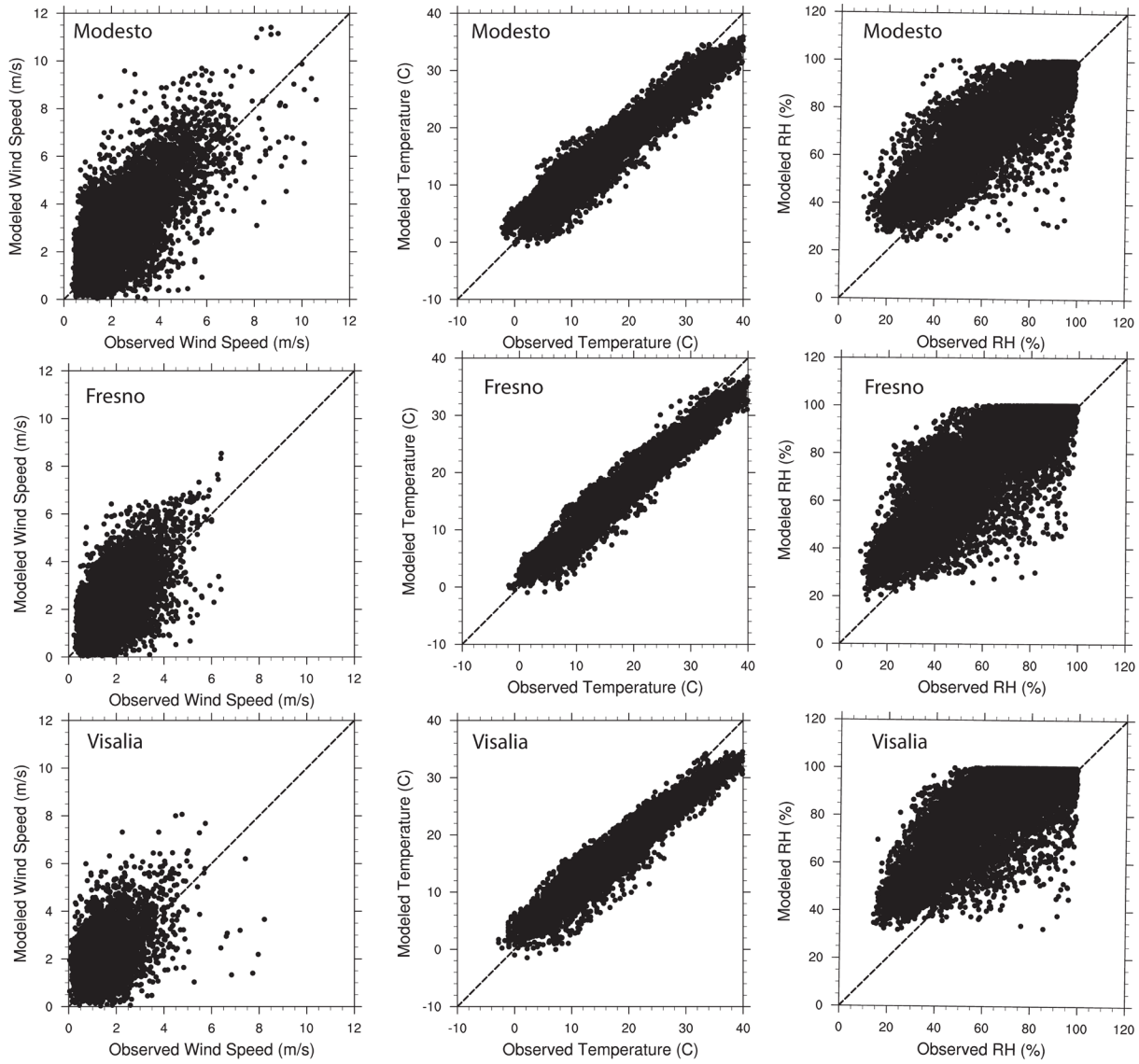

Figure 11. Comparison of modeled and observed hourly wind speed (left column), 2-meter temperature (middle column), and relative humidity (right column). Results for Bakersfield are shown in the top row and SJV in the bottom row.

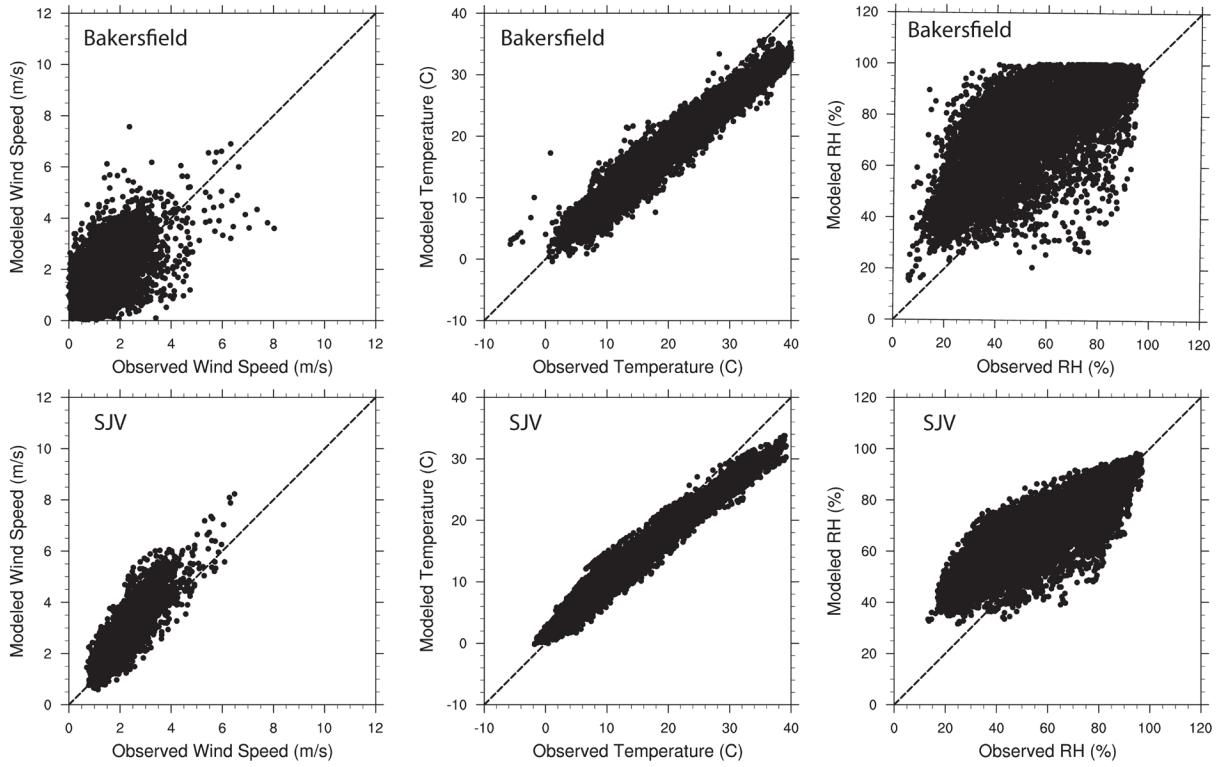

C. Phenomenological Evaluation

Conducting a detailed phenomenological evaluation for all modeled days can be resource intensive given that the entire year was modeled. However, some insight and confidence that the model is able to reproduce the meteorological conditions leading to elevated particulate matter can be gained by investigating the meteorological conditions during a period of peak PM within the Valley in more detail. The highest $PM_{2.5}$-conducive meteorological conditions in the Valley occurred around December 28, 2017. Surface weather analysis shows that on December 28, the western US was under a typical Great Basin high pressure system. In the 500 hPa map (not shown), a strong high pressure system centered over the Pacific off the coast of California. The ridge associated with this high pressure system extends from Northern California along the west Pacific coast all the way to Alaska. As shown in Figure 12 through Figure 14, the winds are mainly offshore along the northern California coast. Under this type of weather system, conditions in SJV are driven by diurnal cycles of the local winds. Figure 12 and Figure 13 show that at 13:00 PST and 14:00 PST, December 28, the upslope flows along the eastern side of the Coastal Ranges and the western side of the Sierras, lead to a weak northwesterly flow on the floor of the valley. The downslope winds form at nighttime (Figure 14), which converge towards the valley and the winds in the center of the valley floor turn southeasterly. At the southern end of the valley, an eddy-like pattern occurs during nighttime due to the interaction of the katabatic flows. The surface wind distributions of the modeled and observed winds indicate the model was able to capture many of the important features of the meteorological fields in the SJV.

Figure 12. Surface wind field at 13:00 PST December 28, 2017.

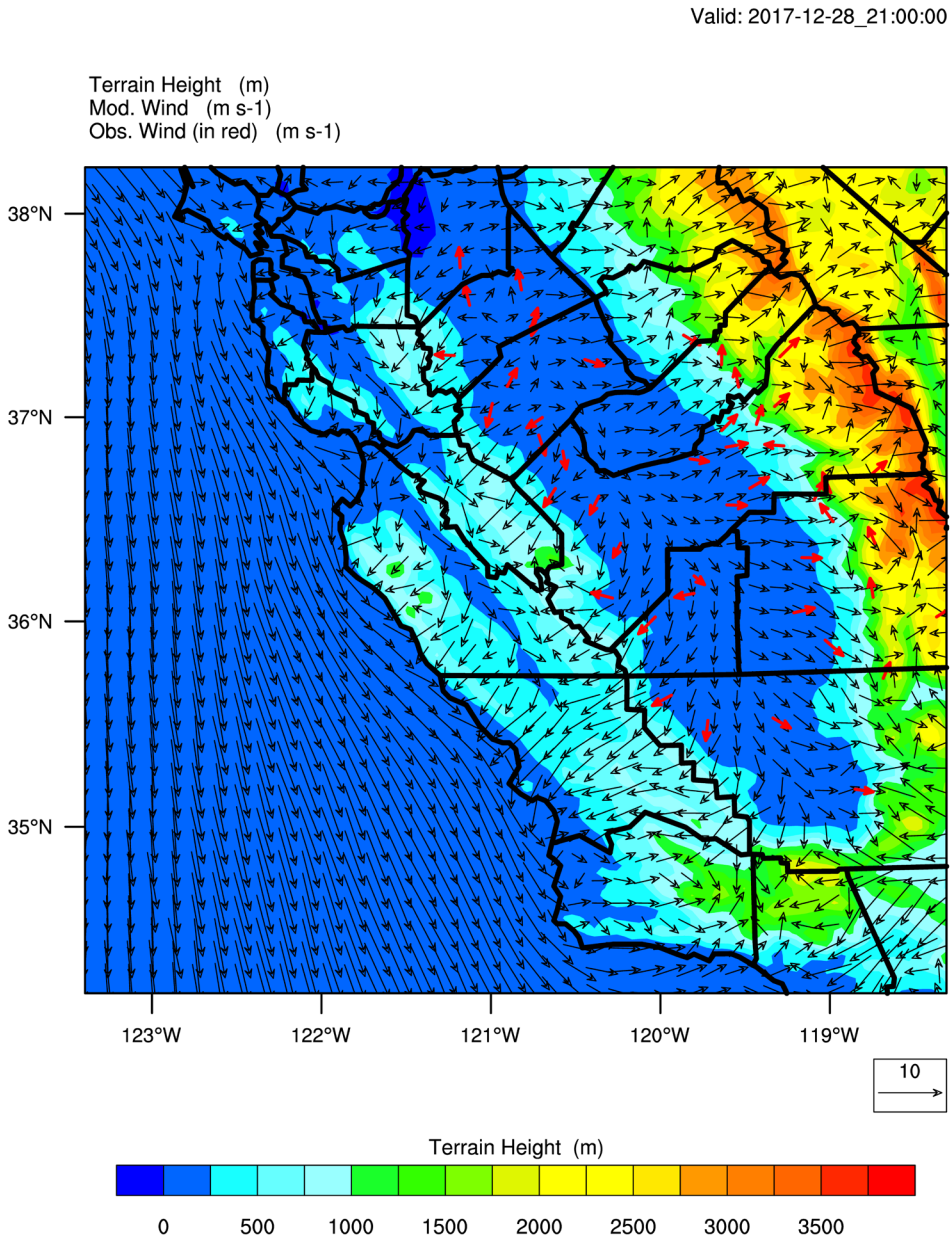

Figure 13. Surface wind field at 14:00 PST December 28, 2017.

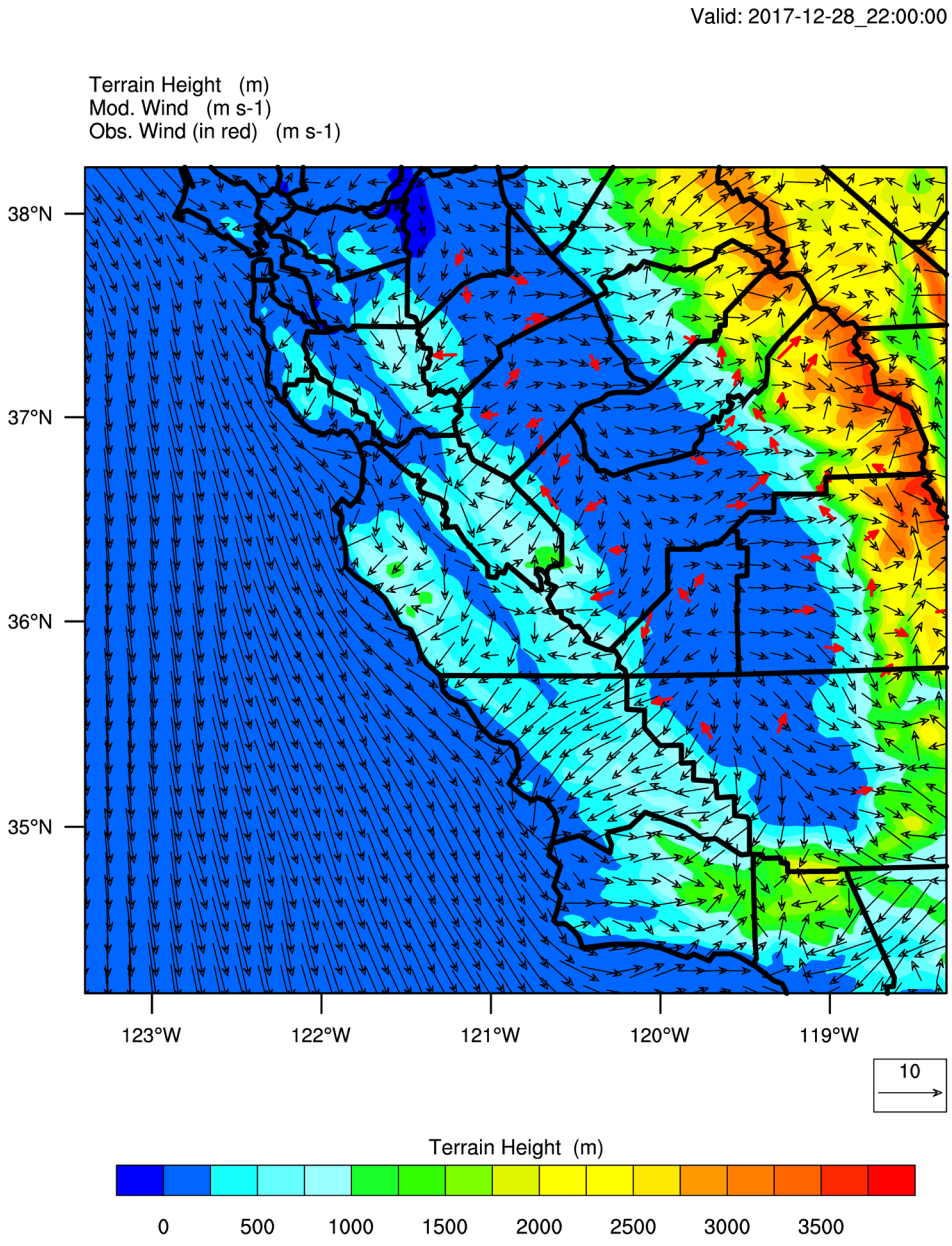

Figure 14. Surface wind field at 20:00 PST December 28, 2017.

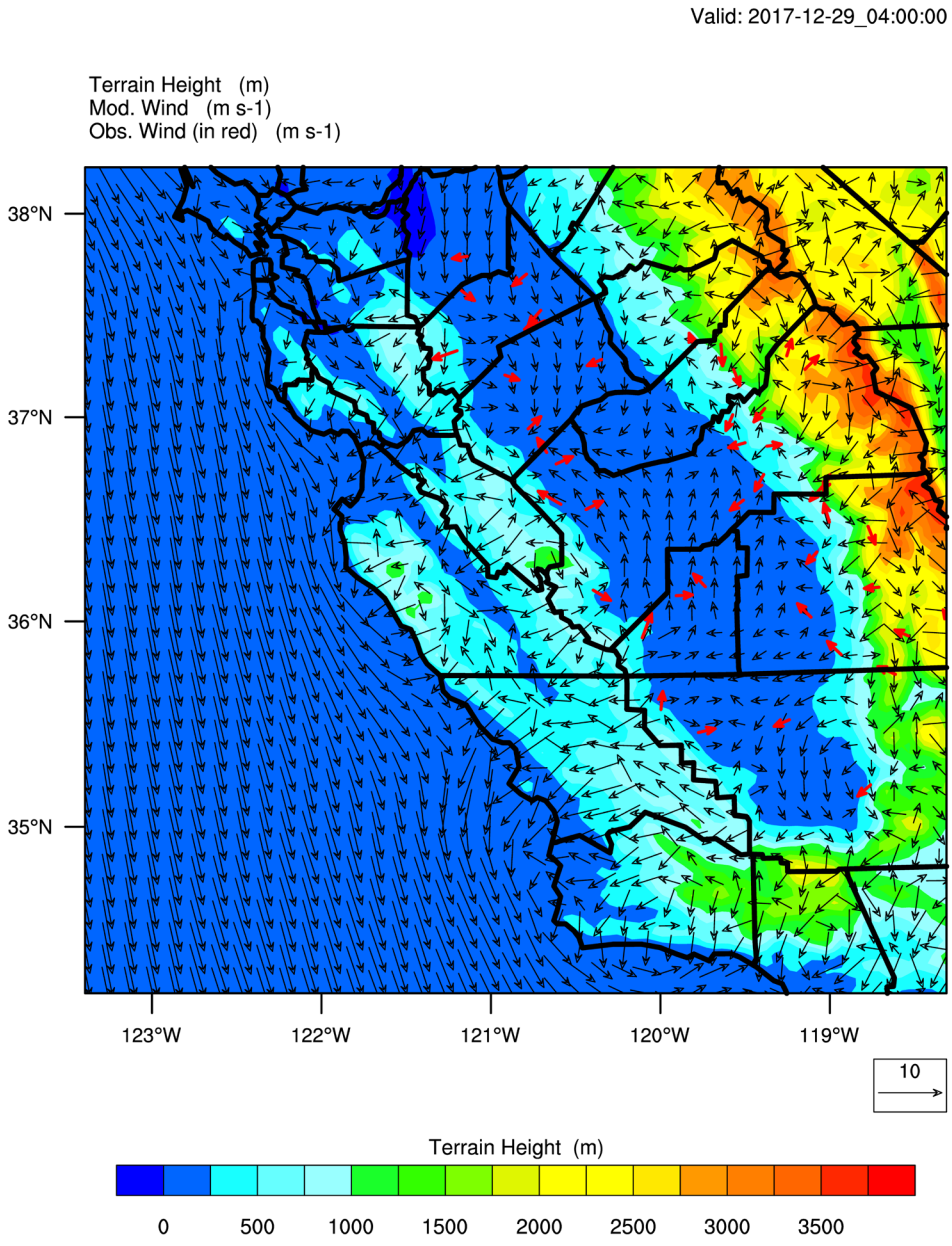

IV. Emissions

The anthropogenic emissions inventory used in this modeling was based on the California Emissions Projection Analysis Model (CEPAM2019 v1.04). For a detailed description of the emissions inventory, updates to the inventory, and how it was processed from the planning totals to a gridded inventory for modeling, see the Modeling Emissions Inventory Appendix.

Table 18 summarizes the 2017, 2030 baseline and 2030 attainment anthropogenic emissions inventories for primary $PM_{2.5}$ and the four $PM_{2.5}$ precursors in the SJV, respectively. These emission totals are based on the model-ready emission inventory and are inherently different from the planning emission inventory because the model-ready inventory considers additional factors such as weekday/weekend differences in on-road mobile emissions, day-to-day changes in residential wood burning activity, and the effects of meteorology on ammonia emissions.

From 2017 to the 2030 attainment inventory, anthropogenic emissions in the SJV will drop approximately 64%, 12%, 19%, 2%, and 2% for NO_x, ROG, primary $PM_{2.5}$, sulfur oxides (SO_x), and ammonia (NH_3), respectively. Among these five precursors, anthropogenic NO_x emissions show the largest relative reduction, dropping from 216 tons/day in 2017 to 77 tons/day in 2030. Anthropogenic $PM_{2.5}$ emissions will drop from 62 tons/day to 50 tons/day, reflecting a 19% reduction from 2017 to 2030.

Additional emission reductions to achieve attainment in 2030 compared to 2030 baseline emissions are summarized in Table 19 for both NO_x and $PM_{2.5}$. As previously stated, the amount of reductions in Table 19 are based on the modeling inventory and therefore can appear different from the reductions based on the planning inventory. A description of these emission control measures (i.e., state SIP strategy for on-road and off-road mobile sources, extending RWC curtailment program through the end of March, and agricultural incentives) can be found in the SIP.

Table 18. SJV Model-Ready Annual Emissions for 2017, 2030 (baseline), and 2030 (attainment).*

	Source Category	Stationary	Area	On-road Mobile	Other Mobile	Total	Change from 2017 to 2030
2017 (ton/day)	NOx	22.9	12.0	95.3	86.0	216.2	
	ROG	89.0	159.9	27.7	42.4	319	
	PM2.5	7.9	44.9	2.6	6.1	61.5	
	SOx	5.1	0.3	0.6	0.2	6.2	
	NH_3	13.0	292.9	4.6	0.	310.5	
2030 baseline (ton/day)	NOx	18.5	6.0	20.3	53.3	98.1	-55%
	ROG	91.6	153.3	12.9	26.9	284.7	-11%
	PM2.5	6.8	38.2	1.4	4.1	50.5	-18%
	SOx	5.1	0.3	0.5	0.3	6.1	-2%
	NH_3	14.2	284.3	6.7	0.1	305.2	-2%
2030 attainment (ton/day)	NOx	18.1	5.3	16.8	37.2	77.4	-64%
	ROG	91.6	153.1	12.7	23.6	281.0	-12%
	PM2.5	6.8	38.0	1.3	3.5	49.6	-19%
	SOx	5.1	0.3	0.5	0.3	6.1	-2%
	NH_3	14.2	284.3	6.3	0.1	304.8	-2%

*: Note: emissions here are based on the model-ready inventory, which considers additional factors such as weekday/weekend difference in on-road mobile emissions. Therefore, emission values here may appear different from the planning inventory.

Table 19. Additional NOx and $PM_{2.5}$ emission reductions (tons/day) implemented in the 2030 attainment inventories.*

Emission control measures	NOx (tpd)	$PM_{2.5}$ (tpd)
State SIP strategy	17.83	0.66
Agricultural incentives (FARMER Program)	3.00	0.18
Extending district's RWC curtailment program through March 31	0.02	0.14

*: Note: emission reductions here are based on the model-ready inventory and can be different from reductions based on planning inventory presented in other documents.

Biogenic emissions were generated using the Model of Emissions of Gases and Aerosols from Nature (MEGAN3.0) biogenics emissions model (https://bai.ess.uci.edu/megan). MEGAN3.0 incorporates a new pre-processor (MEGAN-EFP) for estimating biogenic emission factors based on available landcover and emissions data. The MEGAN3.0 default datasets for plant growth form, ecotype, and emissions were utilized. Leaf Area Index (LAI) for non-urban grid cells was based on the 8-day 500 m resolution MODIS Terra/AQUA combined product (MCD15A2H) for 2018 (https://earthdata.nasa.gov/). The LAI data was converted to LAIv, which represents the LAI for the vegetated fraction within each grid cell, by dividing the gridded MODIS LAI values by the Maximum Green Vegetation Fraction for each grid cell (https://climate.arizona.edu/data/LandCover/MGVF/Average.tif.zip). The MODIS LAI product does not provide information on LAI in urban regions, so urban LAIv was estimated from the US Forest Service's Forest Inventory and Analysis urban tree plot data, processed through the i-Tree v6 software (https://www.itreetools.org/tools/i-tree-eco). Peak summertime urban LAIv for SJV was estimated to be 5.0, and this peak value was adjusted for each 8-day MODIS period based on the relative change in non-urban MODIS LAI across the state. Hourly meteorology was provided by the 4 km WRF simulation described above, and all stress factor adjustments were turned off.

Monthly biogenic ROG totals for 2017 within the Valley are shown in Figure 15 (note that the same biogenic emissions were used in 2017 and 2030 modeling). Biogenic ROG emissions are highest in the summer at over 800 tons/day in July when temperature, insolation, and leaf area are generally at their peak. In addition to biogenic ROG emissions, the MEGAN model also estimates NOx emissions from soils using the Yienger and Levy scheme (Yienger and Levy, 1995), which accounts for natural emissions from soils as well as enhanced emissions from managed crop lands. Figure 16 shows the monthly average soil NOx emissions for 2017 from MEGAN. Soil NOx emissions are highest during summer months, where the emissions peaked at 33 tpd in July.

Figure 15. Monthly average biogenic ROG emissions for 2017.

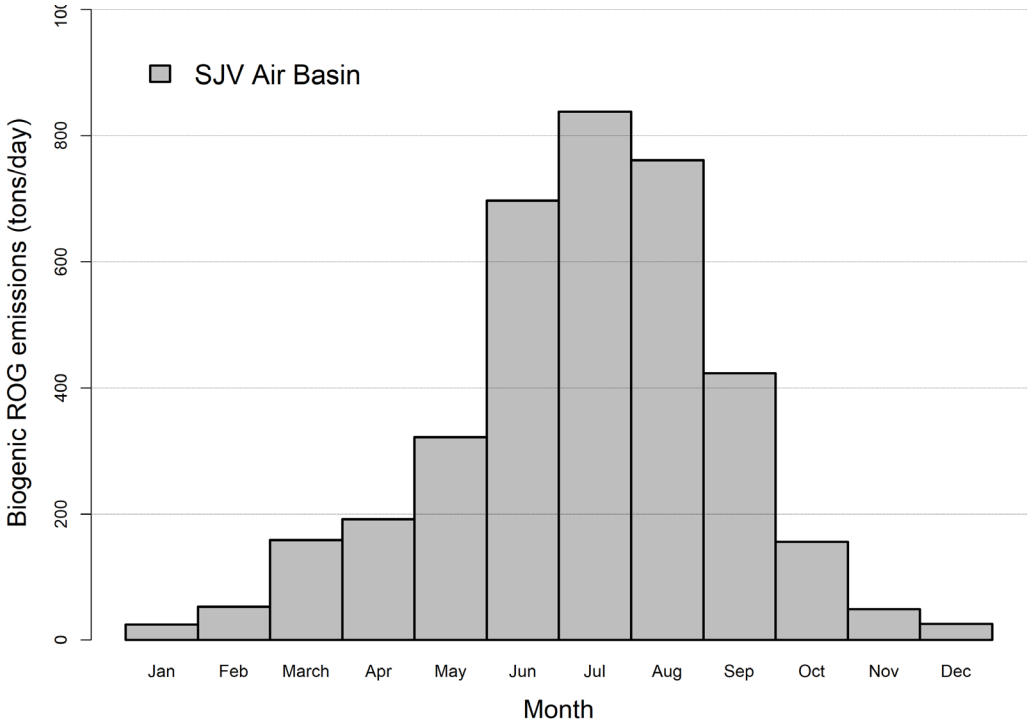

Figure 16. Monthly average soil NOx emissions for 2017.

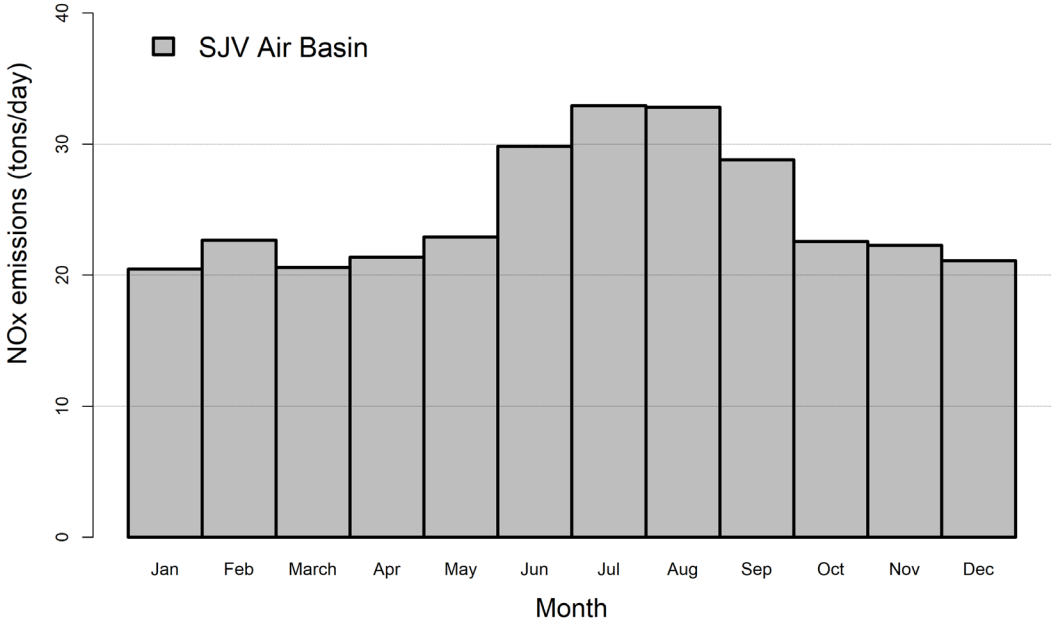

V. $PM_{2.5}$ Modeling

A. CMAQ Model Setup

Figure 17 shows the CMAQ modeling domains used in this work. The larger domain covering all of California has a horizontal grid resolution of 12 km with 107 x 97 lateral grid cells for each vertical layer and extends from the Pacific Ocean in the west to Eastern Nevada in the east and runs from the U.S.-Mexico border in the south to the California-Oregon border in the north. The nested domain covering the SJV region has a finer scale 4 km grid resolution and includes 192 x 192 lateral grid cells. Both the 12 km and 4 km domains are based on a Lambert Conformal Conic projection with reference longitude at – 120.5ºN and 60ºN, which is consistent with the WRF domain settings. In addition, there are 30 vertical layers for CMAQ, consistent with the WRF model, which extends from the surface to 100 mb such that a majority of the vertical layers fall within the planetary boundary layer.

The CMAQ model version 5.3.3 (https://github.com/USEPA/CMAQ/releases/tag/CMAQv5.3.3_17Aug2021) was used for all air quality model simulations. CMAQ is the U.S. EPA's open-source regional air quality model, which is widely used in the regulatory and scientific communities and represents the current state-of-the-science. CMAQ has been utilized for studying ozone and $PM_{2.5}$ formation in California for over a decade (e.g., Cai et al., 2016, 2019; Jin et al., 2008, 2010; Kelly et al., 2010, 2014; Livingstone et al., 2009; Pun et al., 2009; Tonse et al., 2008; Vijayaraghavan et al., 2006; Zhang et al., 2010), and has been the primary CTM used in California SIPs since 2008 (SJV, 2008), having been used in over a dozen ozone and $PM_{2.5}$ SIPs (Eastern Kern, 2017, 2023; Imperial, 2017, 2018; Sacramento, 2017, 2023; SJV, 2012, 2013, 2016a,b, 2018, 2022; South Coast, 2012, 2016; Ventura, 2016; Western Mojave, 2016; Western Nevada, 2018).

The SAPRC07tic chemical mechanism (Carter, 2010a,b) was chosen to represent the gas-phase photochemistry in the atmosphere, along with the aero6 aerosol module for simulating aerosol dynamics and chemistry. Photolysis rates were calculated in-line to better represent changes in photolysis rates due to meteorological conditions and gaseous and particulate pollutant levels in the atmosphere. Other configurations are shown in Table 20. The same configuration was used for all simulations.

Annual simulations were conducted on a simultaneous month-by-month basis, rather than one single continuous simulation. For each month, the CMAQ simulations included a seven-day spin-up period (i.e., the last seven days of the previous month) for the outer 12 km domain, where initial conditions were set to the default CMAQ initial conditions. These outer domain simulations were used to provide lateral boundary conditions for the inner 4 km simulation, which also utilized a seven-day spin-up period.

Figure 17. CMAQ modeling domains utilized in the modeling assessment.

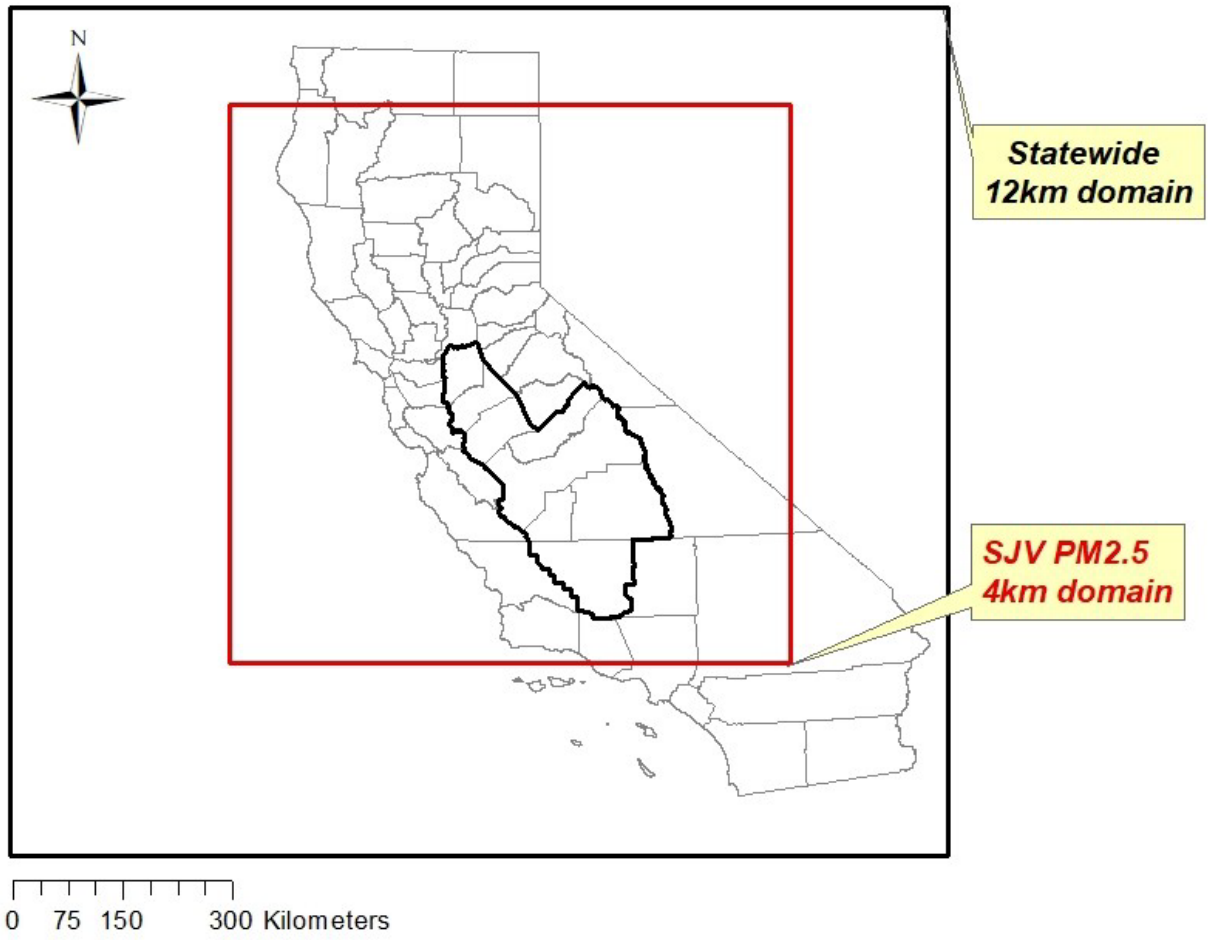

Chemical boundary conditions for the outer 12 km domain were extracted from the Goddard Earth Observing System (GEOS)-Chem model (https://geoschem.github.io/overview.html). The GEOS-Chem model was run internally for the year 2017 and output from GEOS-Chem was mapped to CMAQ model species using U.S. EPA's air quality model boundary condition tool available at https://github.com/barronh/aqmbc/. The same GEOS-Chem derived BCs for the 12 km outer domain were used in all simulations.

Table 20. CMAQ configuration and settings.

Process	Scheme
Horizontal advection	WRF-based scheme for mass-conserving advection
Vertical advection	WRF-based scheme for mass-conserving advection
Horizontal diffusion	Multi-scale
Vertical diffusion	ACM2 (Asymmetric Convective Model version 2)
Gas-phase chemical mechanism	SAPRC-07 gas-phase mechanism version “tic” with extended isoprene chemistry
Chemical solver	EBI (Euler Backward Iterative solver)
Aerosol module	Aero7 (the seventh-generation CMAQ aerosol mechanism)
Cloud module	ACM_AE7 (ACM cloud processor that uses the ACM methodology to compute convective mixing with heterogeneous chemistry for AERO7)
Photolysis rate	phot_inline (calculate photolysis rates in-line using simulated aerosols and ozone concentrations)

B. CMAQ Model Evaluation

CMAQ model performance was evaluated for $PM_{2.5}$ mass, individual $PM_{2.5}$ chemical species, as well as a number of gas-phase species based on observations from an extensive network of monitors in the SJV.

Time series of observed and modeled $PM_{2.5}$ chemical species based on $PM_{2.5}$ speciation measurements are shown in the supplemental material (Figures S24-27 of the supplemental materials for Bakersfield, Fresno, Modesto, and Visalia, respectively). $PM_{2.5}$ species are measured every 3 or 6 days at these sites. Observed $PM_{2.5}$ concentrations are higher in winter months and are much lower in summer months. During winter months, $PM_{2.5}$ in the SJV is dominated by ammonium nitrate and directly emitted OC. The CMAQ model was able to reasonably reproduce these key characteristics of $PM_{2.5}$ pollution in the SJV, including successfully capturing many elevated wintertime ammonium nitrate events, which is key for accurately simulating both peak wintertime $PM_{2.5}$ as well as annual average $PM_{2.5}$ in the SJV.

Table 21 to Table 24 summarize the key model performance metrics for major $PM_{2.5}$ chemical species at the four speciation sites. Model performance was evaluated on a quarterly basis for each species at each monitor. Average observations and modeled values, mean bias, mean error, mean fractional bias (MFB), and mean fractional error (MFE) are given for individual $PM_{2.5}$ species at these four sites. In general, model performance was similar at different monitors. Modeling somewhat over predicted $PM_{2.5}$ concentrations for quarter one, but slightly under predicted $PM_{2.5}$ concentrations for other quarters. Boylan and Russell (2006) proposed two criteria for model performance evaluation: Model performance goals are considered as the level of accuracy that is close to the best a model can be expected to achieve, while model performance criteria are considered as the level of accuracy that is acceptable for modeling applications. For more abundant species (e.g., concentrations ≥ 3 $\mu g/m^3$), model performance criteria are met when MFE ≤ 75% and MFB ≤ ±60%; model performance goals are met when MFE ≤ 50% and MFB ≤ ± 30%. For less abundant species, the performance criteria and goals are less stringent. A graphical representation of the quarterly MFB and MFE values in Tables 21-24 is shown in Figure 18 for each site, along with suggested model performance goals and criteria (green and red lines, respectively) from Boylan and Russell (2006). Based on these metrics, the current CMAQ modelling system met the model performance criteria and in many instances exceeded model performance goals.

Table 21. Quarterly $PM_{2.5}$ model performance based on $PM_{2.5}$ speciation measurement at Fresno - Garland.

Quarter	Species	# of Obs.	Avg. Obs. ($\mu g/m^3$)	Avg. Mod. ($\mu g/m^3$)	Mean bias ($\mu g/m^3$)	Mean error ($\mu g/m^3$)	MFB	MFE
1	$PM_{2.5}$	28	9.6	17.0	7.4	8.3	0.55	0.67
1	Ammonium	24	0.6	1.2	0.6	0.7	0.95	1.03
1	Nitrate	28	2.0	3.5	1.5	1.9	0.35	0.62
1	Sulfate	28	0.6	0.7	0.1	0.4	0.38	0.64
1	OC	28	2.7	5.4	2.8	3.0	0.58	0.70
1	EC	28	0.5	1.7	1.2	1.2	1.05	1.05
2	$PM_{2.5}$	31	7.2	7.2	0.0	2.2	-0.06	0.30
2	Ammonium	29	0.2	0.2	0.0	0.2	0.08	0.82
2	Nitrate	30	0.7	0.9	0.2	0.4	0.09	0.46
2	Sulfate	30	1.0	0.6	-0.4	0.4	-0.38	0.50

Quarter	Species	# of Obs.	Avg. Obs. (µg/m^3)	Avg. Mod. (µg/m^3)	Mean bias (µg/m^3)	Mean error (µg/m^3)	MFB	MFE
2	OC	30	2.1	1.7	-0.3	0.9	-0.28	0.46
2	EC	30	0.3	0.5	0.2	0.3	0.51	0.60
3	$PM_{2.5}$	30	12.1	10.7	-1.4	4.1	-0.20	0.37
3	Ammonium	30	0.3	0.2	-0.1	0.2	-0.39	0.97
3	Nitrate	30	0.6	0.8	0.1	0.5	-0.07	0.62
3	Sulfate	30	1.1	0.8	-0.3	0.4	-0.31	0.45
3	OC	30	3.9	3.1	-0.7	1.5	-0.35	0.52
3	EC	30	0.5	0.5	0.1	0.2	0.06	0.27
4	$PM_{2.5}$	31	29.3	27.0	-2.3	8.9	-0.01	0.36
4	Ammonium	30	2.6	2.3	-0.2	1.1	0.41	0.75
4	Nitrate	30	8.3	8.1	-0.2	2.9	0.21	0.52
4	Sulfate	30	0.9	1.1	0.1	0.4	0.16	0.44
4	OC	30	6.2	5.7	-0.5	2.1	-0.15	0.39
4	EC	30	1.6	1.8	0.2	0.6	0.04	0.39

Table 22. Quarterly $PM_{2.5}$ model performance based on $PM_{2.5}$ speciation measurement at Visalia.

Quarter	Species	# of Obs.	Avg. Obs. (µg/m^3)	Avg. Mod. (µg/m^3)	Mean bias (µg/m^3)	Mean error (µg/m^3)	MFB	MFE
1	$PM_{2.5}$	9	11.3	17.0	5.7	6.8	0.31	0.47
1	Ammonium	15	1.1	1.4	0.3	0.6	0.30	0.63

Quarter	Species	# of Obs.	Avg. Obs. ($\mu g/m^3$)	Avg. Mod. ($\mu g/m^3$)	Mean bias ($\mu g/m^3$)	Mean error ($\mu g/m^3$)	MFB	MFE
1	Nitrate	15	3.6	4.9	1.2	2.3	0.06	0.67
1	Sulfate	15	0.9	0.5	-0.5	0.5	-0.55	0.63
1	OC	15	3.3	3.5	0.1	1.2	-0.11	0.41
1	EC	15	0.5	1.1	0.6	0.7	0.59	0.74
2	$PM_{2.5}$	14	7.7	6.8	-1.0	1.7	-0.13	0.25
2	Ammonium	16	0.6	0.3	-0.3	0.3	-0.71	0.77
2	Nitrate	16	1.4	1.2	-0.2	0.5	-0.24	0.48
2	Sulfate	16	1.3	0.5	-0.8	0.8	-0.73	0.77
2	OC	16	2.3	1.1	-1.2	1.2	-0.70	0.70
2	EC	16	0.3	0.3	0.0	0.1	0.18	0.30
3	$PM_{2.5}$	14	15.2	13.5	-1.7	5.0	-0.19	0.37
3	Ammonium	16	0.8	0.4	-0.3	0.5	-0.74	0.92
3	Nitrate	16	1.6	1.6	0.0	1.1	-0.25	0.62
3	Sulfate	16	1.5	0.7	-0.8	0.8	-0.67	0.70
3	OC	16	4.8	3.2	-1.5	1.7	-0.46	0.51
3	EC	16	0.5	0.6	0.0	0.2	-0.02	0.30
4	$PM_{2.5}$	15	24.5	23.8	-0.7	7.1	0.04	0.37
4	Ammonium	14	3.1	2.7	-0.4	0.9	0.06	0.52
4	Nitrate	14	9.8	9.6	-0.2	2.3	0.14	0.52
4	Sulfate	14	1.1	0.7	-0.4	0.5	-0.34	0.45

Quarter	Species	# of Obs.	Avg. Obs. (µg/m^3)	Avg. Mod. (µg/m^3)	Mean bias (µg/m^3)	Mean error (µg/m^3)	MFB	MFE
4	OC	15	5.9	3.8	-2.2	2.2	-0.43	0.46
4	EC	15	1.1	1.2	0.1	0.3	0.06	0.34

Table 23. Quarterly $PM_{2.5}$ model performance based on $PM_{2.5}$ speciation measurement at Bakersfield.

Quarter	Species	# of Obs.	Avg. Obs. (µg/m^3)	Avg. Mod. (µg/m^3)	Mean bias (µg/m^3)	Mean error (µg/m^3)	MFB	MFE
1	$PM_{2.5}$	22	11.8	16.5	4.7	5.8	0.48	0.53
1	Ammonium	24	1.2	1.2	0.0	0.4	0.46	0.73
1	Nitrate	27	3.7	3.7	0.0	0.9	-0.05	0.33
1	Sulfate	27	0.9	0.6	-0.2	0.5	0.02	0.62
1	OC	24	3.0	5.4	2.5	2.5	0.59	0.61
1	EC	24	0.7	1.7	1.0	1.0	0.91	0.91
2	$PM_{2.5}$	29	8.6	7.0	-1.6	2.6	-0.22	0.36
2	Ammonium	28	0.4	0.2	-0.2	0.2	-0.32	0.80
2	Nitrate	29	0.9	0.8	-0.1	0.4	-0.13	0.58
2	Sulfate	29	1.1	0.6	-0.5	0.6	-0.50	0.64
2	OC	27	2.4	1.7	-0.7	0.7	-0.42	0.43
2	EC	27	0.4	0.5	0.1	0.2	0.36	0.52
3	$PM_{2.5}$	29	12.2	10.8	-1.4	4.1	-0.19	0.37
3	Ammonium	29	0.3	0.2	-0.1	0.2	-0.32	0.90

Quarter	Species	# of Obs.	Avg. Obs. (µg/m^3)	Avg. Mod. (µg/m^3)	Mean bias (µg/m^3)	Mean error (µg/m^3)	MFB	MFE
3	Nitrate	30	0.7	0.8	0.1	0.5	-0.16	0.59
3	Sulfate	30	1.2	0.7	-0.5	0.5	-0.48	0.53
3	OC	28	4.1	3.3	-0.8	1.5	-0.31	0.45
3	EC	28	0.6	0.6	0.1	0.2	0.10	0.31
4	$PM_{2.5}$	29	28.5	25.9	-2.6	7.9	0.00	0.30
4	Ammonium	25	3.1	2.6	-0.5	1.3	0.24	0.68
4	Nitrate	28	9.0	8.0	-1.0	3.2	0.08	0.49
4	Sulfate	28	1.1	0.9	-0.2	0.4	-0.04	0.42
4	OC	29	5.2	5.7	0.5	2.5	0.01	0.43
4	EC	29	1.5	1.8	0.3	0.6	0.10	0.37

Table 24. Quarterly $PM_{2.5}$ model performance based on $PM_{2.5}$ speciation measurement at Modesto.

Quarter	Species	# of Obs.	Avg. Obs. (µg/m^3)	Avg. Mod. (µg/m^3)	Mean bias (µg/m^3)	Mean error (µg/m^3)	MFB	MFE
1	$PM_{2.5}$	16	11.7	16.6	5.0	6.1	0.17	0.41
1	Ammonium	7	0.6	1.1	0.6	0.6	0.81	0.81
1	Nitrate	7	2.4	3.5	1.2	1.2	0.31	0.33
1	Sulfate	7	0.6	0.9	0.3	0.4	0.42	0.55
1	OC	7	2.7	3.8	1.1	1.5	0.29	0.41
1	EC	7	0.5	1.2	0.7	0.7	0.89	0.89

Quarter	Species	# of Obs.	Avg. Obs. ($\mu g/m^3$)	Avg. Mod. ($\mu g/m^3$)	Mean bias ($\mu g/m^3$)	Mean error ($\mu g/m^3$)	MFB	MFE
2	$PM_{2.5}$	17	5.9	5.0	-0.9	1.5	-0.14	0.26
2	Ammonium	17	0.3	0.2	-0.1	0.2	-0.64	0.78
2	Nitrate	17	0.8	0.6	-0.3	0.4	-0.36	0.57
2	Sulfate	17	0.9	0.7	-0.2	0.3	-0.25	0.42
2	OC	17	1.7	1.0	-0.8	0.8	-0.61	0.61
2	EC	17	0.2	0.3	0.1	0.1	0.35	0.39
3	$PM_{2.5}$	15	12.1	12.0	-0.1	4.7	-0.07	0.37
3	Ammonium	15	0.5	0.3	-0.2	0.2	-0.62	0.71
3	Nitrate	15	0.8	0.8	0.0	0.4	-0.12	0.44
3	Sulfate	15	1.2	0.9	-0.3	0.4	-0.23	0.34
3	OC	15	4.3	3.4	-0.9	1.8	-0.32	0.52
3	EC	15	0.5	0.5	0.1	0.1	0.15	0.30
4	$PM_{2.5}$	16	20.4	25.5	5.0	7.3	0.23	0.42
4	Ammonium	15	1.9	2.1	0.2	0.6	0.23	0.55
4	Nitrate	15	6.3	7.4	1.2	2.3	0.24	0.59
4	Sulfate	15	0.8	1.1	0.3	0.6	0.39	0.64
4	OC	15	4.8	4.8	0.0	1.9	-0.12	0.45
4	EC	15	1.2	1.4	0.3	0.6	0.12	0.52

Figure 18. Bugle plot of quarterly $PM_{2.5}$ model performance in terms of MFB and MFE at the four $PM_{2.5}$ speciation sites in the SJV (i.e., Bakersfield, Fresno, Modesto, and Visalia).

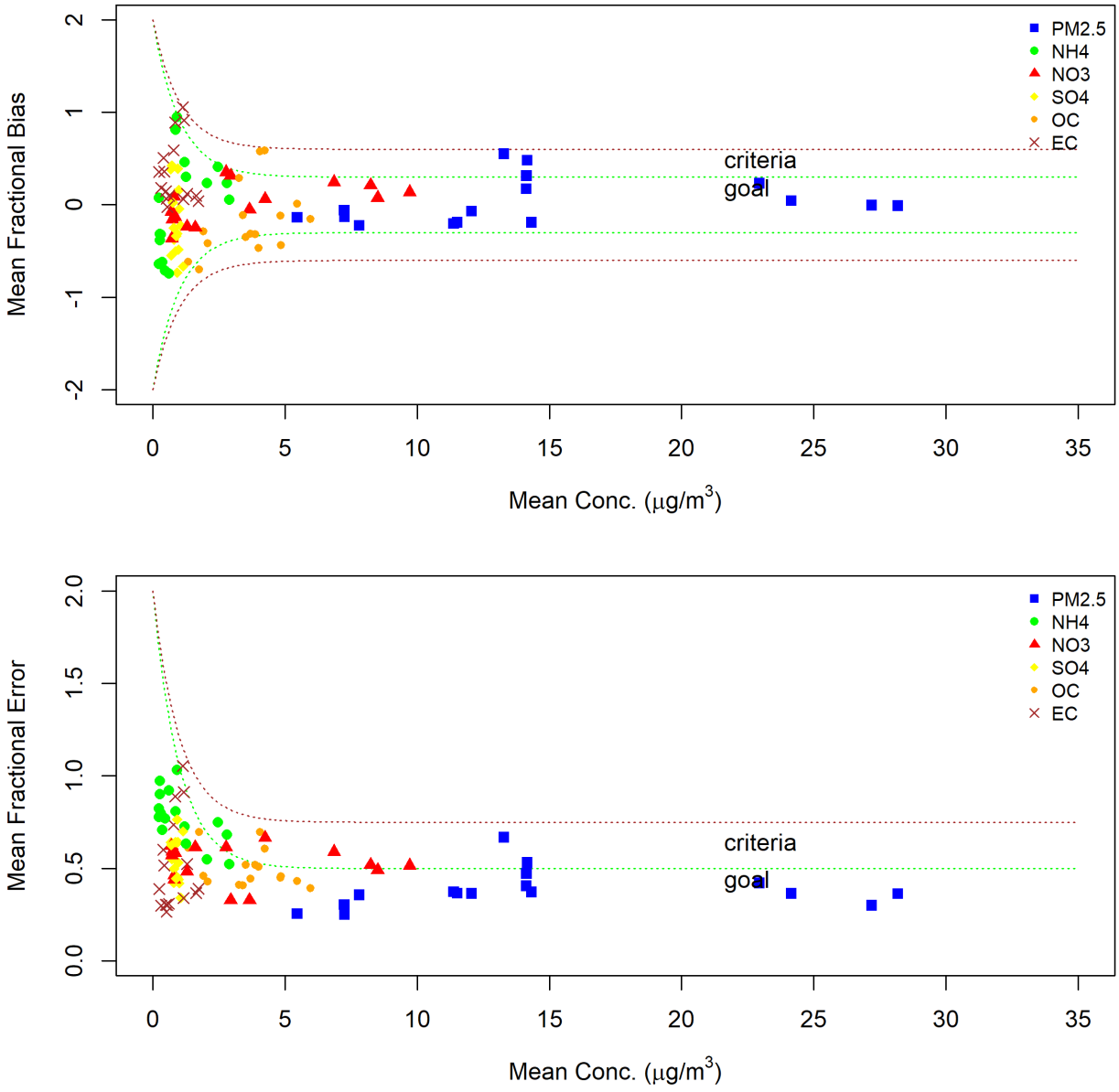

In addition to evaluating the standard statistical performance metrics, it is also informative to put these performance statistics in the context of other studies published in the scientific literature. Figure 19 compares key performance statistics from the modeling platform presented in this document to the range of published performance statistics from 2006 to 2012 and summarized in Simon et al. (2012). In Figure 19, the black centerline shows the median value (i.e., median model performance) from those

studies, the boxes outline the 25th and 75th percentile values, and the whiskers show the 10th and 90th percentile values.

Figure 19. Comparison of annual $PM_{2.5}$ model performance to other modeling studies in Simon et al. (2012). Red symbols represent performance at the four $PM_{2.5}$ speciation sites in the SJV.

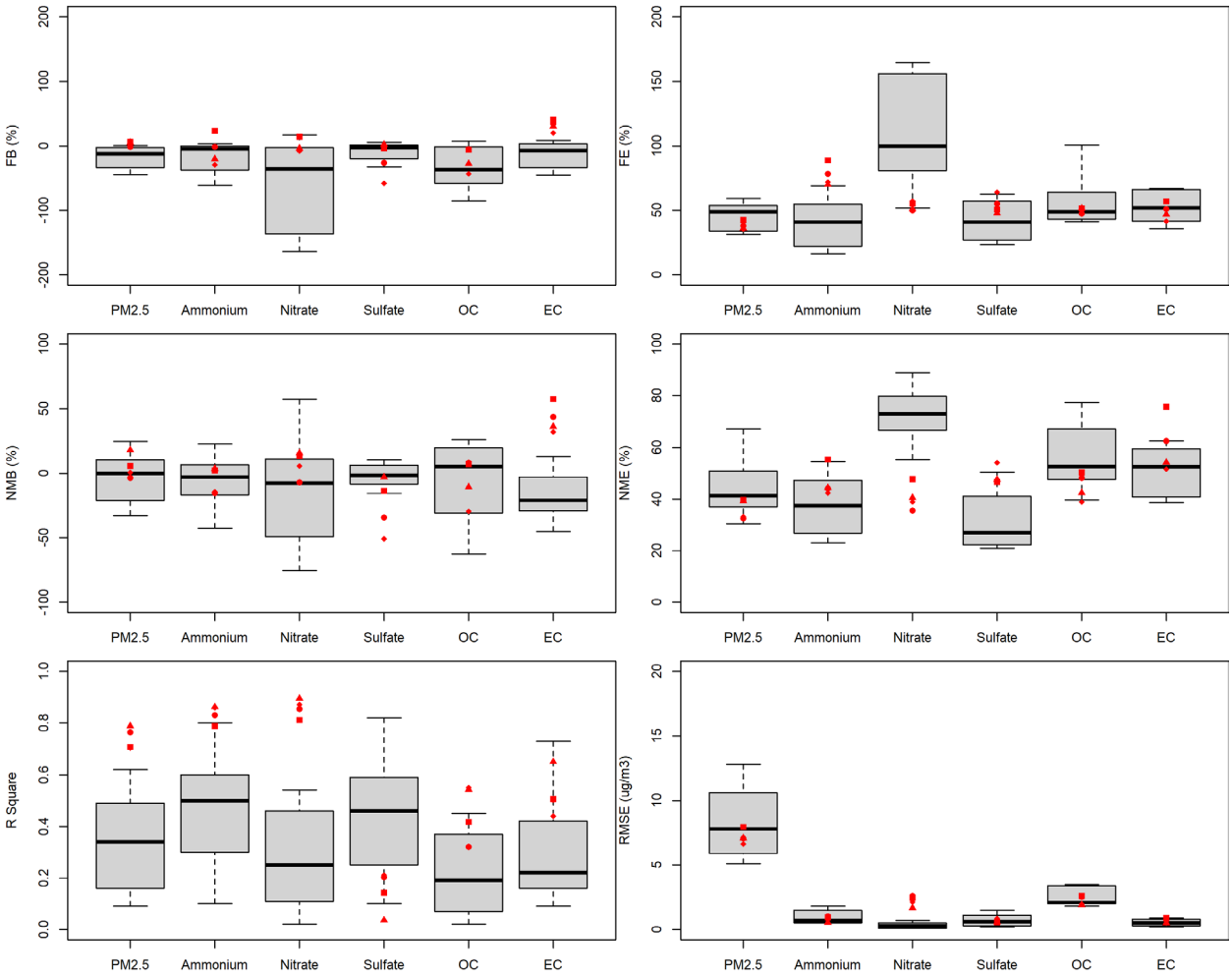

The model performance for each of the four speciation sites in the SJV is shown in red. Performance metrics including MFB, MFE, normalized mean bias (NMB), normalized mean error (NME), R squared, and root mean square error (RMSE) are compared. Model performance metrics in the SJV are typically equal to or better than the corresponding statistics from other studies. One exception is the higher RMSE for nitrate in the SJV, which is simply a reflection of the higher nitrate concentrations in the SJV compared to other regions. In fact, MFB, MFE, NME, and R squared for nitrate in the SJV are on par with the majority of the model studies summarized in Simon et al. (2012). Finally, the model performance is also comparable to that of the 2012 SJV $PM_{2.5}$ SIP and 2018 SJV $PM_{2.5}$ SIP.

Since speciation monitors do not measure $PM_{2.5}$ on a daily basis, it is also advantageous to compare modeled 24-hour average $PM_{2.5}$ concentrations to observations from continuous $PM_{2.5}$ samplers, which typically report 24-hour average $PM_{2.5}$ concentrations on a daily basis. Figures S28 to S38 in the supplemental materials show the time series of modeled and observed 24-hour average $PM_{2.5}$ concentrations at these sites located throughout the SJV. Distinct seasonal variations in $PM_{2.5}$ concentrations are observed throughout the Valley, and they are also reasonably captured by the model. Of particular importance, the modeling system was able to capture the elevated $PM_{2.5}$ events during the winter months and the lower $PM_{2.5}$ which is common in the summer months. In addition, Table 25 summarizes the corresponding model performance statistics at these sites. All the sites met or exceeded the $PM_{2.5}$ model performance criteria defined in Boyland and Russell (2006).

In addition to the $PM_{2.5}$ performance evaluation, gas phase model performance was also evaluated for NO_2, ozone (O_3) and NH_3, which are key products of the photochemical processes in the atmosphere. Scatter plots of observed and modeled one-hour NO_2 mixing ratios at 15 sites are shown in Figures S39 to S53 in the supplemental materials. On average, there is good agreement between observed and modeled NO_2 mixing ratios. The slope of the regression line between the observed and modeled hourly NO_2 mixing ratios is within ±30% of the 1:1 correlation line at most of the sites. Scatter plots of observed and modeled hourly O_3 mixing ratios at 25 sites are shown in Figures S54 to S78 in the supplemental materials. Modeled O_3 mixing ratios show excellent agreement with observed mixing ratios and the slopes of the regression lines between observed and modeled O_3 are within ±15% of the 1:1 correlation line for most of the sites.

The IASI instrument, which is housed aboard the European Space Agency's MetOP-A satellite, passes over California each day around 10:00 am local time, providing measurements of column-integrated NH_3. The IASI measurement data processed by CARB are recorded in 12 x 12 km grid cells. In order for IASI data to be directly compared against NH_3 column densities predicted by CMAQ, CMAQ outputs were computed into vertical-column integrals in the same 12 km grid used for IASI data, then filtered to only select grid cells that overlap in space-time with a valid IASI pixel. Figure S79 shows the annual average of column NH_3 in 2017 from IASI and CMAQ, which indicates a low bias of ~18% in the modeled column NH_3 in the SJV. Since NH_3 is already in excess with respect to ammonium nitrate formation, this underprediction in column NH_3 will have little impact on simulated ammonium nitrate but does mean the modeled sensitivity to changes in NH_3 is likely overestimated and real world ammonium nitrate will be even less sensitive to changes in NH_3 emissions.

Table 25. Model performance for 24-hour $PM_{2.5}$ concentrations measured from continuous beta-attention $PM_{2.5}$ monitors.

Sites	# of Obs.	Avg. Obs. (µg/m^3)	Avg. Mod. (µg/m^3)	Mean bias (µg/m^3)	Mean error (µg/m^3)	MFB	MFE
Fresno - Garland	358	14.5	15.8	1.3	5.3	0.06	0.40
Tranquillity	357	8.4	8.1	-0.3	4.0	-0.15	0.43
Clovis	365	13.2	14.6	1.4	5.1	0.03	0.41
Corcoran	359	15.7	12.4	-3.3	5.8	-0.29	0.45
Hanford	362	17.2	13.7	-3.6	6.3	-0.29	0.45
Madera	359	12.5	12.5	0.0	4.7	-0.07	0.42
Merced	362	13.3	12.2	-1.1	5.4	-0.21	0.45
Stockton	352	12.3	13.1	0.8	5.2	-0.06	0.42
Manteca	362	11.2	11.7	0.5	5.1	-0.14	0.44
Modesto	362	12.9	14.6	1.6	5.0	0.04	0.36
Turlock	362	12.8	14.5	1.7	5.2	0.14	0.45

C. Future Year 2030 Design Values

Projected future year 2030 annual $PM_{2.5}$ DVs for each site are shown in Table 26. The Bakersfield-Planz site has the highest projected DV at 12.0 µg/m^3, rounded to the nearest tenths digit following the U.S. EPA's guidance (U.S. EPA 2018). This DV meets the 12 µg/m^3 annual $PM_{2.5}$ standard established by the U.S. EPA in 2012.

The corresponding Relative Response Factors (RRFs) for annual $PM_{2.5}$ are given in Table 27 (Note, RRF is calculated on a quarterly basis in the actual DV calculation, so the annual RRF is shown for illustrative purposes only). From 2017 to 2030, there are substantial reductions projected for ammonium nitrate, EC, and organic matter (OM), a slight decrease in sulfate, but a slight increase in crustal material (i.e., other primary $PM_{2.5}$ such as fugitive dust emissions). The reduction in ammonium nitrate is a direct result of NO_x emission reductions in 2030 compared to 2017, while EC and OM reductions are primarily tied to the reduction in primary $PM_{2.5}$ emissions. Because future

year projection is performed for each individual $PM_{2.5}$ species, the base year annual $PM_{2.5}$ compositions are given in Table 28. In addition, the projected 2030 annual $PM_{2.5}$ compositions are shown in Table 29. In 2030, for the annual $PM_{2.5}$ standard, OM is the dominant $PM_{2.5}$ component.

Table 26. Projected future year 2030 annual $PM_{2.5}$ DVs at each monitor.

Site AQS ID	Name	Base DV (µg/m^3)	2030 Annual DV (µg/m^3)	2030 Annual DV (µg/m^3, rounded to the tenths digit)
060290016	Bakersfield - Planz	16.97	11.98	12.0
060311004	Hanford	15.73	11.04	11.0
060290010	Bakersfield - Golden	15.52	10.82	10.8
061072002	Visalia	15.43	10.50	10.5
060290014	Bakersfield - California Ave.	15.12	10.52	10.5
060310004	Corcoran	14.95	10.90	10.9
060195025	Fresno – Hamilton	13.99	9.81	9.8
060190011	Fresno – Garland	13.69	9.49	9.5
060990006	Turlock	12.7	9.69	9.7
060195001	Clovis	12.69	8.99	9.0
060470003	Merced - S. Coffee	12.28	9.31	9.3
060771002	Stockton	12.21	10.16	10.2
060392010	Madera	12.11	8.75	8.8
060472510	Merced - M. Street	11.73	8.73	8.7
060990005	Modesto	11.16	8.54	8.5
060772010	Manteca	10.37	8.38	8.4
060192009	Tranquillity	8.19	6.37	6.4

Table 27. 2030 Annual RRFs for $PM_{2.5}$ components.

Site	RRF for $PM_{2.5}$	RRF for NH_4	RRF for NO_3	RRF for SO_4	RRF for OM	RRF for EC	RRF for Crustal	RRF for salt
Bakersfield-Planz	0.71	0.57	0.39	0.88	0.76	0.38	1.12	1.00
Hanford	0.70	0.61	0.38	0.99	0.75	0.47	0.99	1.00
Bakersfield-Golden	0.70	0.54	0.35	0.87	0.77	0.39	1.12	1.00
Visalia	0.68	0.57	0.34	0.96	0.73	0.45	1.06	1.00
Bakersfield-California Ave	0.70	0.56	0.38	0.88	0.75	0.38	1.12	1.00
Corcoran	0.73	0.63	0.39	1.02	0.79	0.54	0.98	1.00
Fresno-Hamilton	0.70	0.63	0.44	0.94	0.71	0.42	1.12	1.00
Fresno-Garland	0.69	0.61	0.42	0.94	0.71	0.44	1.08	1.00
Turlock	0.76	0.68	0.50	0.98	0.80	0.50	1.07	1.00
Clovis	0.71	0.62	0.39	0.96	0.73	0.49	1.08	1.00
Merced-S. Coffee	0.76	0.65	0.42	0.98	0.81	0.50	1.05	1.00
Stockton	0.83	0.74	0.55	1.01	0.87	0.57	1.21	1.00
Madera	0.72	0.63	0.41	0.97	0.76	0.46	1.06	1.00
Merced-M. Street	0.74	0.63	0.42	0.98	0.80	0.50	1.05	1.00
Modesto	0.77	0.69	0.51	0.98	0.79	0.50	1.08	1.00
Manteca	0.81	0.74	0.55	1.01	0.84	0.53	1.08	1.00
Tranquillity	0.78	0.66	0.40	1.00	0.83	0.53	1.03	1.00

Table 28. 2017 Base year annual $PM_{2.5}$ compositions (μg/m^3).*

Name	$PM_{2.5}$	NH_4	NO_3	SO_4	OM	EC	Crustal	Salt
Bakersfield-Planz	16.97	1.31	2.83	1.30	7.69	0.90	1.87	0.05
Hanford	15.73	1.31	2.83	1.30	7.30	0.61	1.29	0.08
Bakersfield-Golden	15.52	1.21	2.68	1.16	6.97	0.83	1.67	0.05
Visalia	15.43	1.28	2.75	1.28	7.17	0.60	1.28	0.08
Bakersfield-Cal. Ave	15.12	1.19	2.64	1.12	6.78	0.81	1.61	0.05
Corcoran	14.95	1.24	2.66	1.24	6.95	0.58	1.25	0.08
Fresno-Hamilton	13.99	0.96	2.06	0.95	7.37	0.74	1.06	0.05
Fresno-Garland	13.69	0.94	2.04	0.92	7.20	0.73	1.03	0.05
Turlock	12.70	0.94	2.01	0.96	6.20	0.68	0.95	0.18
Clovis	12.69	0.84	1.74	0.90	6.74	0.66	1.02	0.05
Merced-S. Coffee	12.28	0.89	1.77	0.99	6.08	0.65	0.96	0.19
Stockton	12.21	0.90	1.83	0.97	5.99	0.64	0.93	0.18
Madera	12.11	0.82	1.71	0.85	6.40	0.63	0.95	0.04
Merced-M. Street	11.73	0.87	1.84	0.89	5.72	0.62	0.88	0.17
Modesto	11.16	0.82	1.72	0.86	5.45	0.59	0.84	0.16
Manteca	10.37	0.75	1.50	0.84	5.11	0.54	0.80	0.16
Tranquillity	8.19	0.52	1.01	0.61	4.36	0.41	0.70	0.03

*: Particle-bound water and blank mass are not shown.

Table 29. Projected 2030 Annual $PM_{2.5}$ compositions (µg/m^3).*

Name	Future $PM_{2.5}$	Future NH_4	Future NO_3	Future SO_4	Future OM	Future EC	Future Crustal	Future Salt	Future Water
Bakersfield-Planz	11.98	0.75	1.11	1.14	5.82	0.34	2.09	0.05	0.48
Hanford	11.04	0.80	1.08	1.29	5.50	0.29	1.28	0.08	0.51
Bakersfield-Golden	10.82	0.65	0.93	1.01	5.37	0.32	1.87	0.05	0.41
Visalia	10.5	0.73	0.94	1.23	5.22	0.27	1.36	0.08	0.47
Bakersfield-Cal. Ave	10.52	0.66	1.01	0.98	5.09	0.31	1.81	0.05	0.42
Corcoran	10.9	0.78	1.05	1.26	5.52	0.31	1.22	0.08	0.49
Fresno-Hamilton	9.81	0.60	0.92	0.90	5.27	0.31	1.19	0.05	0.38
Fresno-Garland	9.49	0.57	0.86	0.86	5.13	0.32	1.12	0.05	0.36
Turlock	9.69	0.64	1.00	0.94	4.97	0.34	1.01	0.18	0.41
Clovis	8.99	0.52	0.67	0.87	4.92	0.32	1.10	0.05	0.34
Merced-S. Coffee	9.31	0.58	0.74	0.97	4.92	0.32	1.00	0.19	0.38
Stockton	10.16	0.66	1.01	0.98	5.20	0.37	1.13	0.18	0.42
Madera	8.75	0.51	0.69	0.83	4.84	0.29	1.01	0.04	0.33
Merced-M. Street	8.73	0.55	0.77	0.88	4.58	0.31	0.92	0.17	0.35
Modesto	8.54	0.57	0.88	0.84	4.33	0.30	0.91	0.16	0.36
Manteca	8.38	0.56	0.82	0.85	4.28	0.29	0.87	0.16	0.36
Tranquillity	6.37	0.35	0.41	0.61	3.60	0.22	0.71	0.03	0.23

*: For each site, blank filter mass equal to 0.2 µg/m^3 is not shown in this table.

D. $PM_{2.5}$ Precursor Sensitivity Analysis

To evaluate the impact of reducing emissions of different $PM_{2.5}$ precursors on $PM_{2.5}$ DVs, a series of model sensitivity simulations were performed. In these simulations anthropogenic emissions of the precursor species were reduced by a specific percentage from the baseline emissions. The U.S. EPA (USEPA, 2016) recommends a

range of 30-70% reduction in precursor emissions in the nonattainment area, and that recommendation is followed here.

Comparing the difference in $PM_{2.5}$ DVs from the precursor reduction simulations and the baseline modeling shows the sensitivity of the $PM_{2.5}$ DVs to changes in baseline precursor emissions. Given the nature of $PM_{2.5}$ formation, the effect of reductions in the following $PM_{2.5}$ precursors were investigated: primary $PM_{2.5}$, NOx, SOx, NH_3, and ROG. For each precursor sensitivity, only anthropogenic emissions in the San Joaquin Valley were reduced. Natural emissions and emissions outside of the SJV were kept constant. Since it is known that NOx and direct $PM_{2.5}$ contribute significantly to $PM_{2.5}$ formation in the SJV (Pusede et al., 2016) and these species already meet U.S. EPA's criteria for significant precursors, sensitivity runs for NOx and direct $PM_{2.5}$ were only performed with a 30% emission reduction. Given the lower contribution of other precursor species to total $PM_{2.5}$ (i.e., ammonia, ROG, and SOx), both 30% and 70% emission reductions were performed for those species.

The precursor sensitivity modeling was performed for both the 2017 base year and 2030 future year. Table 30 shows the impact from precursor reductions on annual $PM_{2.5}$ DVs for 2017. 30% $PM_{2.5}$ and 30% NOx reductions clearly show significant impact on $PM_{2.5}$ DVs. Direct PM reduction is more effective than NOx for the annual standard. Although both NOx and ammonia contribute to ammonium nitrate formation, the impact on $PM_{2.5}$ DVs from ammonia reduction is much less than that from NOx reductions, because ammonium nitrate formation in the SJV is limited by the availability of nitric acid instead of by ammonia (Lurmann et al., 2006; Markovic, 2014; Parworth, et al., 2017; Prabhakar et al., 2017). This is consistent with previous modeling studies (Chen et al., 2014; Kleeman et al., 2005; Pun et al., 2009). Reducing SOx emissions has a very small impact on annual DVs, and may even have a dis-benefit for annual DVs at many sites. The negative impact on DVs from SOx emission reductions is due to the non-linearity in inorganic thermodynamics that governs the partitioning of nitrate onto particles (e.g., West et al., 1999). Reducing ROG emissions has a small positive impact on annual DVs. In 2017, reducing ROG emissions reduced secondary organic aerosol (SOA) formation as well as slightly lowering ammonium nitrate formation, as demonstrated in Kleeman et al. (2005) and Pun et al. (2009).

Table 31 shows the impact on annual DVs from precursor reductions in 2030. Similar to 2017, 30% PM and 30% NOx reductions lead to substantial reductions in annual $PM_{2.5}$ DVs in 2030. While ammonia reduction also leads to reductions in annual $PM_{2.5}$ DVs, an equivalent percentage of ammonia reduction is typically less effective than NOx reductions, due to the excess of ammonia in the SJV (Parworth et al., 2017; Prabhaker et al., 2017). While NOx emissions in 2030 exhibit substantial reductions from 2017 levels, ammonia emission trends are relatively flat, meaning ammonia is even more in excess in 2030 (i.e., NH_3 reductions will be even less effective at reducing $PM_{2.5}$ in 2030). Reducing SOx emissions has a very small impact on annual DVs and reducing ROG emissions has essentially no effect on the annual DVs. However, under 2030 emission levels, reducing ROG emissions can slightly increase ammonium nitrate formation in the wintertime. This is different from the reference year 2017, because modeled ammonium nitrate concentration is much smaller in 2030 than in 2017, such that the response in ammonium nitrate formation to ROG emission reductions is

reversed. A previous modeling study by CARB (2016) utilizing the Integrated Reaction Rate (IRR) technique in the CMAQ model shows that reduced ROG emissions can lead to less peroxyacetyle nitrate (PAN) formation (Meng et al., 1997), increased availability of nitrogen dioxide and more nighttime nitric acid formation. However, since lower ROG levels also reduce daytime hydroxyl radical concentrations and result in less daytime nitric acid formation, these processes compete with each other and lead to a different net impact on ammonium nitrate formation depending on the NOx and ROG emission levels.

Table 30. Difference in Annual $PM_{2.5}$ DVs between the 2017 baseline run and precursor emission reduction runs.*

Sites	Baseline DV	30% PM*	30% NOx	30% NH_3	70% NH_3	30% ROG	70% ROG	30% SOx	70% SOx
Bakersfield-Planz	16.97	-2.63	-0.7	-0.35	-1.3	-0.07	-0.21	-0.02	-0.01
Hanford	15.73	-1.86	-0.77	-0.19	-0.85	-0.01	-0.13	0.01	-0.05
Bakersfield-Golden	15.52	-2.38	-0.8	-0.36	-1.41	-0.01	-0.11	0.01	0.01
Visalia	15.43	-1.95	-0.85	-0.27	-1.09	-0.06	-0.2	-0.02	-0.07
Bakersfield-Cal. Ave	15.12	-2.32	-0.68	-0.32	-1.22	-0.02	-0.14	0.01	0.01
Corcoran	14.95	-1.64	-0.86	-0.24	-1	-0.04	-0.14	0	-0.01
Fresno-Hamilton	13.99	-2.11	-0.33	-0.2	-0.86	-0.04	-0.2	0.02	-0.03
Fresno-Garland	13.69	-2.04	-0.34	-0.17	-0.79	-0.01	-0.14	0.04	0.02
Turlock	12.7	-1.44	-0.12	-0.08	-0.5	0	-0.11	0.05	0.02
Clovis	12.69	-1.8	-0.37	-0.19	-0.76	0	-0.11	0.06	0.08
Merced-S Coffee	12.28	-1.3	-0.27	-0.15	-0.68	0.01	-0.07	0.04	0.01
Stockton	12.21	-1.12	-0.02	-0.02	-0.38	0.06	-0.02	0.09	0.06
Madera	12.11	-1.45	-0.25	-0.14	-0.75	0.03	-0.08	0.08	0.05
Merced-M Street	11.73	-1.25	-0.28	-0.15	-0.72	0.01	-0.07	0.04	0.01

Sites	Baseline DV	30% PM*	30% NOx	30% NH_3	70% NH_3	30% ROG	70% ROG	30% SOx	70% SOx
Modesto	11.16	-1.27	-0.06	-0.04	-0.42	0.04	-0.05	0.07	0.04
Manteca	10.37	-0.82	0.01	-0.02	-0.31	0.04	-0.05	0.07	0.04
Tranquillity	8.19	-0.73	-0.29	-0.14	-0.51	0	-0.03	0.03	0.04

*: 30% PM means that anthropogenic PM emissions within SJV are reduced by 30% from the baseline emissions inventory. Same meaning applies to other precursor reduction runs.

Table 31. Difference in Annual $PM_{2.5}$ DVs between the 2030 baseline run and precursor emission reduction runs.*

Sites	Baseline DV	30% PM*	30% NOx	30% NH_3	70% NH_3	30% ROG	70% ROG	30% SOx	70% SOx
Bakersfield-Planz	16.97	-2.4	-0.47	-0.12	-0.37	-0.02	-0.05	-0.06	-0.1
Hanford	15.73	-1.53	-0.39	-0.1	-0.35	0	0	-0.07	-0.14
Bakersfield-Golden	15.52	-2.15	-0.4	-0.12	-0.39	-0.01	-0.01	-0.05	-0.08
Visalia	15.43	-1.71	-0.43	-0.1	-0.34	-0.01	-0.01	-0.08	-0.16
Bakersfield-Cal. Ave	15.12	-2.12	-0.41	-0.11	-0.35	-0.01	-0.03	-0.05	-0.09
Corcoran	14.95	-1.34	-0.41	-0.11	-0.39	-0.02	-0.03	-0.04	-0.09
Fresno-Hamilton	13.99	-1.86	-0.3	-0.09	-0.31	-0.05	-0.12	-0.07	-0.14
Fresno-Garland	13.69	-1.84	-0.28	-0.09	-0.28	-0.04	-0.09	-0.06	-0.11

Sites	Baseline DV	30% PM*	30% NOx	30% NH_3	70% NH_3	30% ROG	70% ROG	30% SOx	70% SOx
Turlock	12.7	-1.35	-0.25	-0.07	-0.25	-0.03	-0.07	-0.04	-0.08
Clovis	12.69	-1.61	-0.25	-0.07	-0.24	-0.02	-0.06	-0.03	-0.06
Merced-S Coffee	12.28	-1.15	-0.21	-0.08	-0.26	-0.02	-0.04	-0.03	-0.07
Stockton	12.21	-1.19	-0.14	-0.06	-0.21	-0.02	-0.05	-0.02	-0.05
Madera	12.11	-1.2	-0.24	-0.09	-0.29	-0.02	-0.05	-0.04	-0.09
Merced-M Street	11.73	-1.1	-0.21	-0.08	-0.27	-0.01	-0.03	-0.03	-0.07
Modesto	11.16	-1.26	-0.19	-0.07	-0.22	-0.03	-0.07	-0.04	-0.08
Manteca	10.37	-0.81	-0.15	-0.05	-0.18	-0.02	-0.06	-0.03	-0.06
Tranquillity	8.19	-0.52	-0.13	-0.06	-0.19	-0.01	-0.01	0	0

*: 30% PM means that anthropogenic PM emissions within SJV are reduced by 30% from the baseline emissions inventory. Same meaning applies to other precursor reduction runs.

E. Unmonitored Area Analysis

The unmonitored area analysis is performed to ensure that there are no regions outside of the existing monitoring network that could exceed the NAAQS if a monitor was present at that location (U.S. EPA, 2018). The U.S. EPA recommends combining spatially interpolated design value fields with modeled gradients for the pollutant of interest and grid-specific RRFs in order to generate gridded future year gradient adjusted design values. The spatial Interpolation of the observed design values is done only within the geographic region constrained by the monitoring network, since extrapolating to outside of the monitoring network is inherently uncertain.

This analysis can be done using SMAT-CE (Software for the Modeled Attainment Test – Community Edition, *https://www.epa.gov/scram/photochemical-modeling-tools*). However, this software is not open source and comes as a precompiled software package. To maintain transparency and flexibility in the analysis, in-house R codes (https://www.r-project.org/) developed at CARB are utilized in this analysis.

For annual $PM_{2.5}$ standards, the unmonitored area analysis involves the following steps:

Step 1: At each grid cell, the quarterly RRFs of each species are calculated based on the reference- and future-year modeling results following the same approach outlined in the Methodology section of this document.

Step 2: At each grid cell, the quarterly average of the modeled $PM_{2.5}$ species is calculated from the reference year simulation, and the gradients in these quarterly speciated averages between each grid cell and grid cells which contain a monitor is calculated.

Step 3: The quarterly reference year speciated $PM_{2.5}$ design values are obtained for each monitoring site from the attainment test. For each grid cell, the monitors within its Voronoi Region are identified, and the quarterly speciated $PM_{2.5}$ values are then interpolated using normalized inverse distance squared weightings for all monitors within a grid cell's Voronoi Region. The quarterly interpolated speciated $PM_{2.5}$ fields are further adjusted based on the appropriate gradients from Step 2.

Step 4: The quarterly future year speciated $PM_{2.5}$ value for each grid cell is obtained by multiplying reference year speciated $PM_{2.5}$ value with the quarterly RRF for that grid from step 1. The future year annual $PM_{2.5}$ design value for each grid cell is thus calculated by averaging the quarterly speciated $PM_{2.5}$ values.

Step 5: The future year gridded annual average $PM_{2.5}$ estimates are then compared to the annual $PM_{2.5}$ NAAQS to determine compliance.

Under the Voronoi diagram method, each monitoring site was assigned to a Voronoi region based on location and the distance to each grid cell (Sen 2016), and the interpolations were done between each grid cell and all the monitors in surrounding Voronoi regions. Voronoi diagram with inverse distance weighting method has been

used in various 2-D data analysis areas, including air quality measurements interpolations (Atsuyuki, et al., 2009; Deligiorgi and Philippopoulos 2011).

Figure 20 shows the spatial distribution of projected 2030 annual $PM_{2.5}$ DVs (left) and RRFs (right) in the SJV nonattainment area. Projected 2030 annual $PM_{2.5}$ DVs at every grid cell are below the threshold needed for attainment (12.04 µg/m^3), except for a few cells surrounding the Lemoore military facility (grids borders are marked in the plot), where the greater $PM_{2.5}$ levels are due to localized emissions associated with that facility. A similar $PM_{2.5}$ hotspot associated with the Lemoore military facility was observed in past SJV $PM_{2.5}$ SIPs as well. This demonstrates that all unmonitored areas within the SJV will attain the 12 µg/m^3 annual $PM_{2.5}$ standard (technically, DVs not greater than 12.04 µg/m^3 are considered as attainment) established by the USEPA in 2012, except for a small area surrounding the Lemoore military facility (the areas with marked grid cells in Figure 20) which will need further evaluation given the uncertainties associated with emissions from military facilities**.**

Figure 20. Spatial distribution of projected 2030 annual $PM_{2.5}$ DVs (left) and RRFs based on the unmonitored area analysis within the SJV nonattainment area.

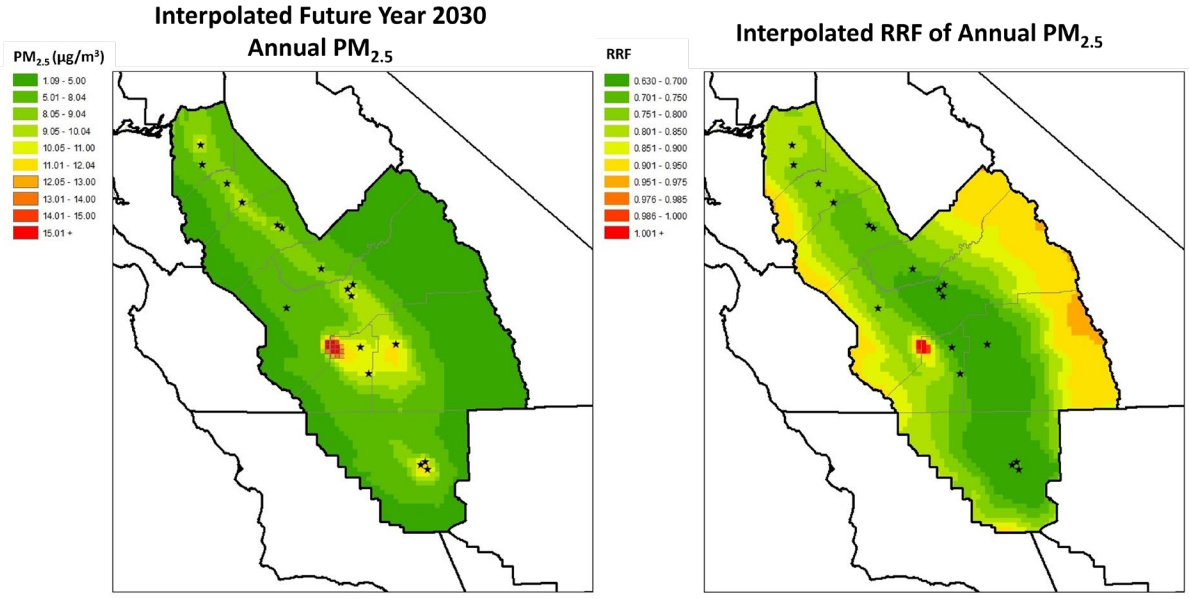

F. Discussions on the Impact from Different Soil NOx Parameterizations and Increasing Prescribed Burn Emissions

Soils can be a source of atmospheric nitrogen oxides (NOx), especially in regions with significant cropland where nitrogen fertilizers are widely used. However, the magnitude of soil NOx emissions can vary substantially, depending on local land use, management activities, and meteorological/irrigation conditions (Guo et al., 2020). Various parameterizations and models have been proposed to simulate soil NOx emissions, and

these various approaches have a wide range of soil NOx emission estimates for the SJV (e.g., Almaraz et al., 2018; Guo et al., 2020; Sha et al., 2021; Zhu et al., 2023). While the attainment demonstration simulations used soil NOx emission estimates from the default YL95 scheme (Yienger and Levy, 1995) in the MEGAN model, to assess the response of future DVs to changes in the soil NOx inventory, a sensitivity analysis was conducted using the Berkeley-Dalhousie soil NOx parameterization or BDSNP (Hudman et al., 2012) in the MEGAN model. The BDSNP model has been referenced in recent air quality studies over the SJV (e.g., Sha et al., 2021; Zhu et al., 2023). On an annual basis, the BDSNP algorithm estimated much higher soil NOx emissions than the default scheme in MEGAN3.0. However, on a monthly basis, the BDSNP algorithm estimated soil NOx emissions can be smaller than the default scheme for winter months. Figure 21 shows monthly soil NOx emissions estimates for the SJV from the default YL95 scheme as well as the BDSNP algorithm.

Table 32 shows the future year annual DV difference between the default soil NOx emissions and the BDSNP algorithm. For the annual DVs, using BDSNP slightly reduced annual DVs. This is likely because the BDSNP estimated soil NOx emissions are actually lower than the default YL95 scheme for winter months, leading to smaller ammonium nitrate prediction when ambient ammonium nitrate concentrations are highest. Since ammonium nitrate levels are low in the summer months when BDSNP predicts the highest soil NOx emissions, there is very little impact on the overall DVs.

In addition, we also performed the 2017 model performance simulation based on the BDSNP scheme and compared it to the observations as well as the model prediction based on the default YL95 scheme in MEGAN3.0. Figures S80-S83 in the supplemental material show these comparisons for $PM_{2.5}$ species at Fresno, Bakersfield, Visalia, and Modesto, respectively. The BDSNP scheme only modestly increased nitrate prediction in warmer months. Despite much higher NOx emissions from the BDSNP in warmer months, meteorological conditions do not favor ammonium nitrate formation in warmer months in the SJV, leading to only modest increase in nitrate prediction in warmer months. The BDSNP scheme has minimal impact on the predictions of other species such as OC, EC, and sulfate. Overall, $PM_{2.5}$ model performance based on BDSNP scheme is close to those based on the default YL95 soil NOx scheme in MEGAN.

Figure 21. Daily soil NOx emissions for each month of 2017 estimated from the MEGAN3.0 default soil NOx scheme and the MEGAN BDSNP soil NOx scheme.

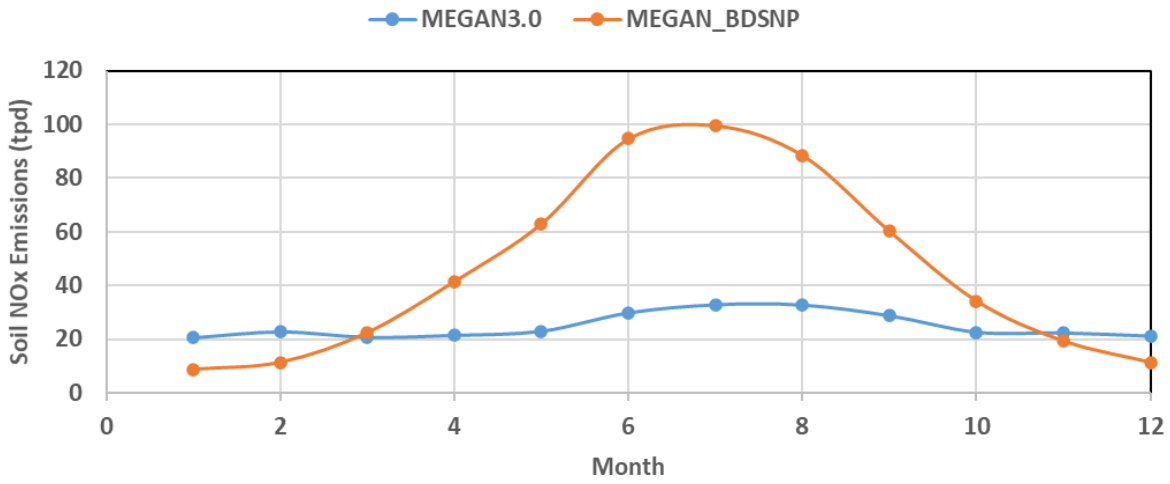

Table 32. 2030 annual DVs difference calculated using the BDSNP soil NOx algorithm compared to the default soil NOx algorithm in MEGAN3.0.

AQ site	Site name	Base year annual $PM_{2.5}$ DVs ($\mu g/m^3$)	Difference in 2030 annual $PM_{2.5}$ DVs ($\mu g/m^3$)
60290016	Bakersfield - Planz	16.97	-0.13
60311004	Hanford	15.73	-0.18
60290010	Bakersfield - Golden	15.52	-0.11
61072002	Visalia	15.43	-0.14
60290014	Bakersfield - California Ave.	15.12	-0.11
60310004	Corcoran	14.95	-0.18
60195025	Fresno - Hamilton	13.99	-0.07
60190011	Fresno - Garland	13.69	-0.05
60990006	Turlock	12.7	-0.04
60195001	Clovis	12.69	-0.02
60470003	Merced - S. Coffee	12.28	-0.03
60771002	Stockton	12.21	-0.04

AQ site	Site name	Base year annual $PM_{2.5}$ DVs ($\mu g/m^3$)	Difference in 2030 annual $PM_{2.5}$ DVs ($\mu g/m^3$)
60392010	Madera	12.11	-0.04
60472510	Merced - M. Street	11.73	-0.03
60990005	Modesto	11.16	-0.04
60772010	Manteca	10.37	-0.04
60192009	Tranquillity	8.19	-0.07

To evaluate the potential impact increased prescribed burning may have on future DVs and attainment of the NAAQS, an additional sensitivity analysis was conducted. For this sensitivity analysis, the base year 2017 utilized the actual 2017 prescribed burning emissions, while for the future year 2030, aggregated prescribed burning emissions from four years (2017, 2018, 2019, and 2021) were utilized. Since future prescribed burn scenarios are not available, those four years were chosen as a conservative representation of prescribed burn activity under a scenario where prescribed burning increased by a factor of four, consistent with the near-term state goals. Table 33 shows the annual average prescribed burn emissions from 2017 and the aggregated emissions from four years. The aggregated four-year emissions are approximately 10 times higher than the 2017 emissions. Figure 22 shows the locations of prescribed burns for 2017, 2018, 2019, and 2021. As can be seen, the typical locations of prescribed burns are generally away from the populated regions of the valley and so are expected to have only a minor impact on air quality in the valley.

Table 34 shows the difference in annual DVs from the sensitivity run compared to the default run. With the aggregated prescribed burn emissions, the annual DVs can increase slightly (less than a tenth of a $\mu g/m^3$) and only 0.04 $\mu g/m^3$ in Bakersfield, which is not sufficient to jeopardize attainment of the NAAQS.

Table 33. Annual average prescribed burning $PM_{2.5}$ emissions in the SJV.

Year	Annual $PM_{2.5}$ emissions (tons/day)
2017	4.5

Year	Annual $PM_{2.5}$ emissions (tons/day)
2018	7.0
2019	7.0
2021	28.6

Figure 22. Locations of prescribed burning events for 2017, 2018, 2019, and 2021.

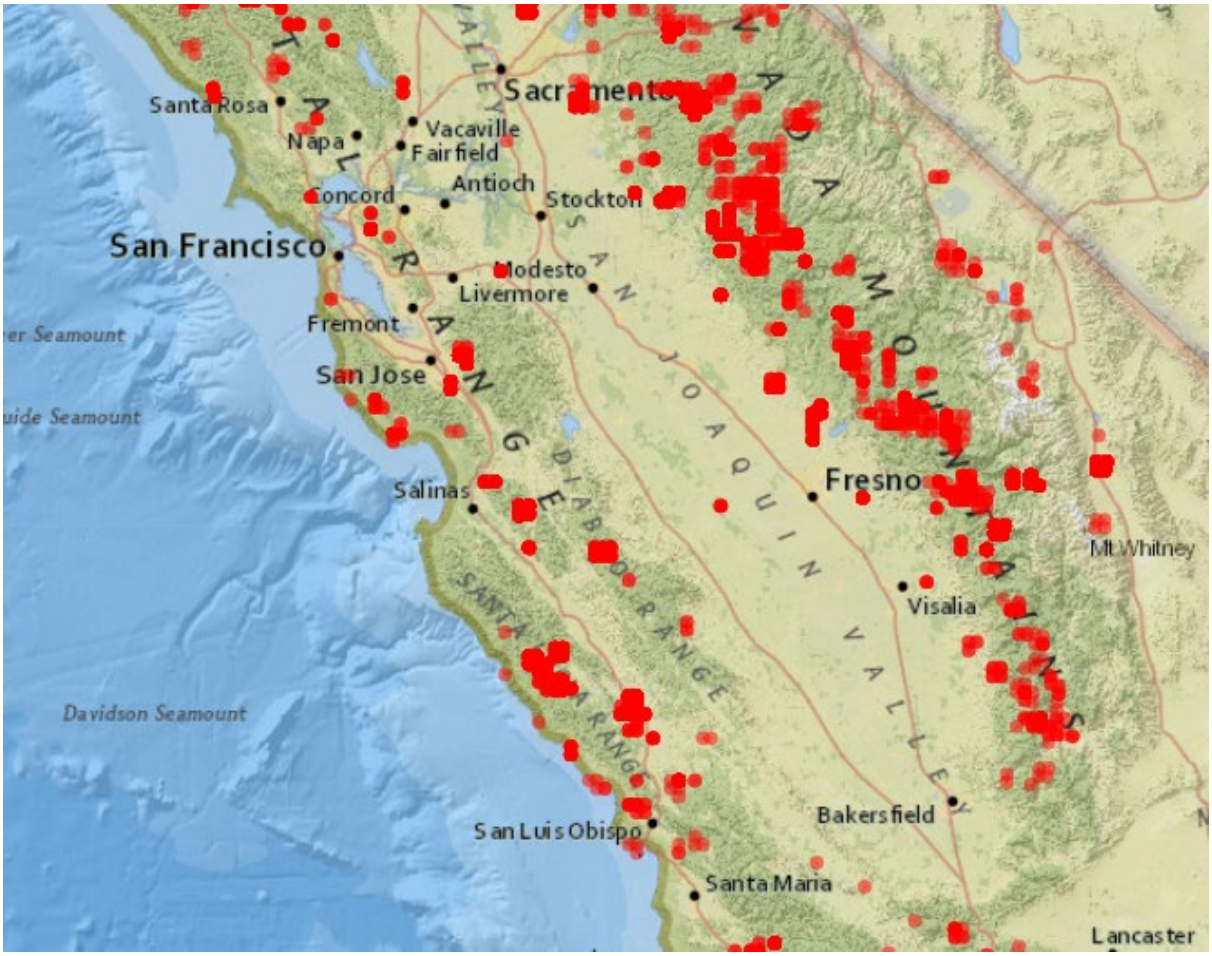

Table 34. 2030 annual DVs difference calculated using the aggregated four year prescribed burning emissions for future year.

AQ site	Site name	Base year annual $PM_{2.5}$ DVs ($\mu g/m^3$)	Difference in 2030 $PM_{2.5}$ DVs ($\mu g/m^3$)
060290016	Bakersfield - Planz	16.97	0.05
060311004	Hanford	15.73	0.08
060290010	Bakersfield - Golden	15.52	0.05
061072002	Visalia	15.43	0.07
060290014	Bakersfield - California Ave	15.12	0.04
060310004	Corcoran	14.95	0.09
060195025	Fresno - Hamilton	13.99	0.05
060190011	Fresno - Garland	13.69	0.05
060990006	Turlock	12.7	0.04
060195001	Clovis	12.69	0.07
060470003	Merced - S. Coffee	12.28	0.06
060771002	Stockton	12.21	0.04
060392010	Madera	12.11	0.07
060472510	Merced - M. Street	11.73	0.06
060990005	Modesto	11.16	0.03
060772010	Manteca	10.37	0.04
060192009	Tranquillity	8.19	0.08

VI. References

Almaraz, M., Bai, E., Wang, C., Trousdell, J., Conley, S., Faloona, I., Houlton, B.Z., 2018, Agriculture is a major source of NOx pollution in California, Science Advances, 4, 3477-3784.

Angevine, W. M., Eddington, L., Durkee, K., Fairall, C., Bianco, L., Brioude, J., 2012, Meteorological model evaluation for CalNex 2010, Monthly Weather Review, 140, 3885-3906.

Atsuyuki, O., B. Boots, K. Sugihara, and S. N. Chiu. 2009. Spatial tessellations: concepts and applications of Voronoi diagrams. Second. John Wiley & Sons.

Baker, K. R., Simon, H., Kelly, J.T., 2011, Challenges to modeling “cold pool” meteorology associated with high pollution episodes. Environmental Science and Technology, 45, 7118–9.

Baker, K. R., Misenis, C., Obland, M. D., Ferrare, R. A., Scarino, A. J., and Kelly, J. T., 2013, Evaluation of surface and upper air fine scale WRF meteorological modeling of the May and June 2010 CalNex period in California, Atmospheric Environment, 80, 299-309.

Bao, J.W., Michelson, S.A., Persson, P.O.G., Djalalova, I.V., Wilczak, J.M., 2008, Observed and WRF-simulated low-level winds in a high-ozone episode during the Central California ozone study, Journal of Applied Meteorology and Climatology, 47, 2372-2394.

Boylan, J.W. and Russell, A.G., 2006, PM and light extinction model performance metrics, goals, and criteria for three-dimensional air quality models, Atmospheric Environment, 40, 4946-4959.

CARB, 2016, Photochemical modeling for the 2016 San Joaquin Valley Annual PM2.5 State Implementation Plan, Modeling Assessment, Prepared by California Air Resources Board and San Joaquin Valley Air Pollution Control District for United States Environmental Protection Agency Region IX, available at http://www.valleyair.org/Air_Quality_Plans/docs/PM25-2016/a.pdf.

Cai, C., J. C. Avise, A. Kaduwela, J. DaMassa, C. Warneke, J. B. Gilman, W. Kuster, et al. 2019, Simulating the Weekly Cycle of NOx-VOC-HOx-O3 Photochemical System in the South Coast ofbCalifornia During CalNex-2010 Campaign, Journal of Geophysical Research: Atmospheres, 3532–3555.

Cai, C., S. Kulkarni, Z. Zhao, A. Kaduwela, J. C. Avise, and J. A. DaMassa. 2016, Simulating Reactive Nitrogen, Carbon Monoxide, and Ozone in California During ARCTAS-CARB 2008 with High Wildfire Activity, Atmospheric Environment, 28-44.

Carter, W.P.L. 2010a, Development of the SAPRC-07 chemical mechanism, Atmospheric Environment, 5324-5335.

Carter, W.P.L. 2010b, Development of a condensed SAPRC-07 chemical mechanism, Atmospheric Environment, 5336-5345.

Chen, J.J., Lu, J., Avise, J.C., DaMassa, J.A., Kleeman, M.J., Kaduwela, A.P., 2014, Seasonal modeling of PM2.5 in California's San Joaquin Valley, Atmospheric Environment, 92, 182-190.

Chen, J.J., et al., 2020, Modeling air quality in the San Joaquin valley of California during the 2013 Discover-AQ field campaign, Atmospheric Environment: X, 5, 100067.

Chow, J.C., Watson, J.G., Lowenthal, D.H., Magliano, K.L., 2005, Loss of PM2.5 nitrate from filter samples in Central California, Journal of Air & Waste Management Association, 55, 1158-1168.

Daly, C., Conklin, D., Unsworth, M., 2009, Local atmospheric decoupling in complex topography alters climate change impacts. International Journal of Climatology, 30, 1857–1864.

Deligiorgi, D., and K. Philippopoulos. 2011. "Spatial Interpolation Methodologies in Urban Air Pollution Modeling: Application for the Greater Area of Metropolitan Athens, Greece." In Advanced Air Pollution. doi:10.5772/17734.

Eastern Kern. 2017, 2017 Ozone Attainment Plan, available at: http://www.kernair.org/Documents/Announcements/Attainment/2017%20Ozone%20Plan_EKAPCD_Adopted_7-27-17.pdf.

Eastern Kern. 2023, 2023 Ozone Attainment Plan, available at: http://www.kernair.org/Documents/Rules/2023%20Attainment%20Plan/EKAPCD_2023_Ozone_Plan_Adopted_5-4-23.pdf

Imperial. 2017, Imperial County 2017 State Implementation Plan for the 2008 8-Hour Ozone Standard, available at: https://ww3.arb.ca.gov/planning/sip/planarea/imperial/2017o3sip_final.pdf.

Imperial. 2018. Imperial County 2018 Annual Particulate Matter Less than 2.5 Microns in Diameter State Implementation Plan, available at: https://ww3.arb.ca.gov/planning/sip/planarea/imperial/final_2018_ic_pm25_sip.pdf.

Fast, J. D., et al., 2012, Transport and mixing patterns over Central California during the carbonaceous aerosol and radiative effects study (CARES), Atmospheric Chemistry and Physics, 12, 1759-1783, doi:10.5194/acp-12-1759-2012.

Ferreria, S.R. and Shipp, E.M., 2005, Historical Meteorological Analysis in Support of the 2003 San Joaquin Valley PM10 State Implementation Plan, San Joaquin Valley Air Pollution District, Fresno, CA.

Fosberg, M.A., Schroeder, M.J., 1966, Marine air penetration in Central California, Journal of Applied Meteorology, 5, 573-589.

Frank, N.H., 2006, Retained nitrate, hydrated sulfates, and carbonaceous mass in federal reference method fine particulate matter for six eastern U.S. cities, Journal of Air & Waste Management Association, 56, 500-511.

Ge, X., A. Setyan, Y. Sun, and Q. Zhang, 2012, Primary and secondary organic aerosols in Fresno, California during wintertime: Results from high resolution aerosol mass spectrometry, J. Geophys. Res., 117, D19301, doi:10.1029/2012JD018026.

Gillies, R. R., S. Wang, and M. R. Booth, 2010, Atmospheric scale interaction on wintertime intermountain west low-level inversions, Weather Forecasting, 25, 1196 – 1210.

Guo, L., et al, 2020, Assessment of nitrogen oxide emissions and San Joaquin Valley PM2.5 impacts from soils in California, Journal of Geophysical Research, https://doi.org/10.1029/2020JD033304.

Hering, S., Cass, G., 1999, The magnitude of bias in the measurement of PM2.5 arising from volatilization of particulate nitrate from Teflon filters, Journal of Air & Waste Management Association, 49, 725-733.

Hu, J., Howard, C. J., Mitloehner, F., Green, P. G., Kleeman, M. J., 2012, Mobile Source and Livestock Feed Contributions to Regional Ozone Formation in Central California, Environmental Science & Technology, 46, 2781-2789.

Hudman, R. C.; Moore, N. E.; Mebust, A. K.; Martin, R. V.;Russell, A. R.; Valin, L. C.; Cohen, R. C., 2012, Steps towards a mechanistic model of global soil nitric oxide emissions: implementation and space based-constraint, Atmos. Chem. Phys.2012,12(16), 7779−7795.

Jackson, B.S., Chau, D., Gurer, K., Kaduwela, A., 2006, Comparison of ozone simulations using MM5 and CALMET/MM5 hybrid meteorological fields for the July/August 2000 CCOS episode, Atmospheric Environment, 40, 2812-2822.

Jin, L., N. J. Brown, R. A. Harley, J-W. Bao, S. A. Michelson, and J. M. Wilczak, 2010, Seasonal versus episodic performance evaluation for an Eulerian photochemical air quality model, Journal of Geophysical Research: Atmospheres, 115, D09302.

Jin, L., S. Tonse, D. S. Cohan, X Mao, R. A. Harley, and N. J. Brown, 2008, Sensitivity analysis of ozone formation and transport for a central California air pollution episode, Environmental Science and Technology, 3683-3689.

Kelly, J.T., J. Avise, C. Cai, and A. Kaduwela, 2010, Simulating particle size distributions over California and impact on lung deposition fraction, Aerosol Science and Technology, 148-162.

Kelly, J. T., et al., 2014, Fine-scale simulation of ammonium and nitrate over the South Coast Air Basin and San Joaquin Valley of California during CalNex-2010, Journal of Geophysical Research, 119, 3600-3614, doi:10.1002/2013JD021290.

Kleeman, M.J., Ying, Q., Kaduwela, A., 2005, Control strategies for the reduction of airborne particulate nitrate in California's San Joaquin Valley, Atmospheric Environment, 39, 5325-5341.

Livingstone, P.L., K. Magliano, K. Gurer, P.D. Allen, K.M. Zhang, Q. Ying, and B.S. Jackson et al., 2009, Simulating PM concentration during a winter episode in a

subtropical valley: Sensitivity simulations and evaluation methods, Atmospheric Environment, 5971-5977.

Lurmann, F.W., Brown, S.G., McCarthy, M.C., Roberts, P.T., 2006, Processes Influencing Secondary Aerosol Formation in the San Joaquin Valley during Winter, Journal of Air and Waste Management Association, 56, 1679-1693.

Markovic, M. Z., VandenBoer, T. C., Baker, K. R., Kelly, J. T., Murphy, J. G., 2014, Measurements and modeling of the inorganic chemical composition of fine particulate matter and associated precursor gases in California's San Joaquin Valley during CalNex 2010, Journal of Geophysical Research - Atmosphere,119, 6853–6866, doi:10.1002/2013JD021408.

Meng, Z., Dabdub, D., Seinfeld, J.H., 1997, Chemical coupling between atmospheric ozone and particulate matter, Science, 277, 116-119.

Parworth, C.L., Young, D.E., Kim, H., Zhang, X., Cappa, C.D., Collier, S., Zhang, Q., 2017, Wintertime water-soluble aerosol composition and particle water content in Fresno, California, Journal of Geophysical Research, Atmosphere, 10.1002/2016JD026173.

Prabhakar, G., Parworth, C., Zhang, X., Kim, H., Young, D., Beyersdorf, A.J., Ziemba, L.D., Nowak, J.B., Bertram, T.H., Faloona, I.C., Zhang, Q., Cappa, C.D., 2017, Observational assessment of the role of nocturnal residual-layer chemistry in determining daytime surface particulate nitrate concentrations, Atmospheric Chemistry Physics, https://doi.org/10.5194/acp-17-14747-2017.

Pun, B.K., Balmori, R.T.F., Seigneur, C., 2009. Modeling wintertime particulate matter formation in central California, Atmospheric Environment 43, 402-409.

Pusede, S.E., et al., 2016, On the effectiveness of nitrogen oxide reductions as a control over ammonium nitrate aerosol, Atmospheric Chemistry Physics, 16, 2575-2596.

Sacramento, 2017, Sacramento Regional 2008 NAAQS 8-Hour Ozone Attainment And Reasonalbe Further Progress Plan, available at http://www.airquality.org/ProgramCoordination/Documents/Sac%20Regional%202008%20NAAQS%20Attainment%20and%20RFP%20Plan.pdf.

Sacramento, 2023, Sacramento Regional 2015 NAAQS 8-Hour Ozone Attainment And Reasonalbe Further Progress Plan, available at https://www.airquality.org/ProgramCoordination/Documents/Sacramento%20Regional%202015%20NAAQS%208%20Hour%20Ozone%20Attainment%20and%20Reasonable%20Further%20Progress%20Plan.pdf.

Varoni, and Thiessen Polygons." In Spatial Modeling Principles in Earth Sciences, 57. Springer.

Sha, T., Ma, X., Zhang, H., Janechek, N., Wang, Y., Wang, Y., Garcia, L.C., Jenerette, G.D., Wang, J., 2021, Impact of soil NOx emission on O3 air quality in rural California, Environmental Science & Technology, 55, 7113-7122.

Simon, H., Baker, K.R., and Phillips, S., 2012, Compilation and interpretation of photochemical model performance statistics published between 2006 and 2012, Atmospheric Environment, 61, 124-139.

Skamarock, W. C., Klemp, J. B., Dudhia, J., Gill, D. O., Liu, Z., Berner, J., Huang, X. - yu, 2021, A Description of the Advanced Research WRF Model Version 4.3 (No. NCAR/TN-556+STR). doi:10.5065/1dfh-6p97.

South Coast, 2012, Final 2012 Air Quality Management Plan, available at: http://www.aqmd.gov/home/air-quality/clean-air-plans/air-quality-mgt-plan/final-2012-air-quality-management-plan.

South Coast, 2016, Final 2016 Air Quality Management Plan, available at: http://www.aqmd.gov/docs/default-source/clean-air-plans/air-quality-management-plans/2016-air-quality-management-plan/final-2016-aqmp/cover-and-opening.pdf?sfvrsn=6.

SJV, 2008, 2008 PM2.5 Plan, available at: http://www.valleyair.org/Air_Quality_Plans/AQ_Proposed_PM25_2008.htm.

SJV, 2012, 2012 PM2.5 Plan, available at: http://www.valleyair.org/Air_Quality_Plans/PM25Plans2012.htm.

SJV, 2013, 2013 Plan for the Revoked 1-Hour Ozone Standard, available at: http://valleyair.org/Air_Quality_Plans/Ozone-OneHourPlan-2013.htm.

SJV, 2016a, 2016 Moderate Area Plan for the 2012 PM2.5 Standard, available at: http://www.valleyair.org/Air_Quality_Plans/docs/PM25-2016/2016-Plan.pdf.

SJV, 2016b, 2016 Plan for the 2008 8-Hour Ozone Standard, available at: http://valleyair.org/Air_Quality_Plans/Ozone-Plan-2016.htm.

SJV, 2018, 2018 PM2.5 Plan for the San Joaquin Valley, available at: http://valleyair.org/pmplans/documents/2018/pm-plan-adopted/2018-Plan-for-the-1997-2006-and-2012-PM2.5-Standards.pdf.

SJV, 2023, 2023 O3 Plan for the San Joaquin Valley, available at: https://ww2.valleyair.org/media/q55posm0/0000-2022-plan-for-the-2015-8-hour-ozone-standard.pdf.

Tonse, S. R., N. J. Brown, R. A. Harley, and L. Jin, 2008, A process-analysis based study of the ozone weekend effect, Atmospheric Environment 7728-7736.

Turkiewicz, K., Magliano, K; and Najita, T., 2006, Comparison of Two Winter Air Quality Episodes during the California Regional Particulate Air Quality Study, Journal of Air & Waste Management Association, 56, 467-473.

U.S. EPA, 2016, PM2.5 Precursor Demonstration Guidance, available at https://www.epa.gov/sites/production/files/2016-11/documents/transmittal_memo_and_draft_pm25_precursor_demo_guidance_11_17_16.pdf.

U.S. EPA, 2018, Modeling Guidance for Demonstrating Attainment of Air Quality Goals for Ozone, PM2.5 and Regional Haze, available at o3-pm-rh-modeling_guidance-2018.pdf (epa.gov)

Watson, J.G., and Chow, J.C.A., 2002, Wintertime PM2.5 Episode at the Fresno, CA, Supersite; Atmospheric Environment, 36, 465-475.

West, J.J., Ansari, A.S., Pandis, S.N., 1999, Marginal PM2.5: Nonlinear aerosol mass response to sulfate reductions in the eastern United States, Journal of the Air & Waste Management Association, 49, 1415-1424.

Whiteman, C. D., Zhong, S., Shaw, W. J., Hubbe, J. M., Bian, X., Mittelstadt, J., 2001, Cold pools in the Columbia Basin. Weather Forecasting, 16, 432–447.

Yienger, J.J., Levy II, H., 1995, Empirical model of global soil-biogenic NOx emissions, Journal of Geophysical Research-Atmosphere, https://doi.org/10.1029/95JD00370.

Young, D.E., Kim, H., Parworth, C., Zhou, S., Zhang, X., Cappa, C.D., Seco, R., Kim, S., and Zhang, Q., 2016, Influences of emission sources and meteorology on aerosol chemistry in a polluted urban environment: results from DISCOVER-AQ California, Atmospheric Chemistry Physics, 16, 5427-5451.

Zhu, Q., et al., 2023, Direct observations of NOx emissions over the San Joaquin Valley using airborne flux measurements during RECAP-CA 2021 field campaign, Atmospheric Chemistry Physics Discussion, https://doi.org/10.5194/acp-2023-3.

VII. Supplemental Materials

Supplemental Materials List of Figures

Figure S 1. Time series of temperature, relative humidity, wind speed, and wind direction for San Joaquin Valley in January 2017.

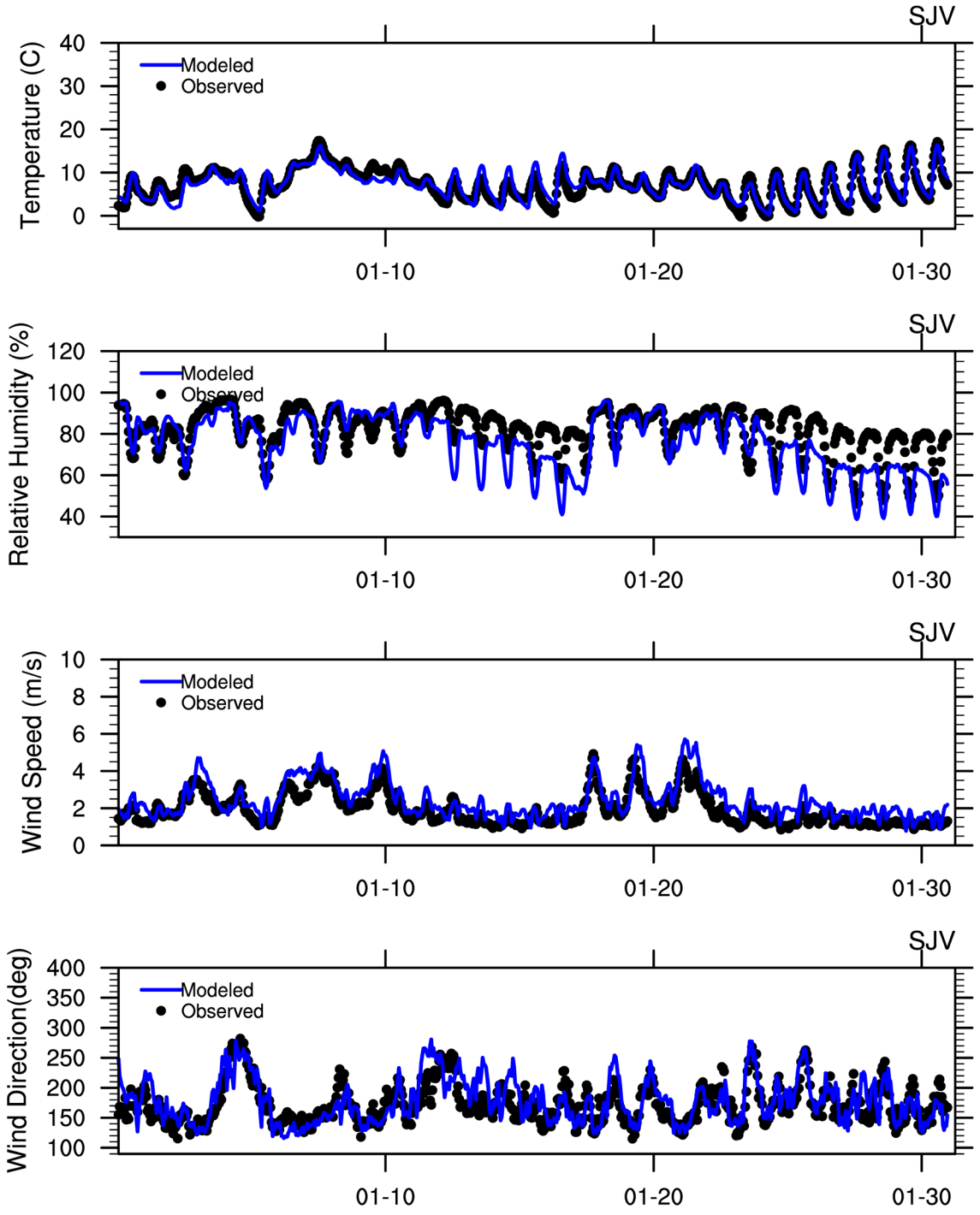

Figure S 2. Time series of temperature, relative humidity, wind speed, and wind direction for San Joaquin Valley in February 2017.

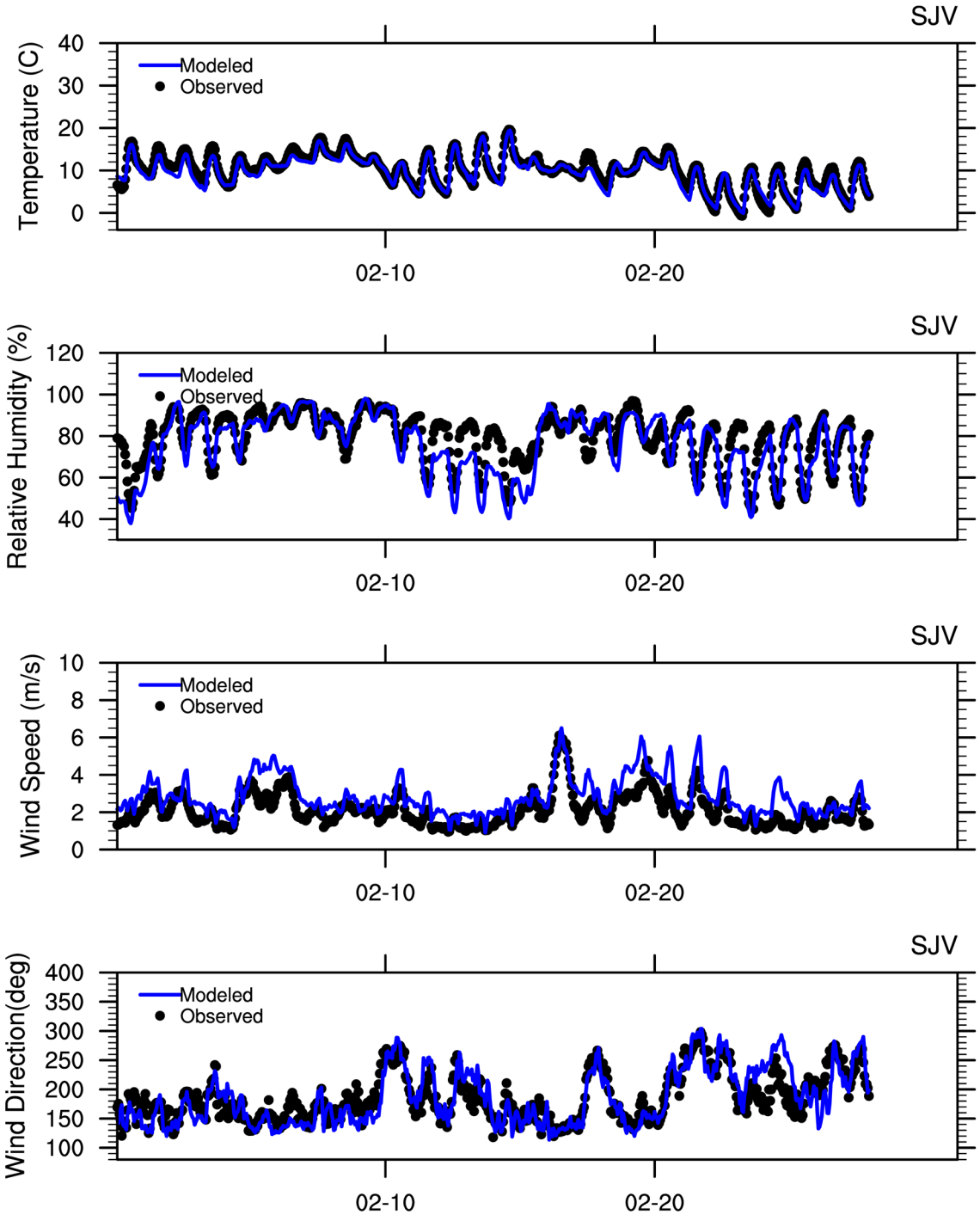

Figure S 3. Time series of temperature, relative humidity, wind speed, and wind direction for San Joaquin Valley in March 2017.

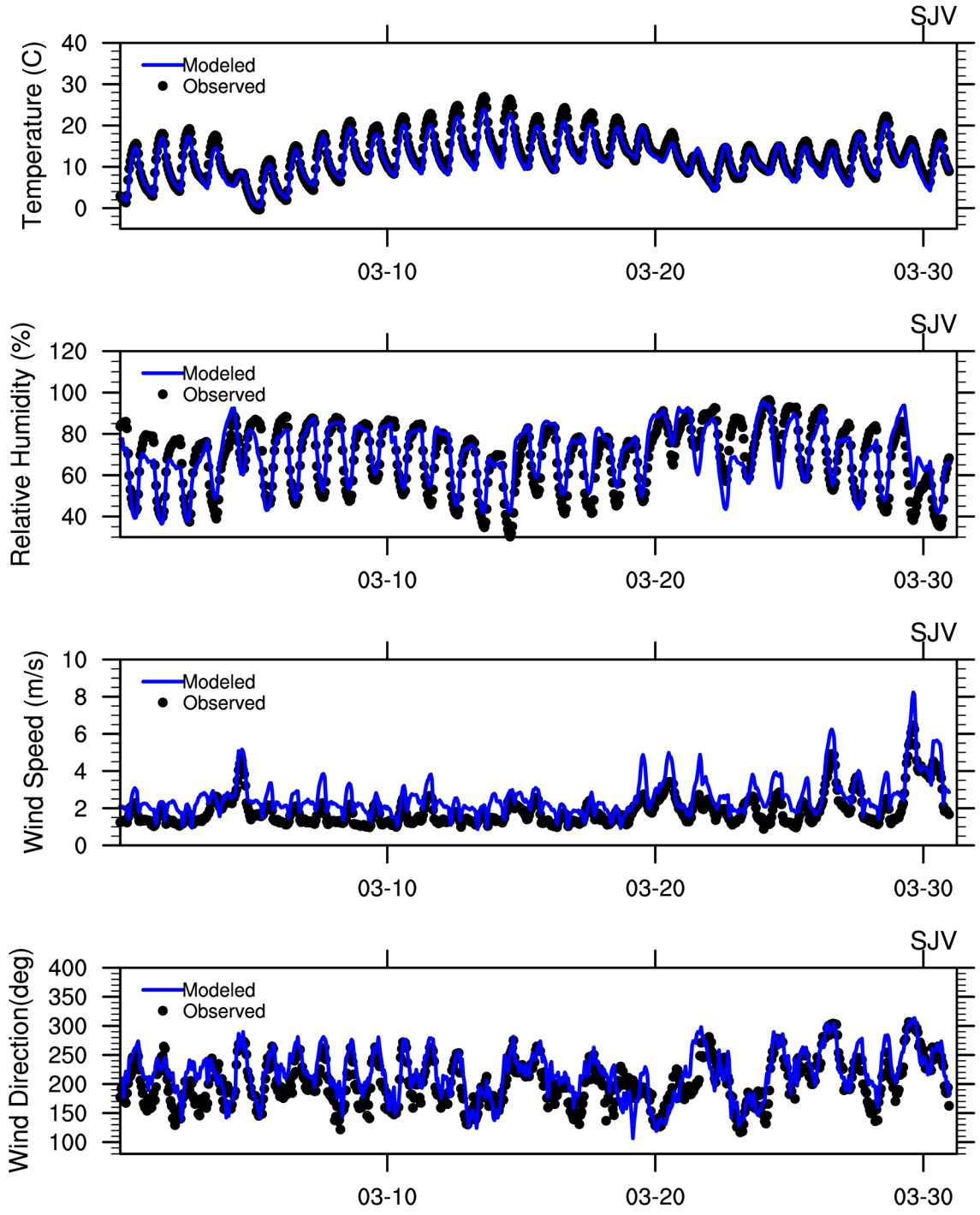

Figure S 4. Time series of temperature, relative humidity, wind speed and wind direction for San Joaquin Valley in April 2017.

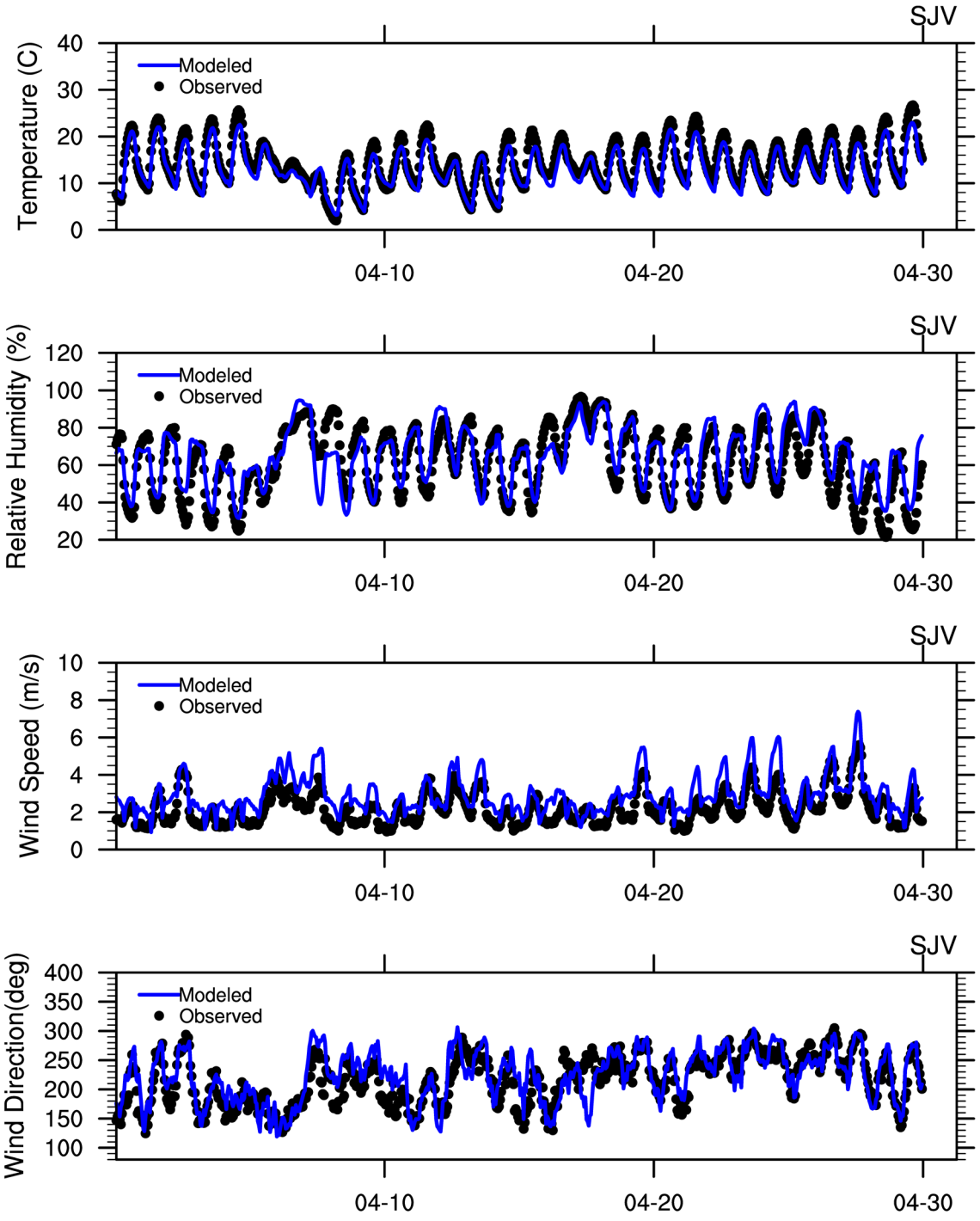

Figure S 5. Time series of temperature, relative humidity, wind speed and wind direction for San Joaquin Valley in May 2017.

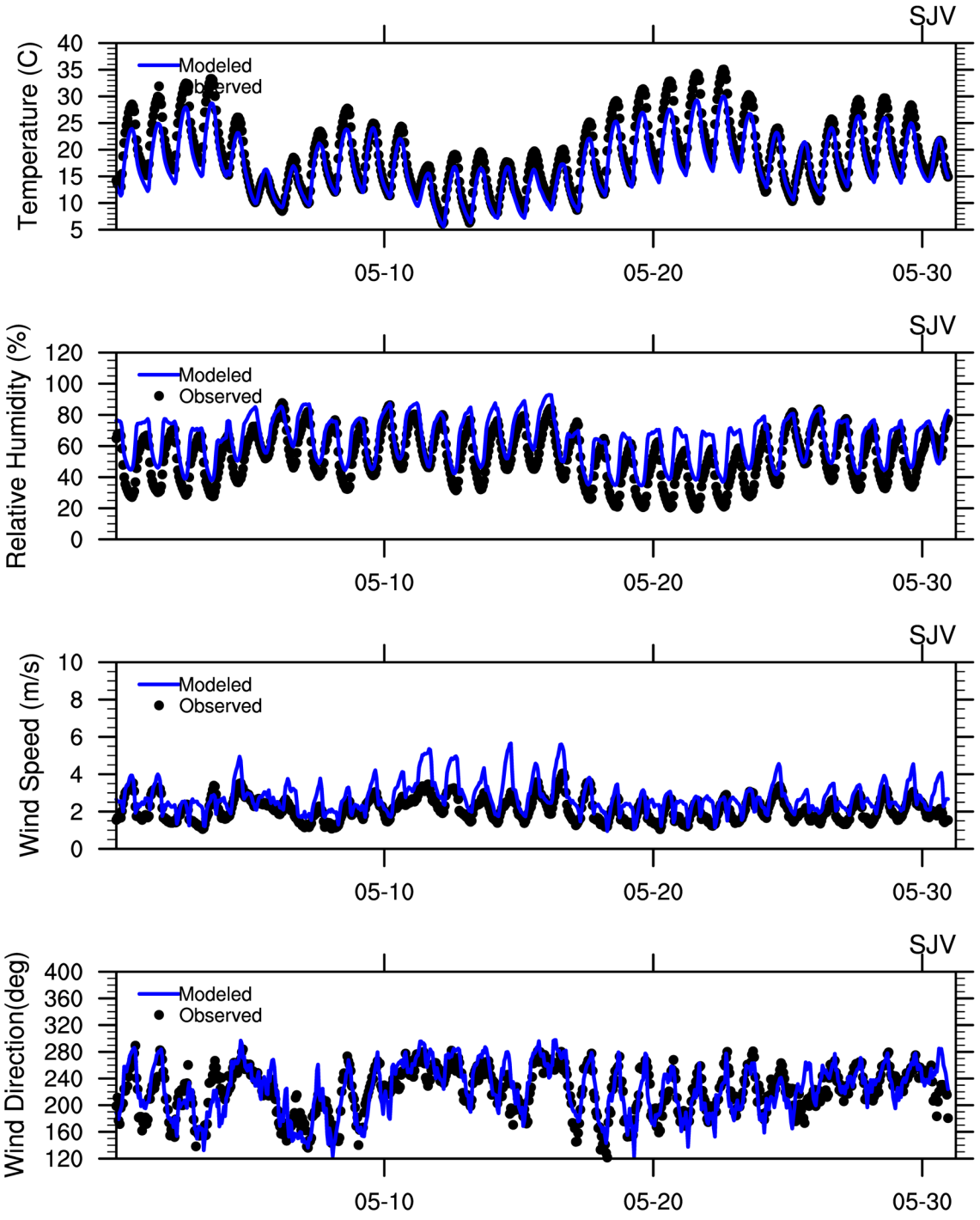

Figure S 6. Time series of temperature, relative humidity, wind speed, and wind direction, for San Joaquin Valley in June 2017.

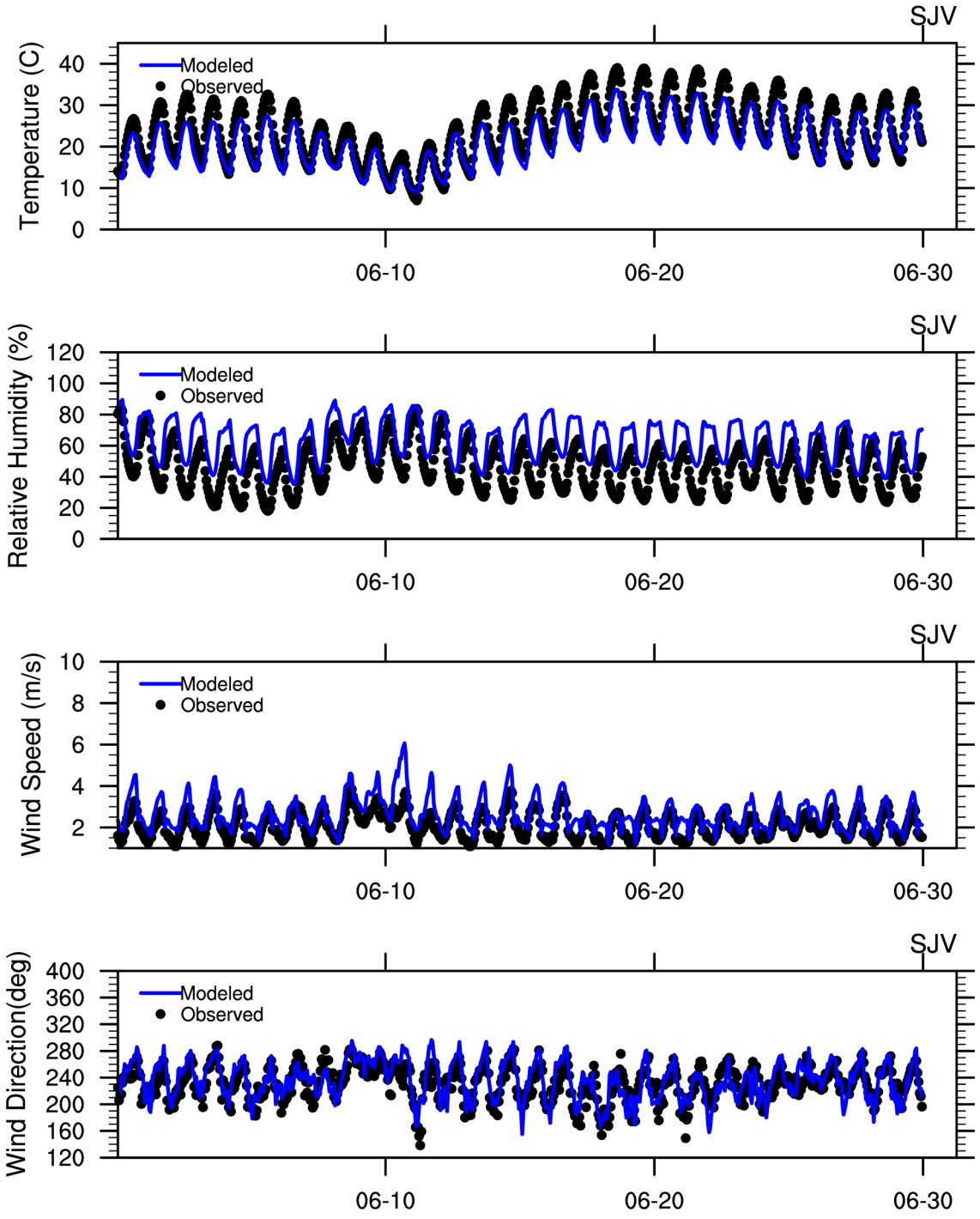

Figure S 7. Time series of temperature, relative humidity, wind speed, and wind direction for San Joaquin Valley in July 2017.

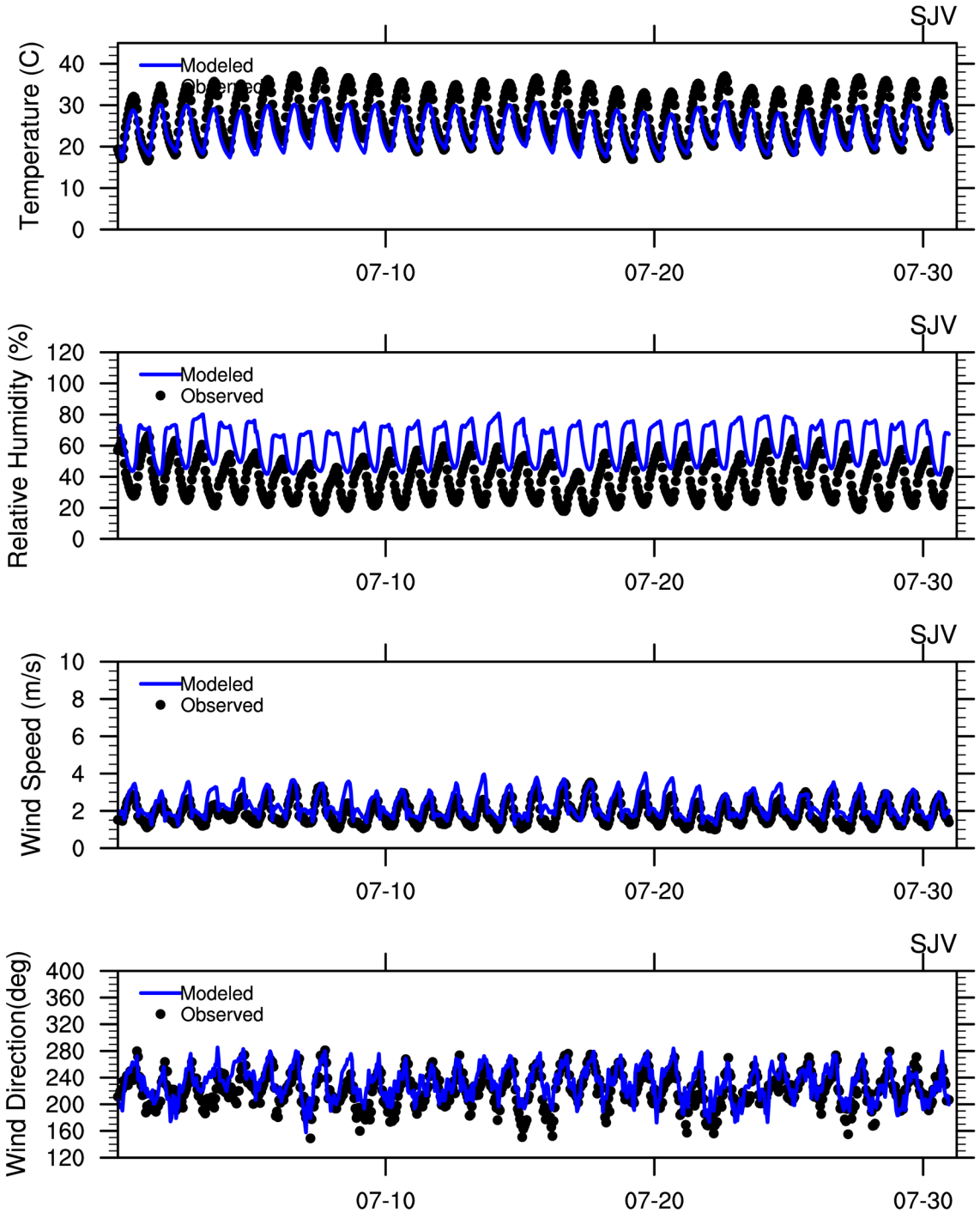

Figure S 8. Time series of temperature, relative humidity, wind speed, and wind direction for San Joaquin Valley in August 2017.

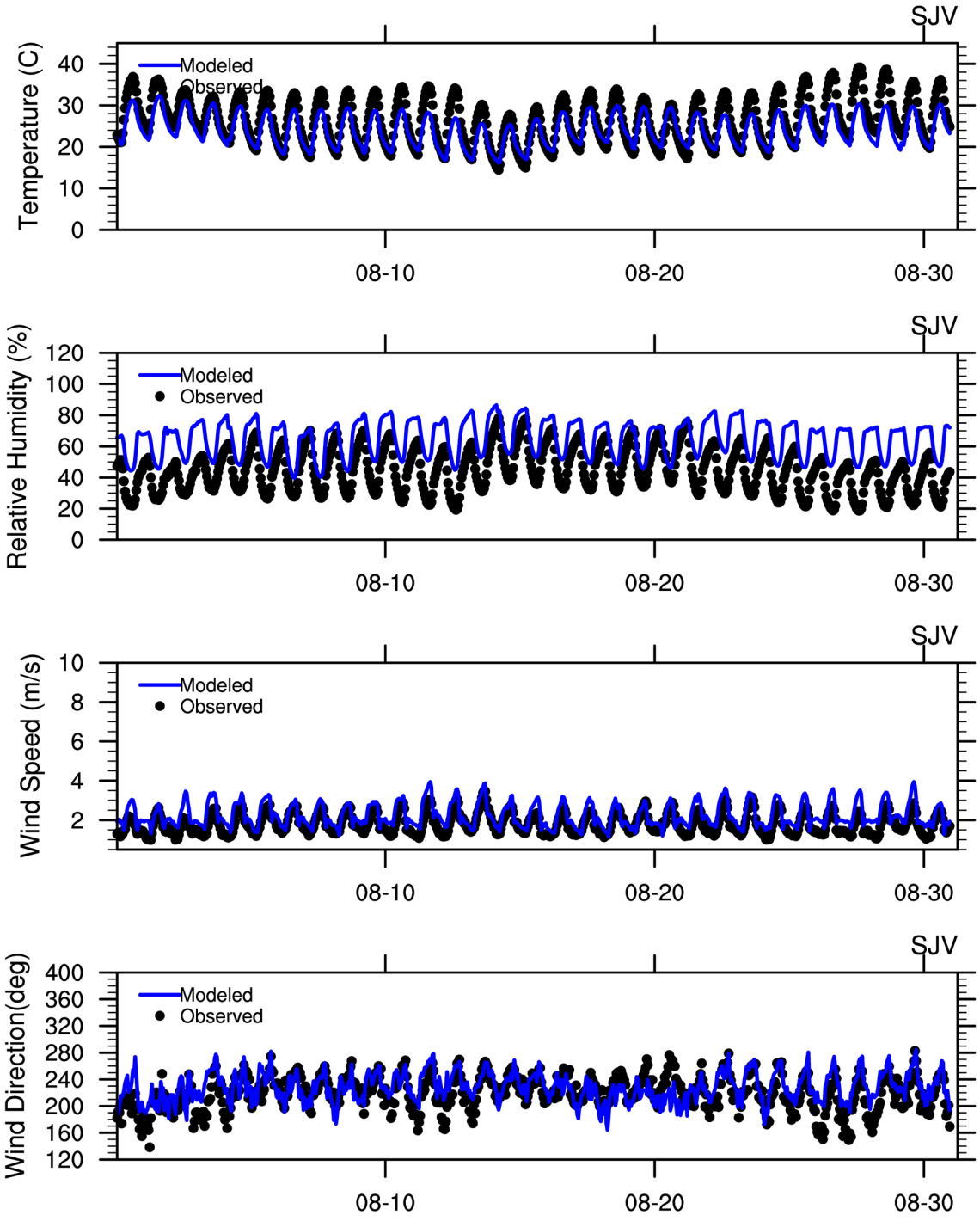

Figure S 9. Time series of temperature, relative humidity, wind speed, and wind direction for San Joaquin Valley in September 2017.

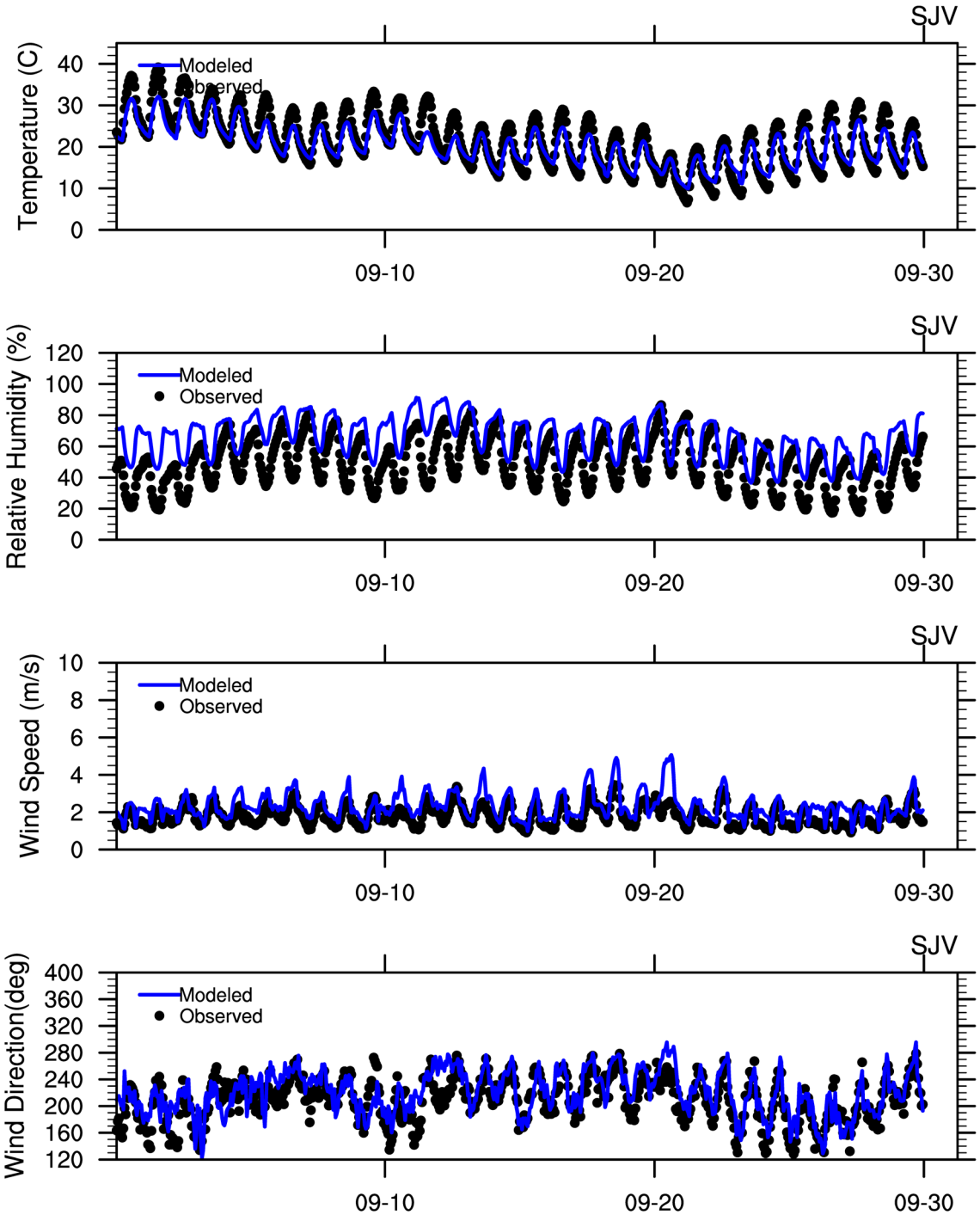

Figure S 10. Time series of temperature, relative humidity, wind speed, and wind direction for San Joaquin Valley in October 2017.

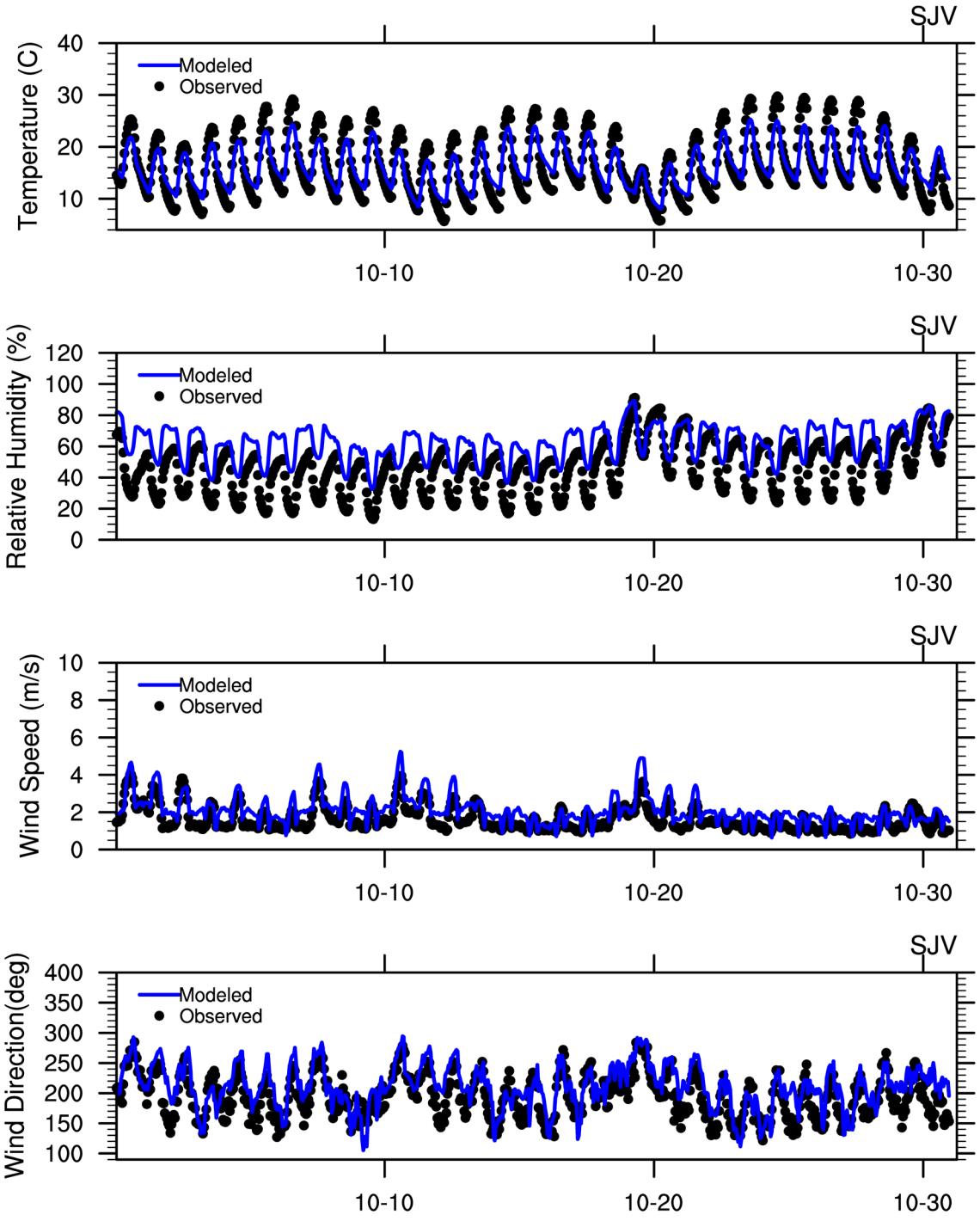

Figure S 11. Time series of wind speed, direction, temperature and relative humidity for San Joaquin Valley in November 2017.

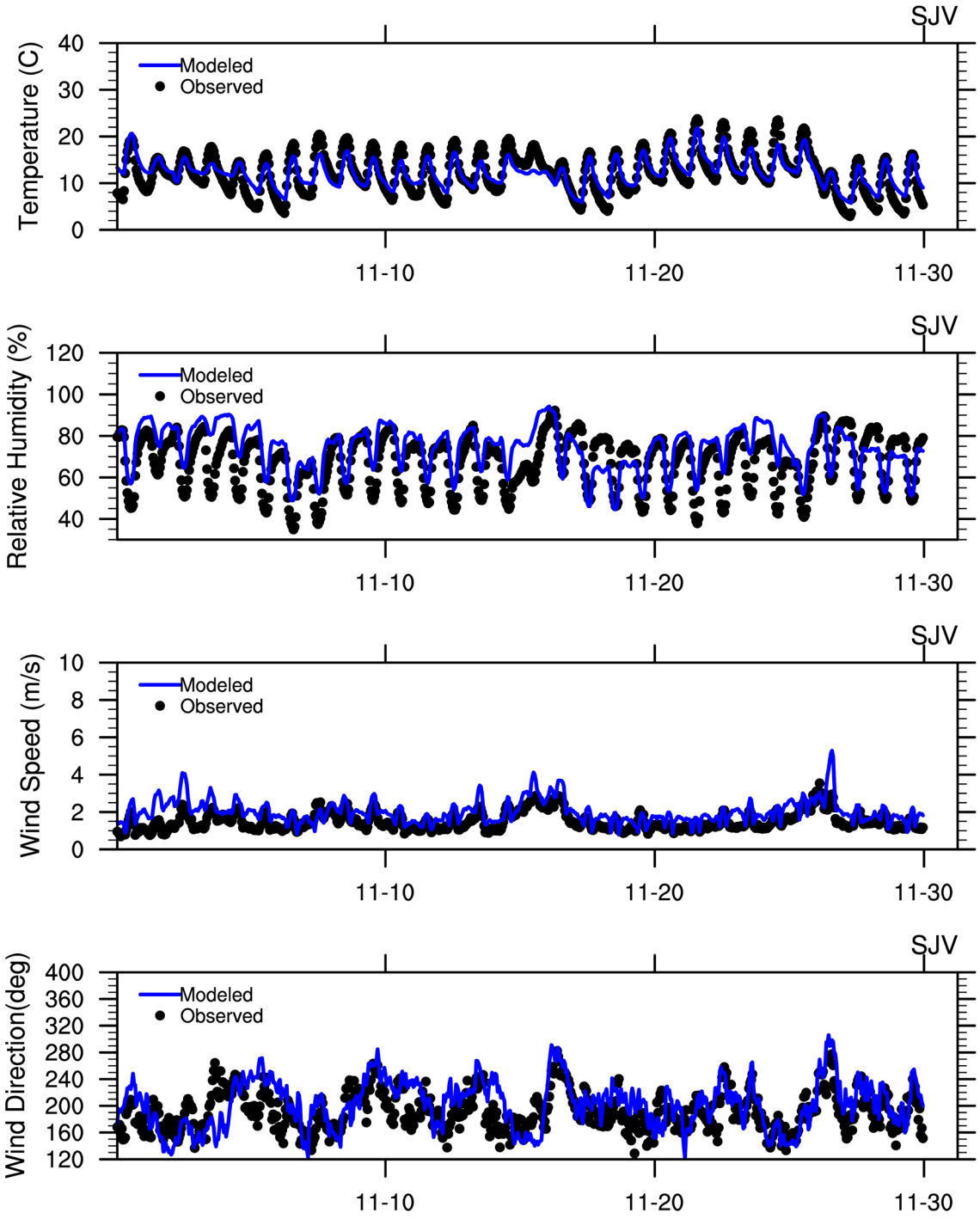

Figure S 12. Time series of temperature, relative humidity, wind speed and wind direction for San Joaquin Valley in December 2017.

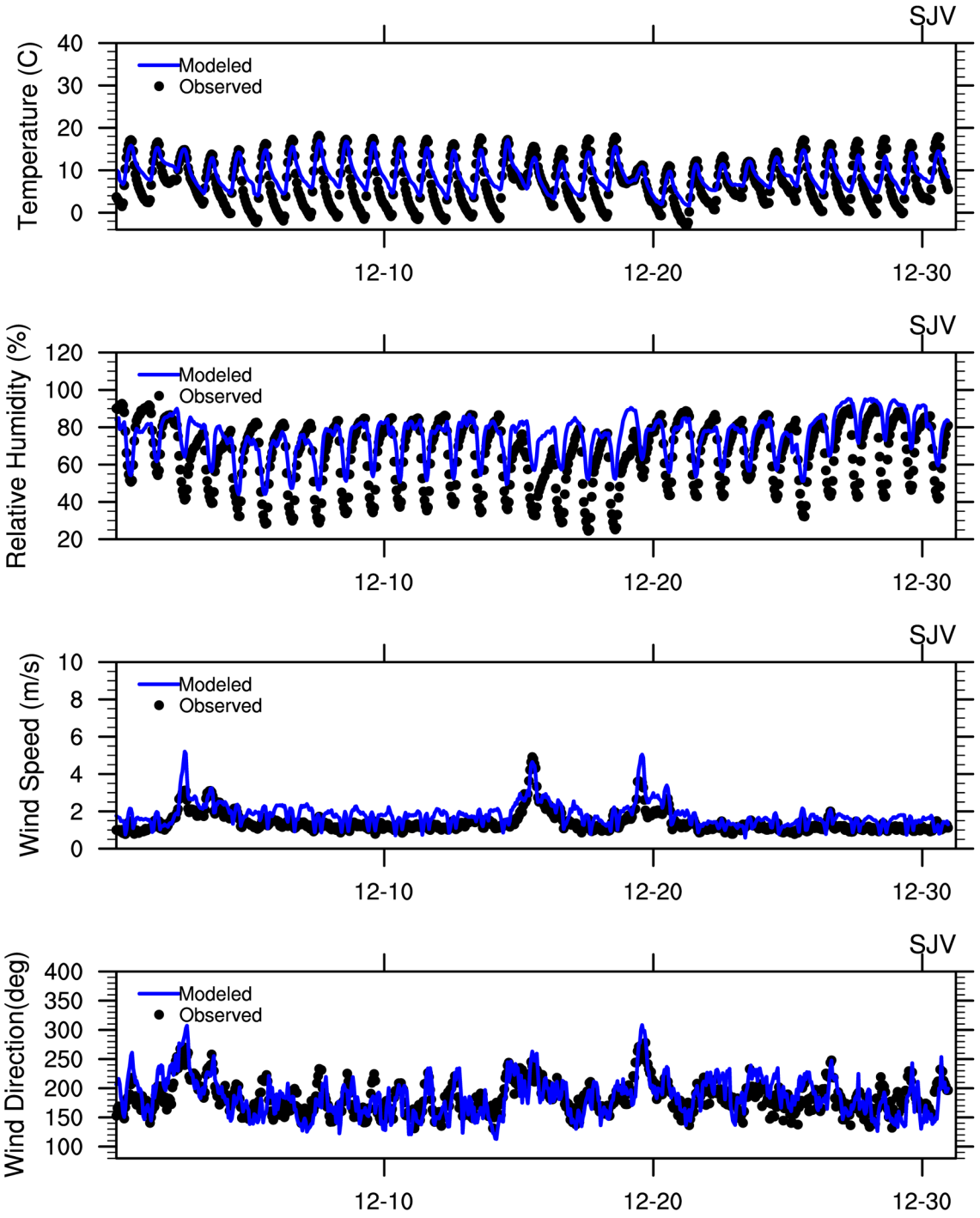

Figure S 13. Hourly surface temperature mean bias in each quarter of 2017.

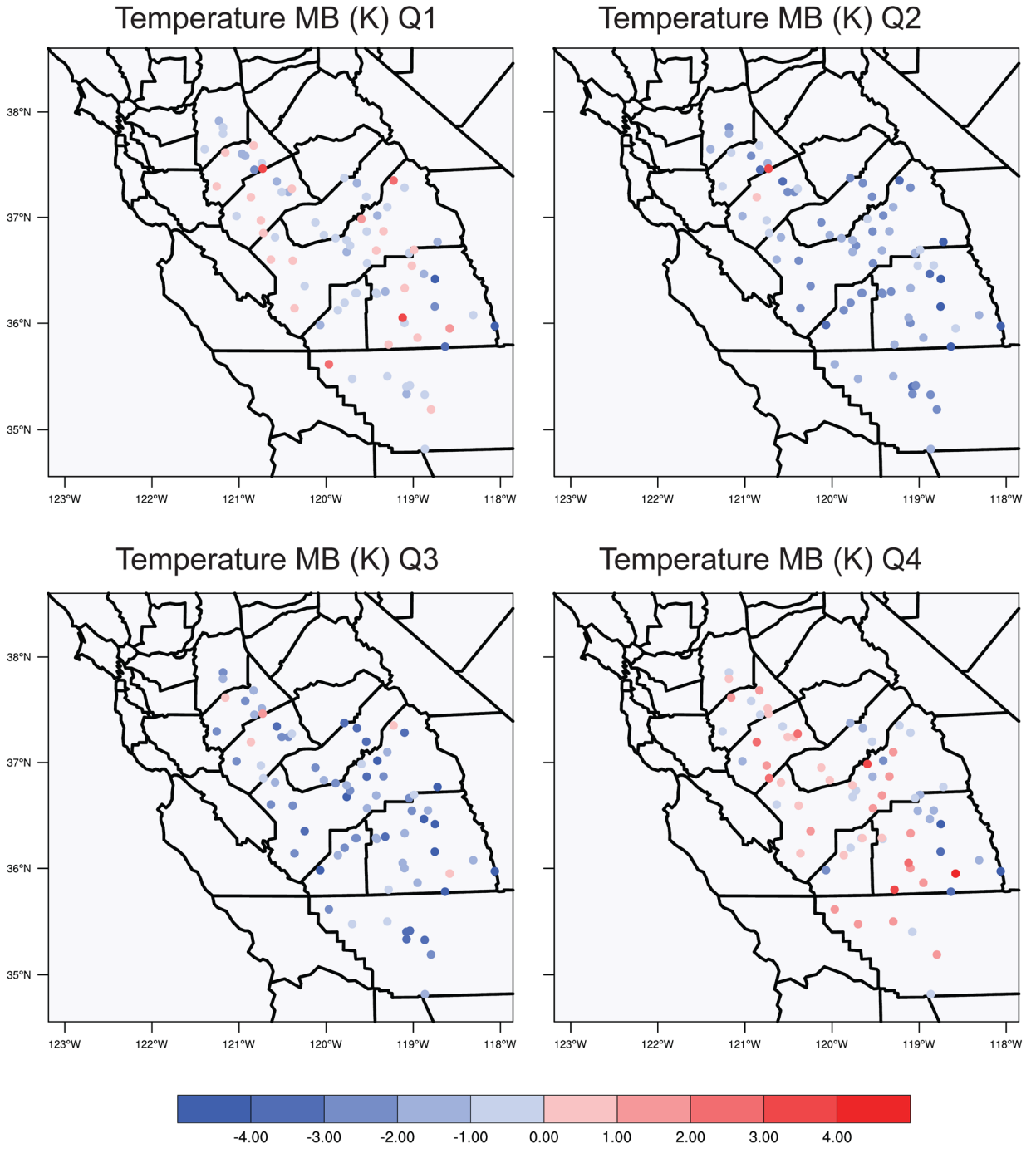

Figure S 14. Hourly surface temperature mean error in each quarter of 2017.

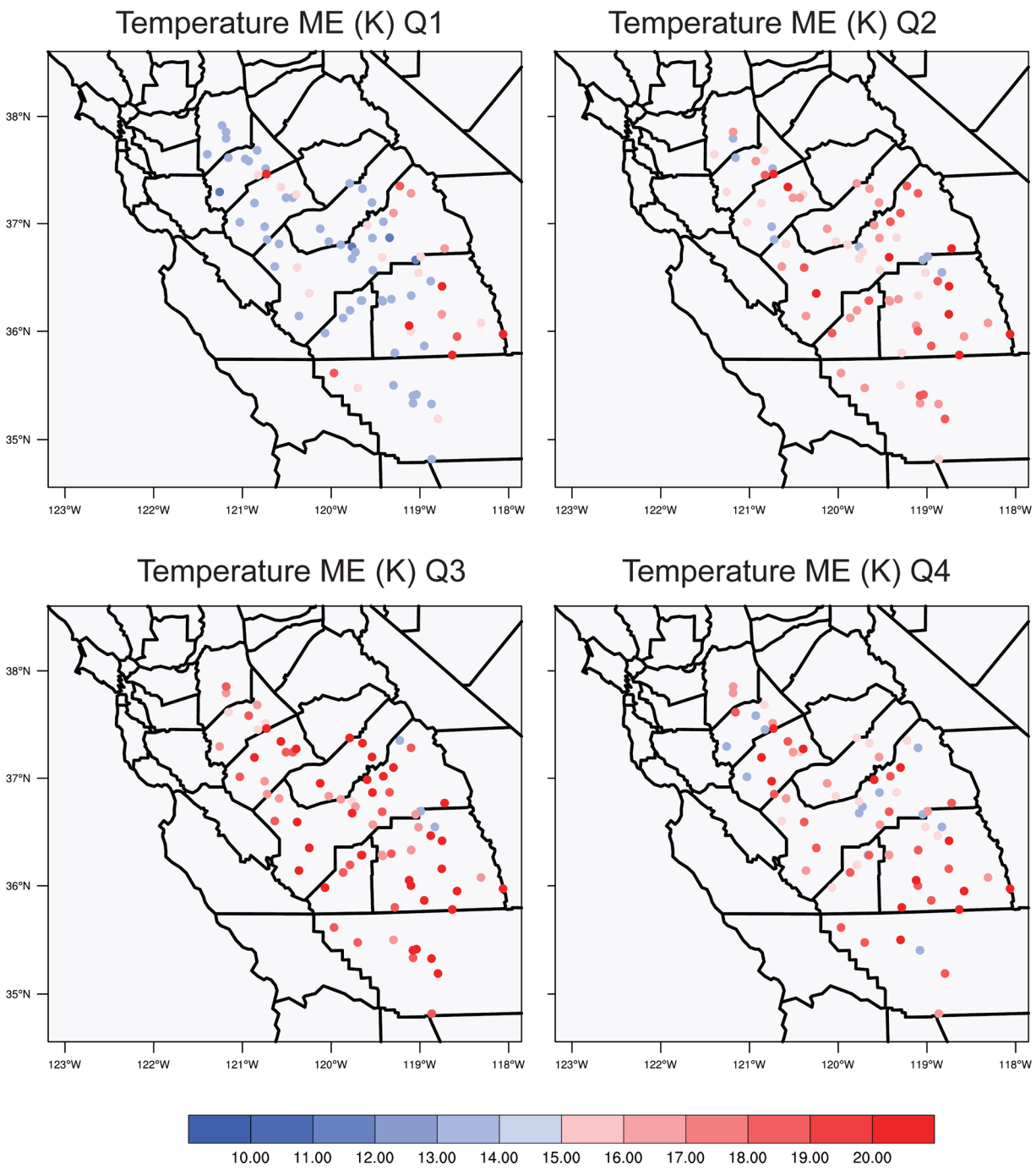

Figure S 15. Hourly surface wind speed mean bias in each quarter of 2017.

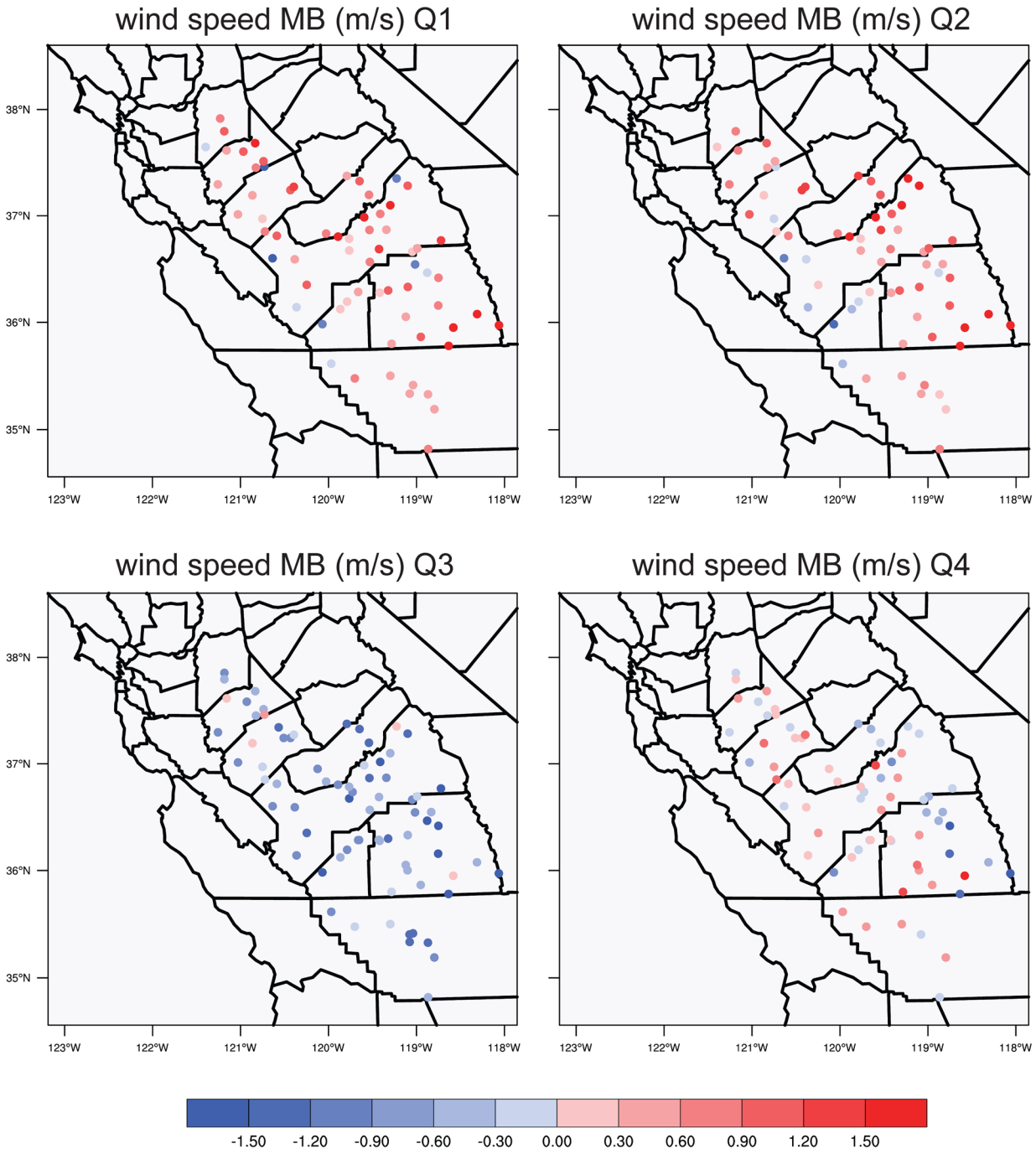

Figure S 16. Hourly surface wind speed mean error in each quarter of 2017.

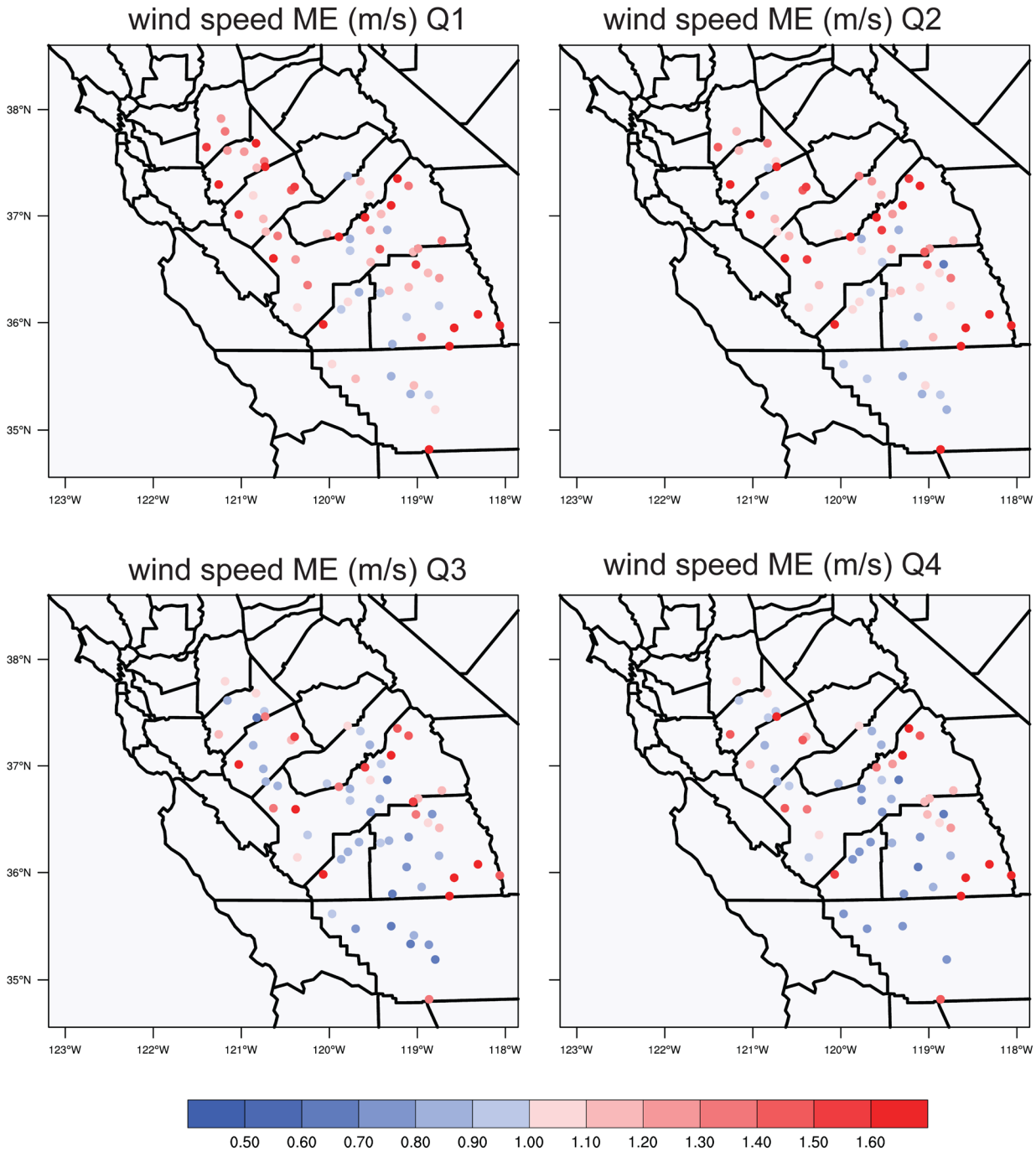

Figure S 17. Hourly surface relative humidity mean bias in each quarter of 2017.

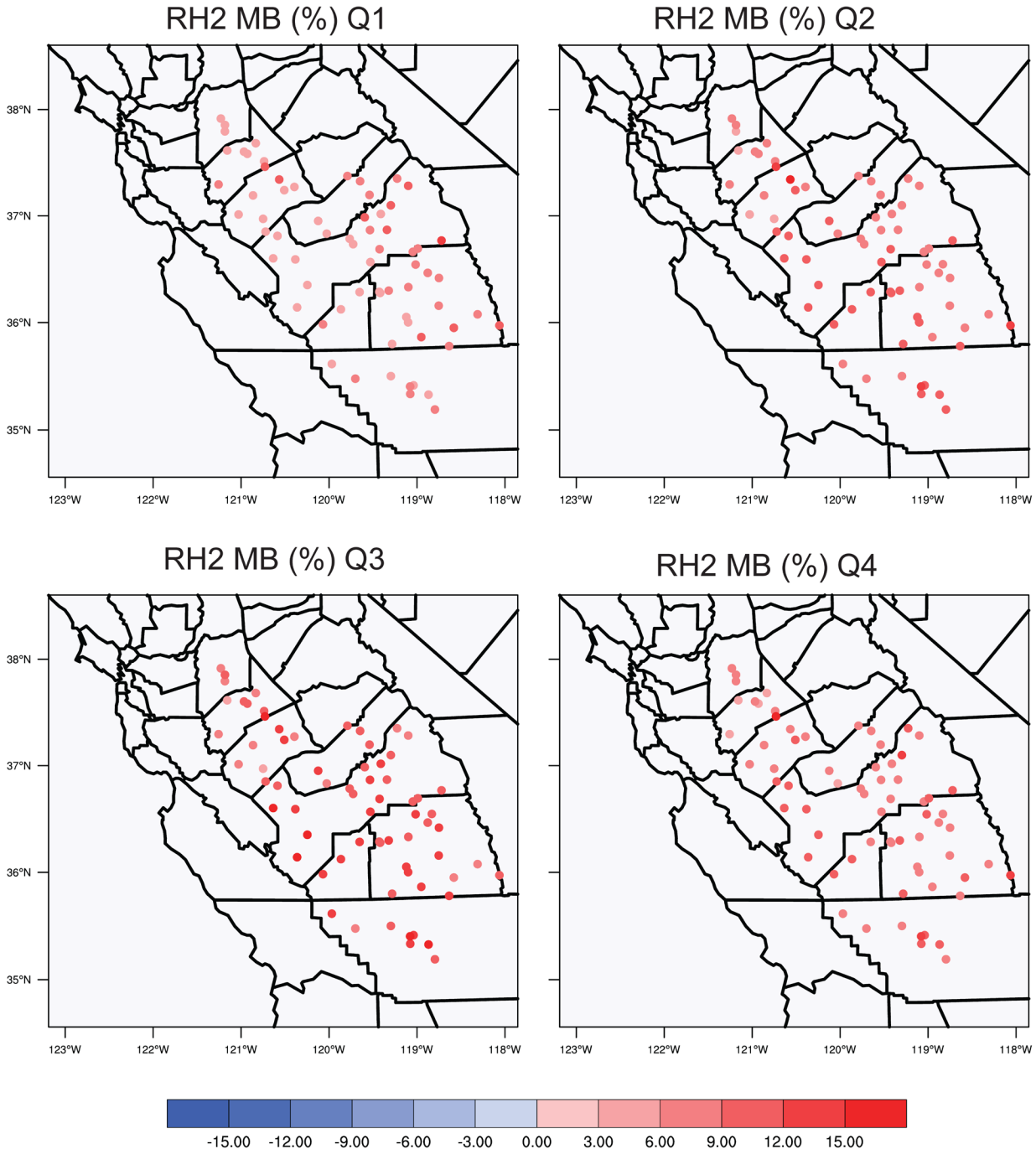

Figure S 18. Hourly surface relative humidity mean error in each quarter of 2017.

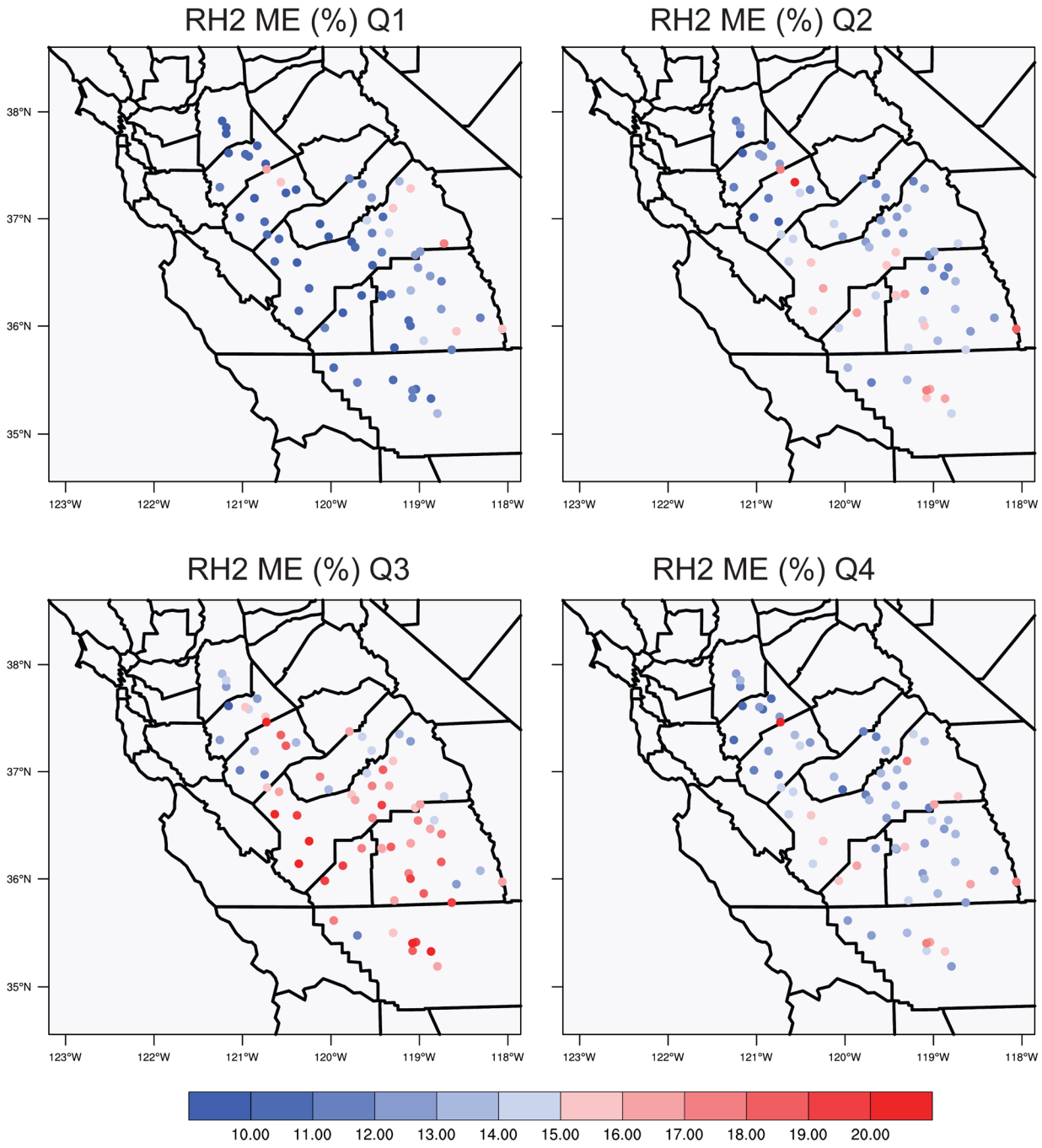

Figure S 19. Hourly precipitation for sites Modesto #3, Fresno State #2, and Belridge for January 2017.

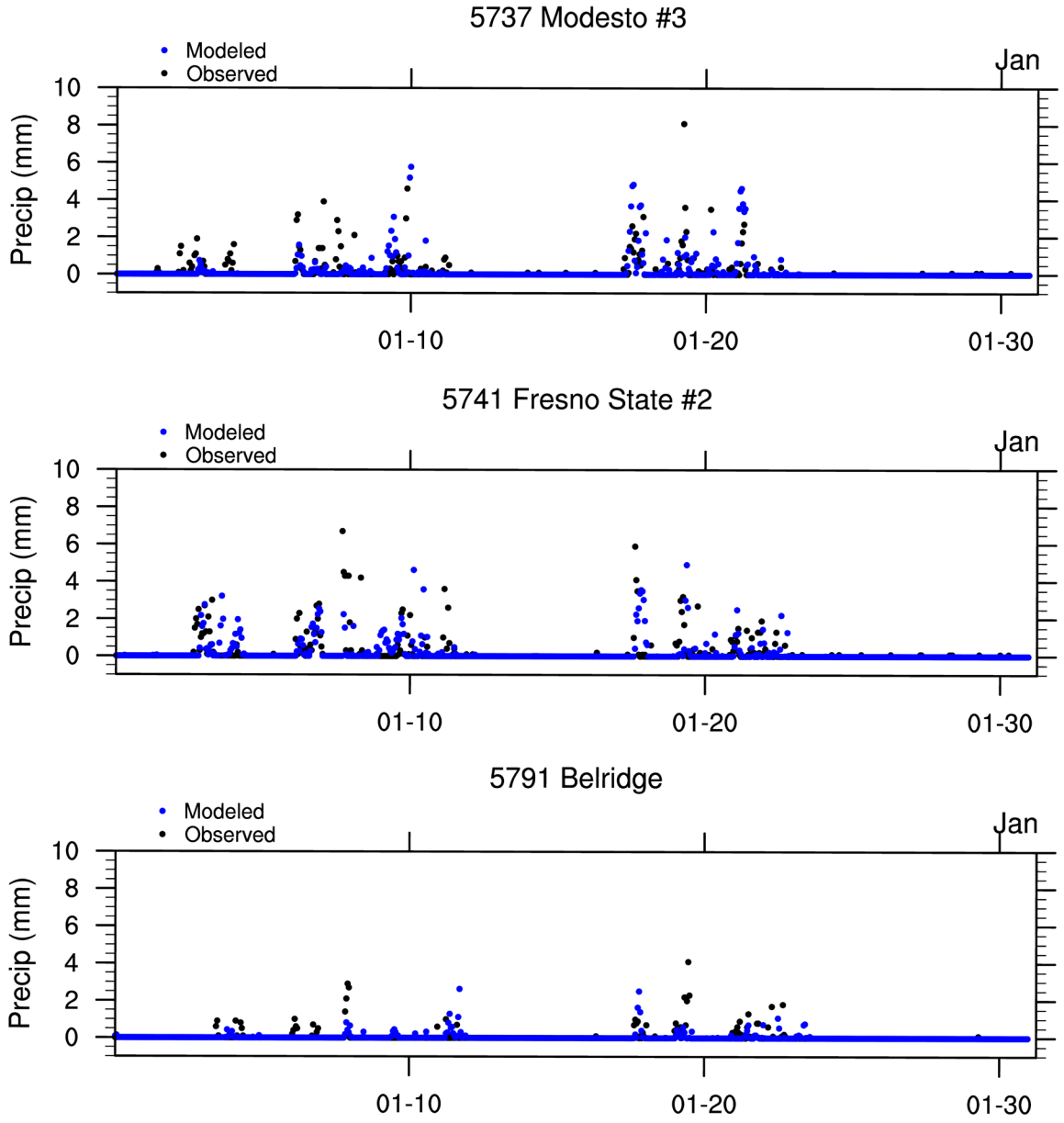

Figure S 20. Same as Figure S 19, but for February 2017.

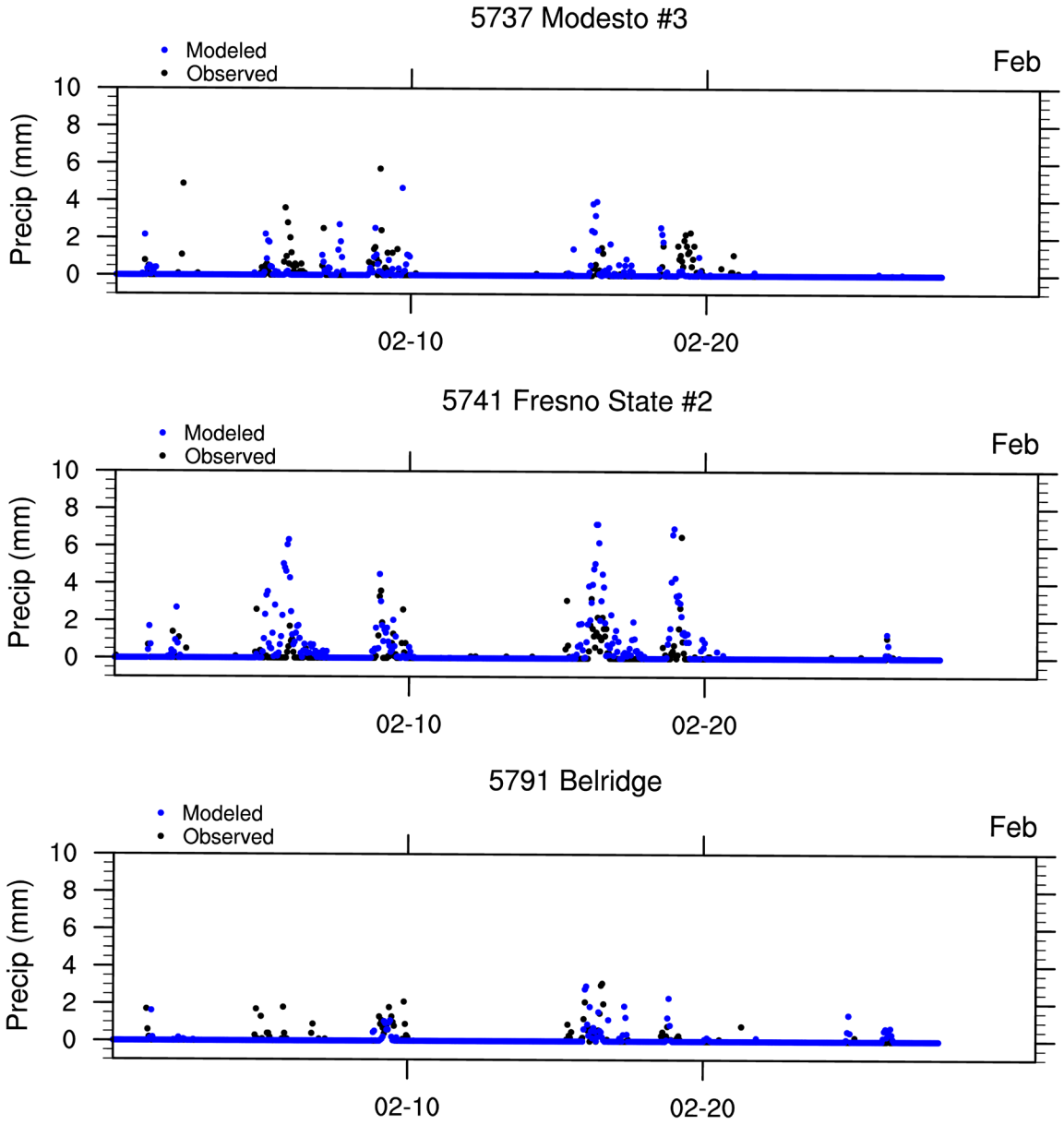

Figure S 21. Same as Figure S 19, but for March 2017.

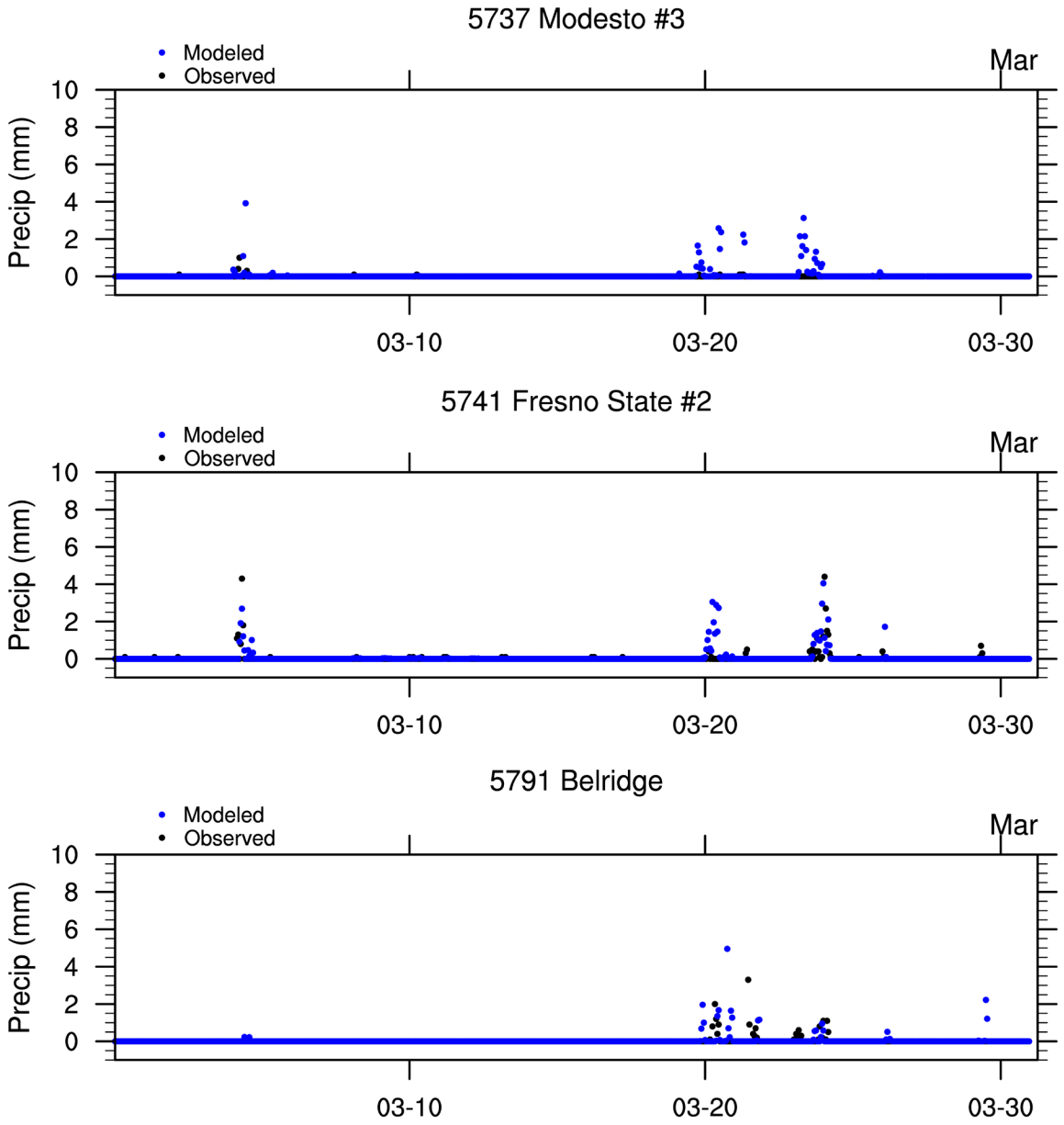

Figure S 22. Same as Figure S 19, but for November 2017.

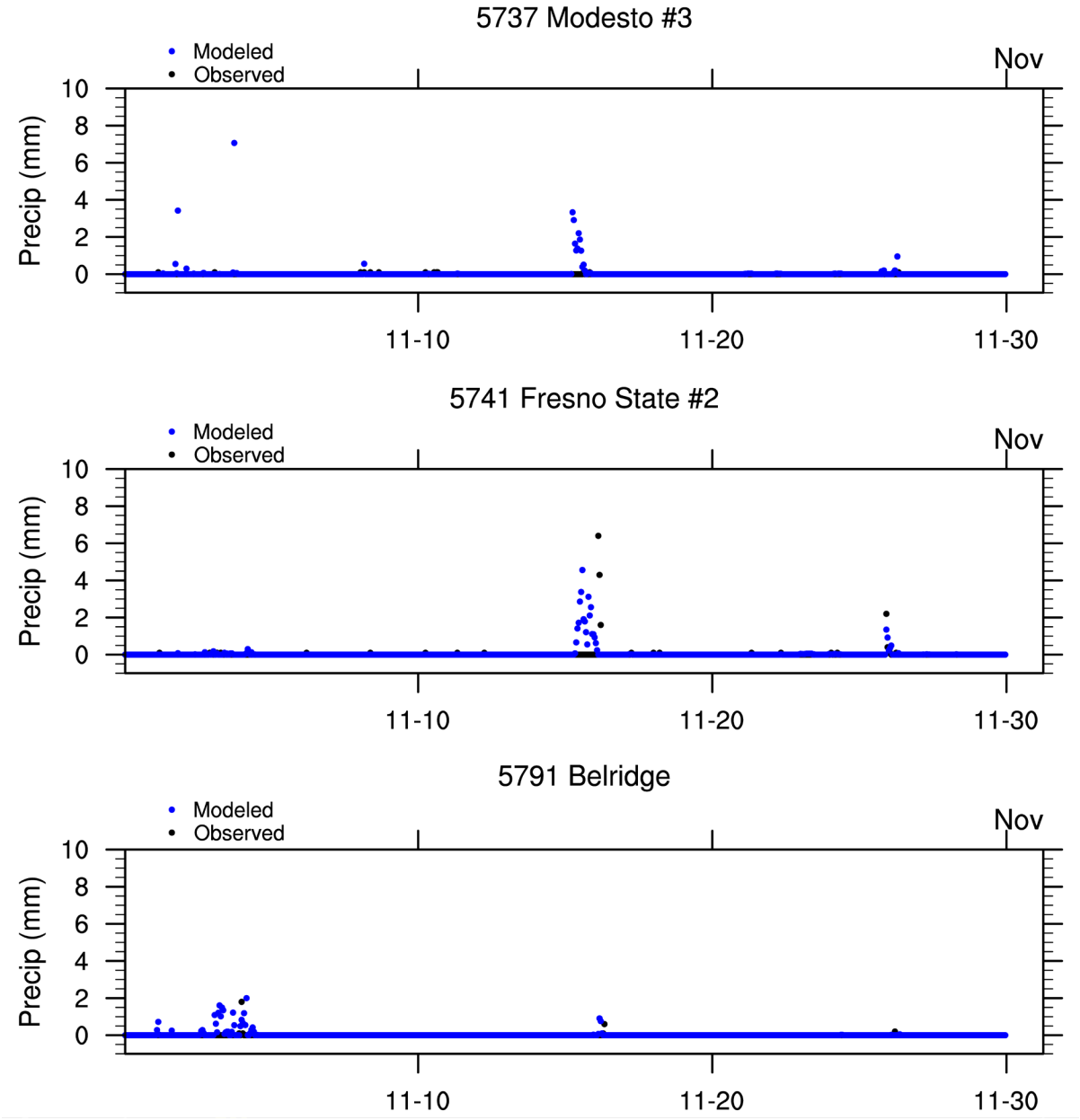

Figure S 23. Same as Figure S 19, but for December 2017.

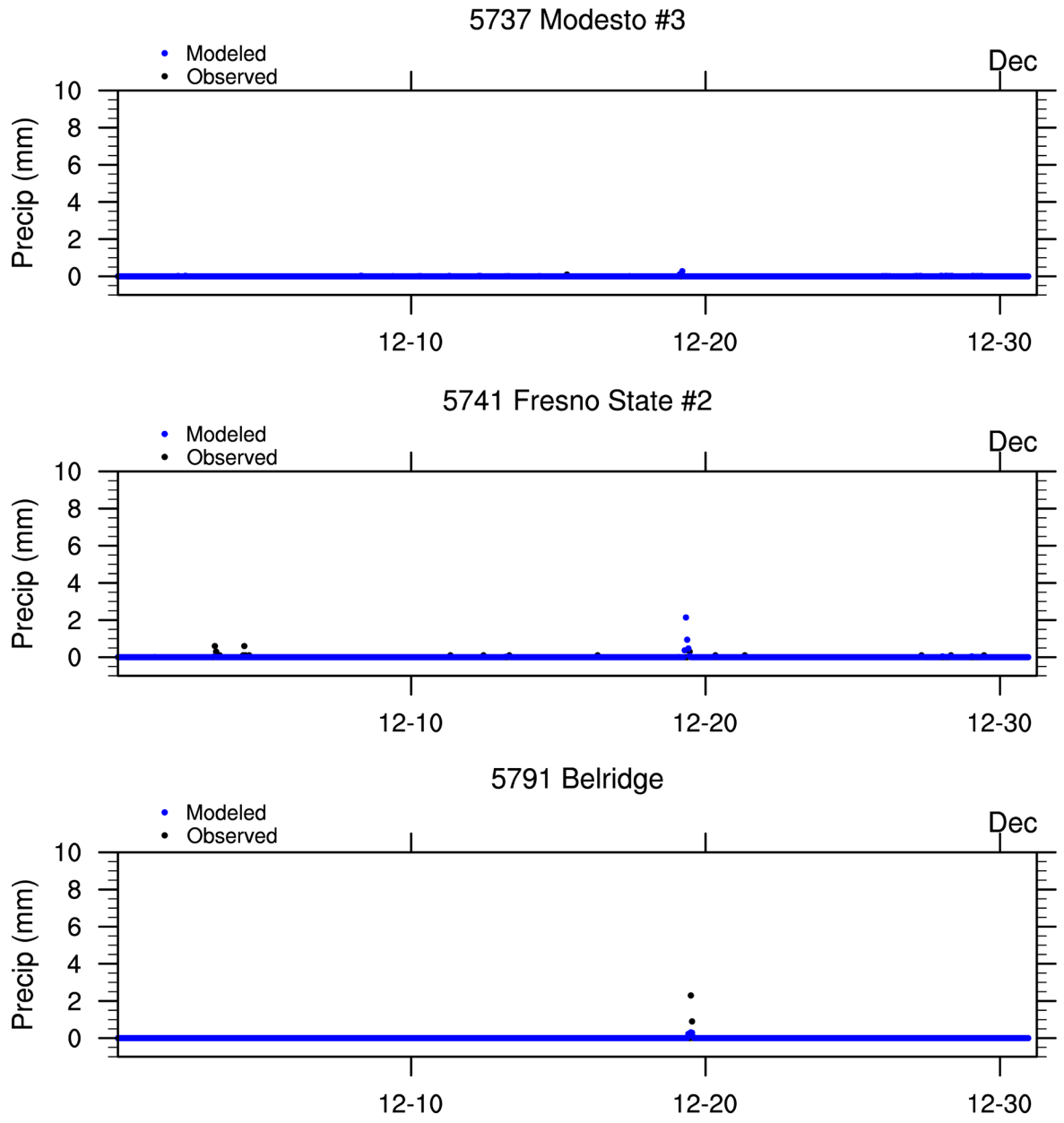

Figure S 24. Comparison of time series of observed (from CSN measurement) and modeled $PM_{2.5}$ species at Bakersfield.

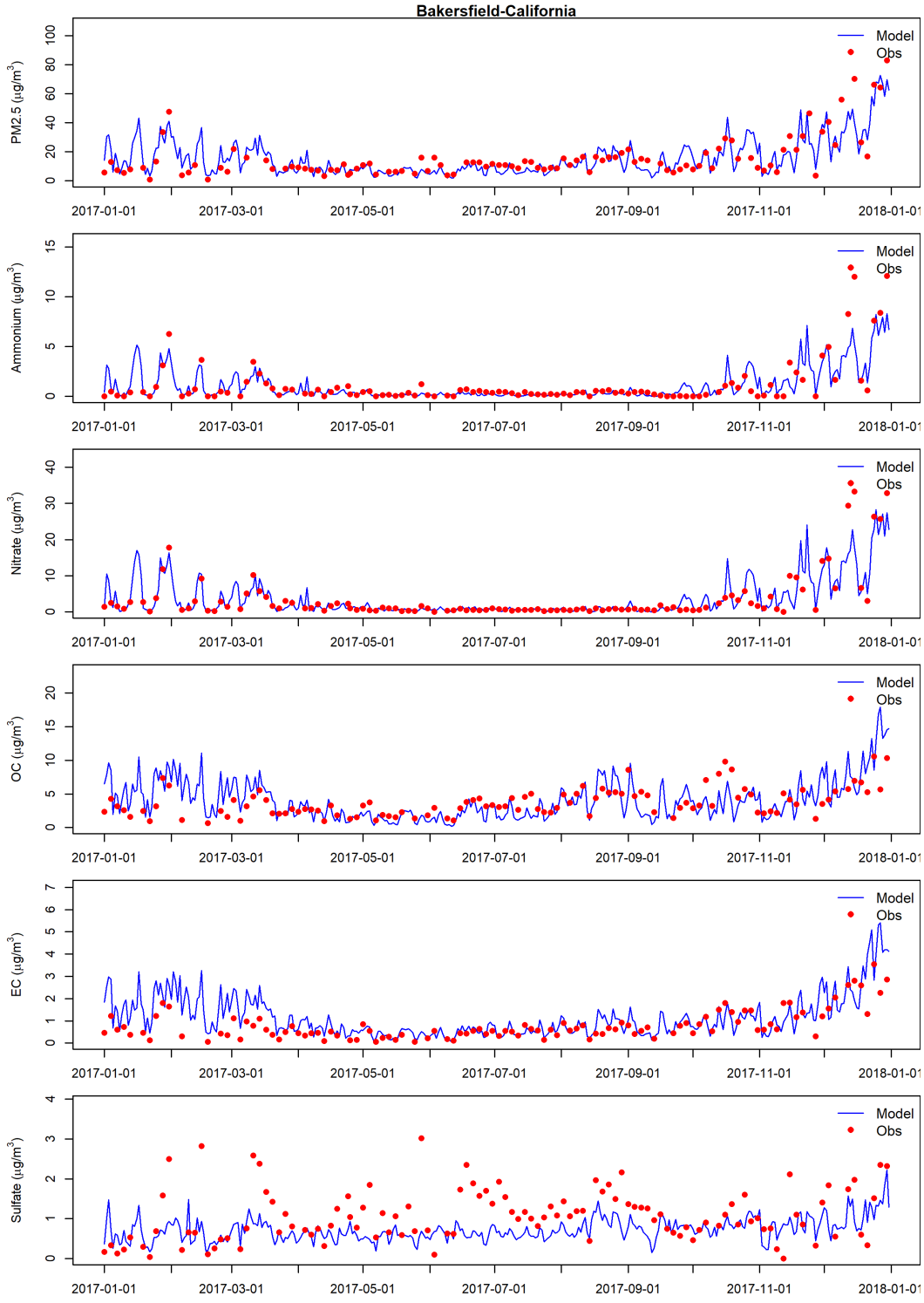

Figure S 25. Comparison of time series of observed (from CSN measurement) and modeled $PM_{2.5}$ species at Fresno.

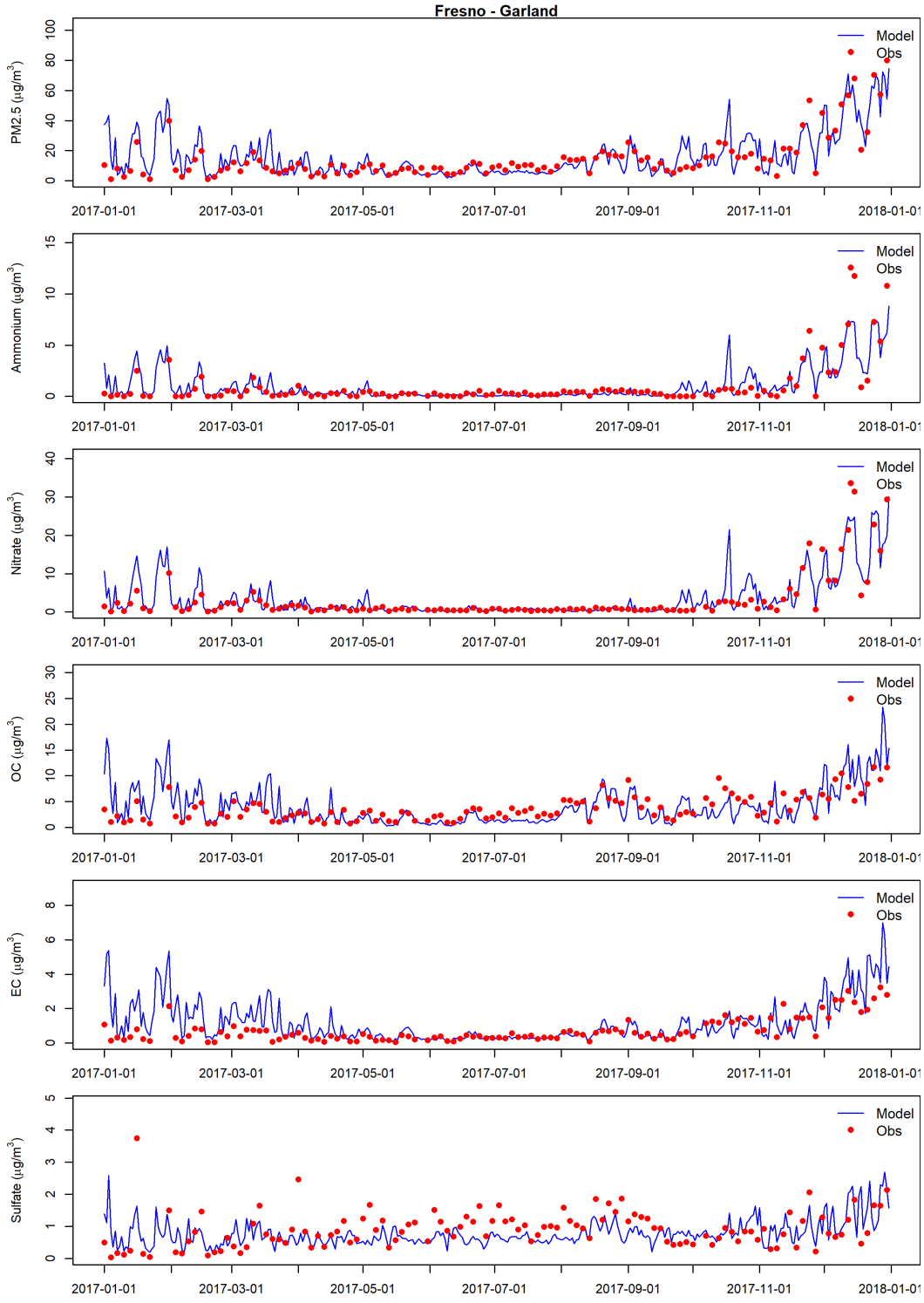

Figure S 26. Comparison of time series of observed (from CSN measurement) and modeled $PM_{2.5}$ species at Visalia.

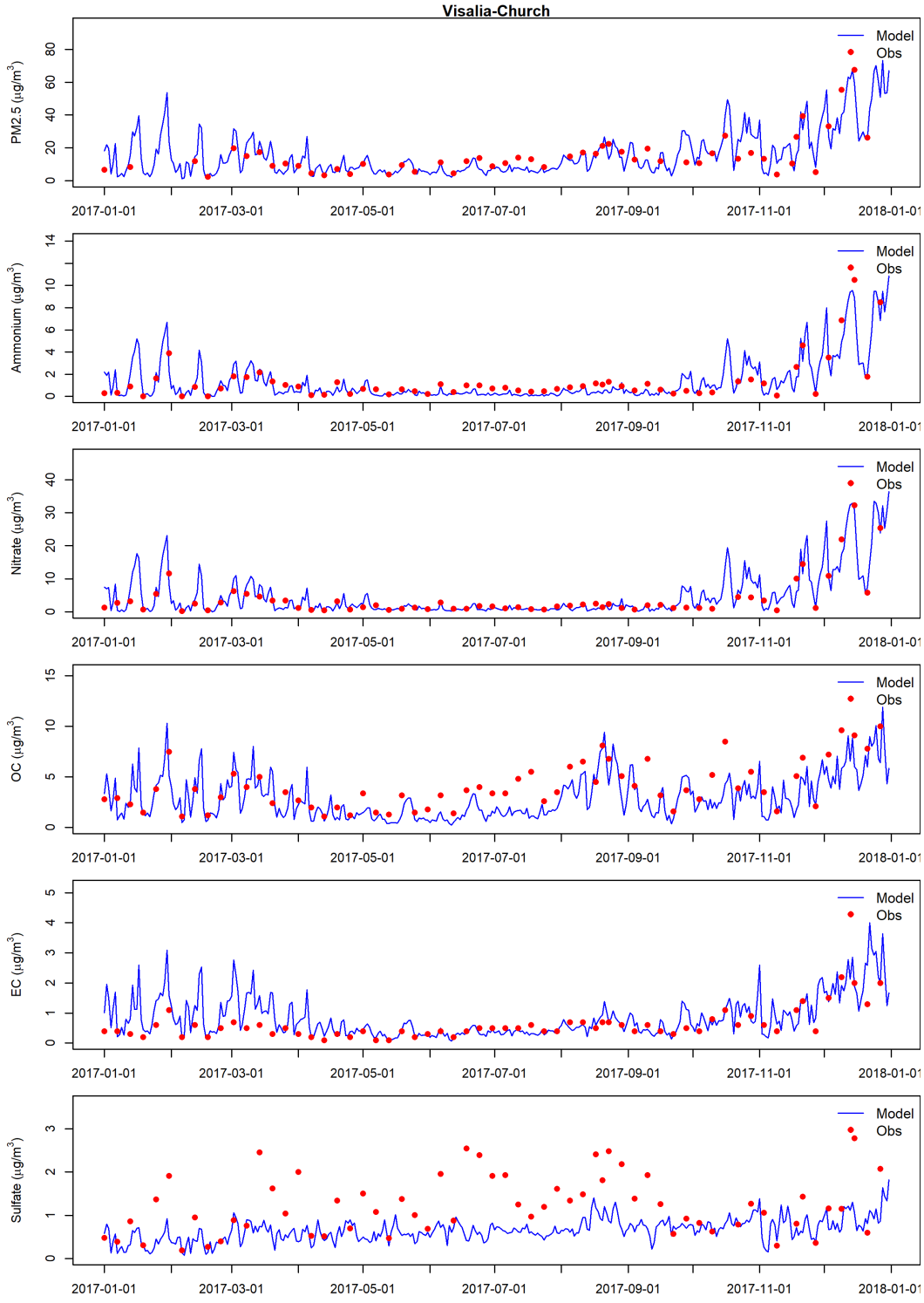

Figure S 27. Comparison of time series of observed (from CSN measurement) and modeled $PM_{2.5}$ species at Modesto

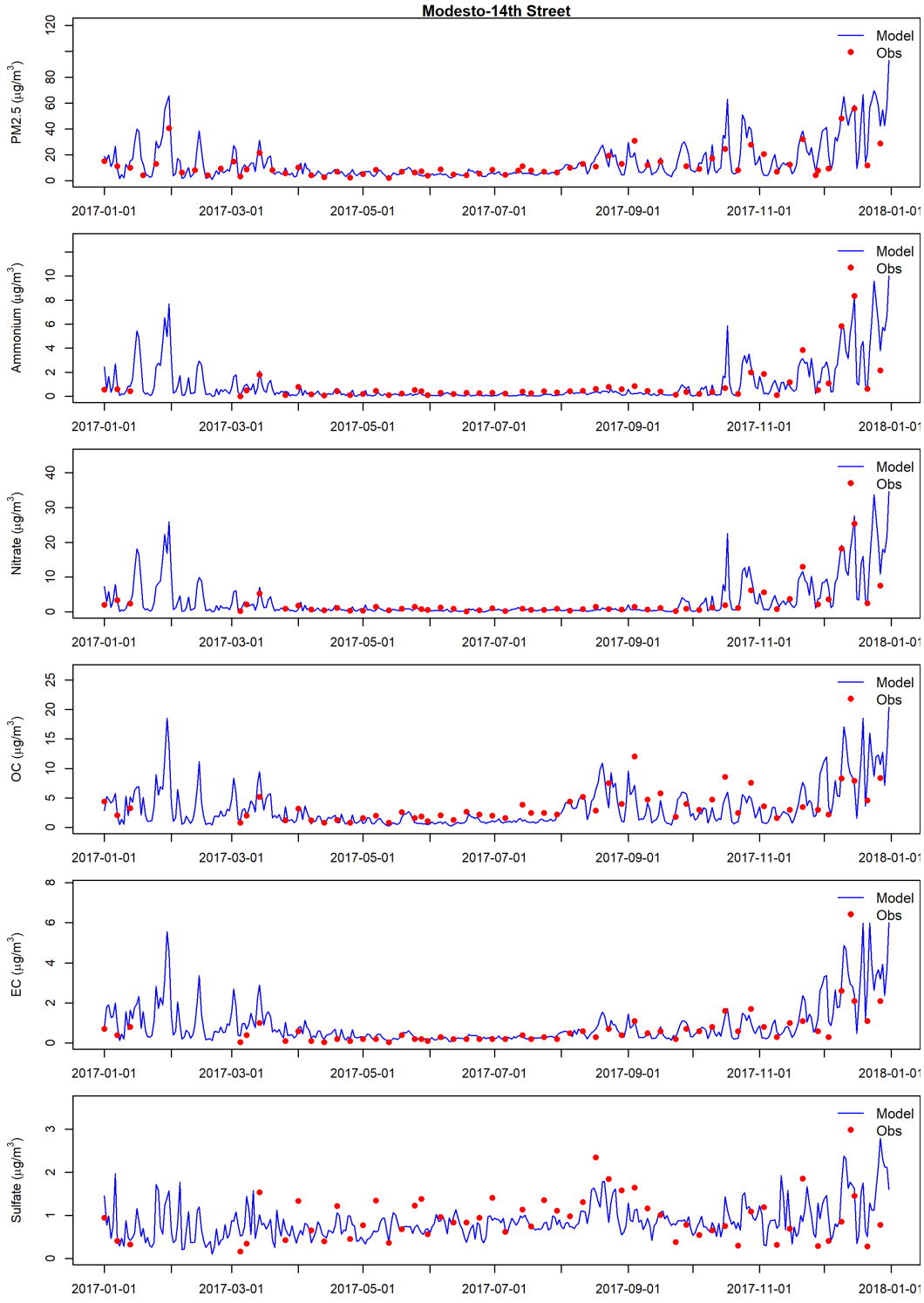

Figure S 28. Observed and modeled 24-hour average $PM_{2.5}$ at Fresno – Garland.

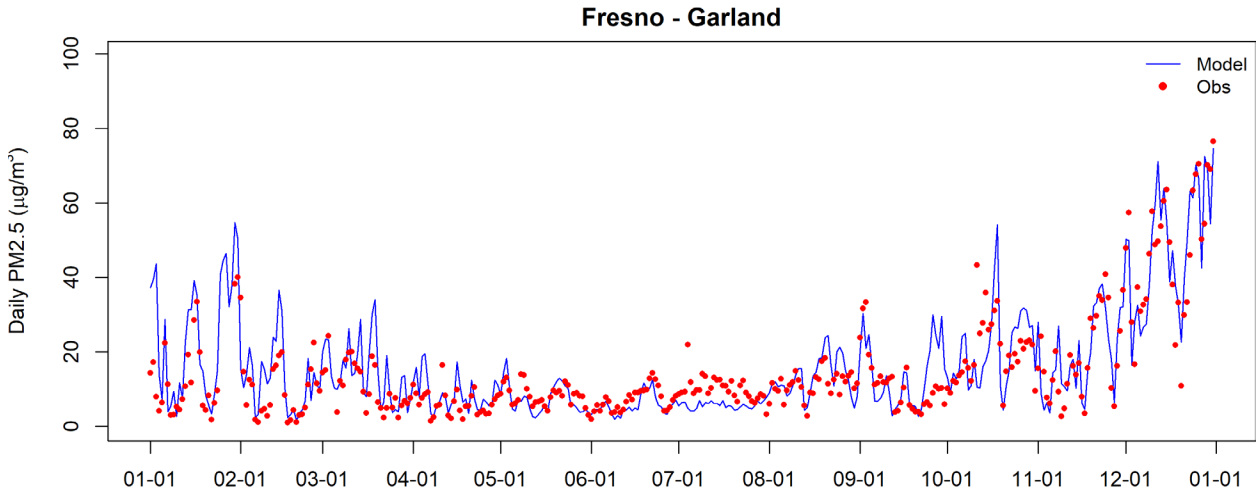

Figure S 29. Observed and modeled 24-hour average $PM_{2.5}$ at Tranquillity.

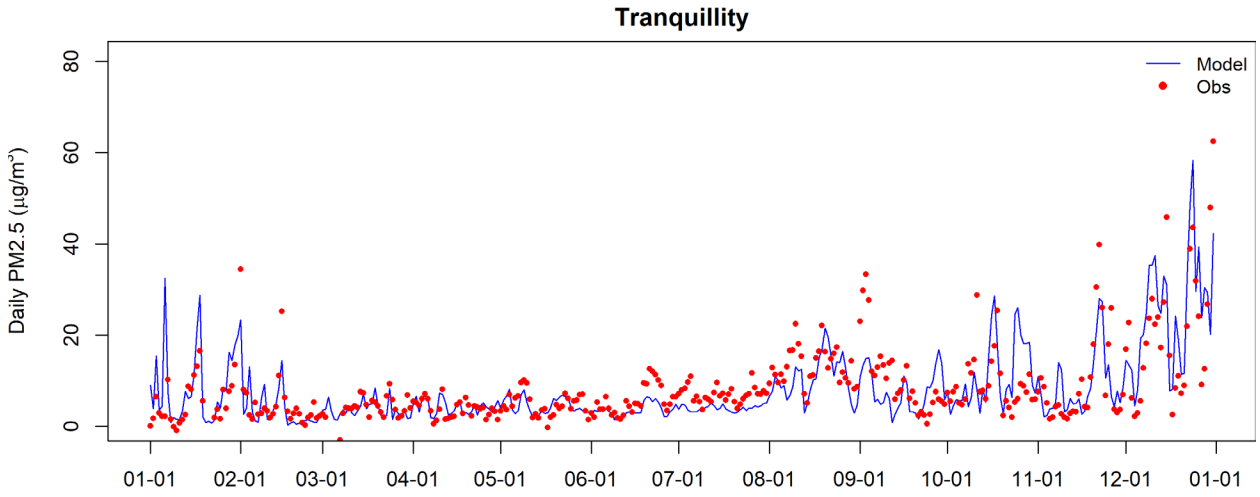

Figure S 30. Observed and modeled 24-hour average $PM_{2.5}$ at Clovis.

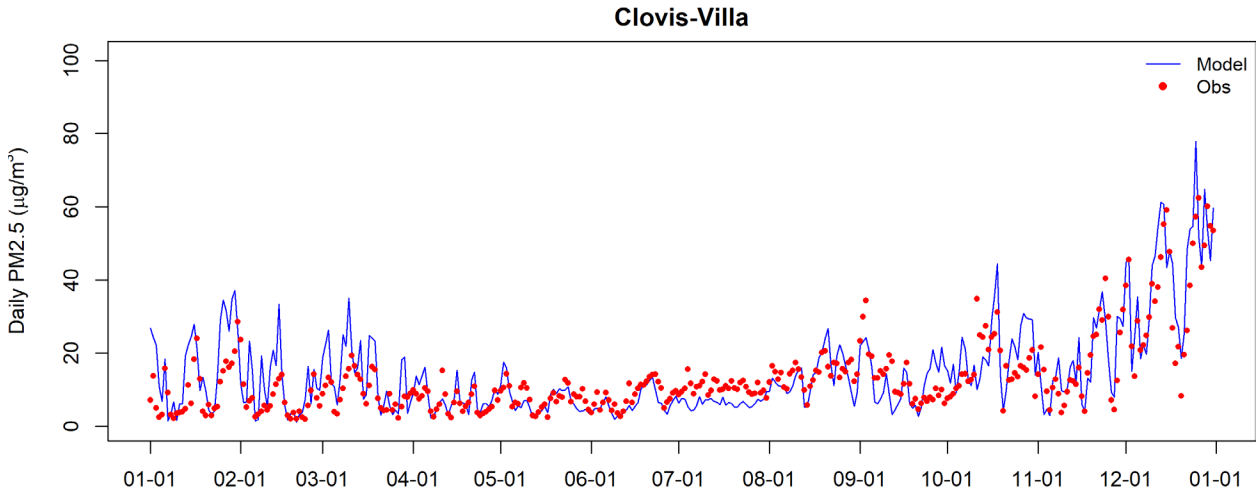

Figure S 31. Observed and modeled 24-hour average $PM_{2.5}$ at Corcoran.

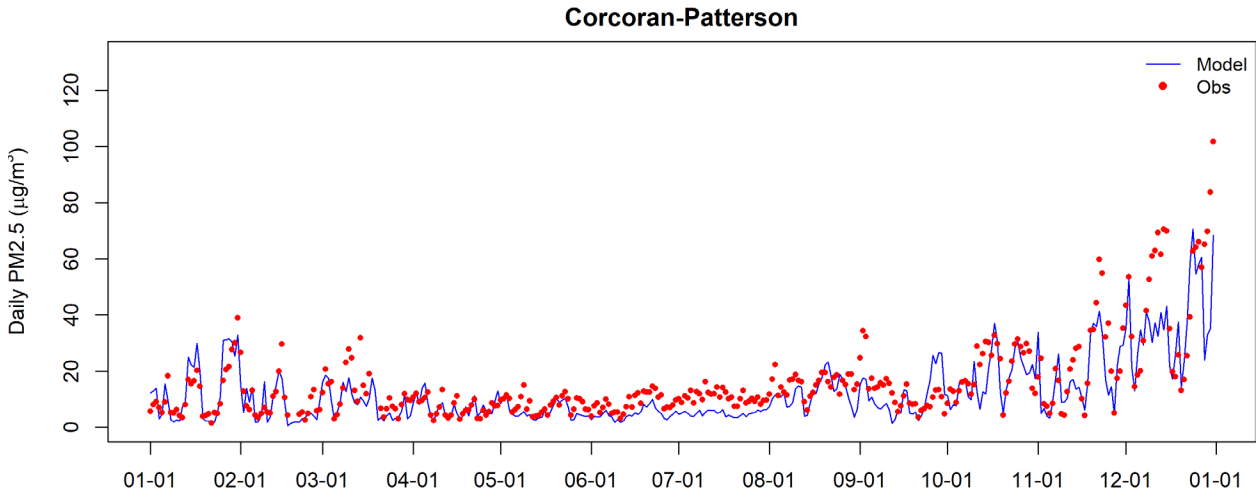

Figure S 32. Observed and modeled 24-hour average $PM_{2.5}$ at Hanford.

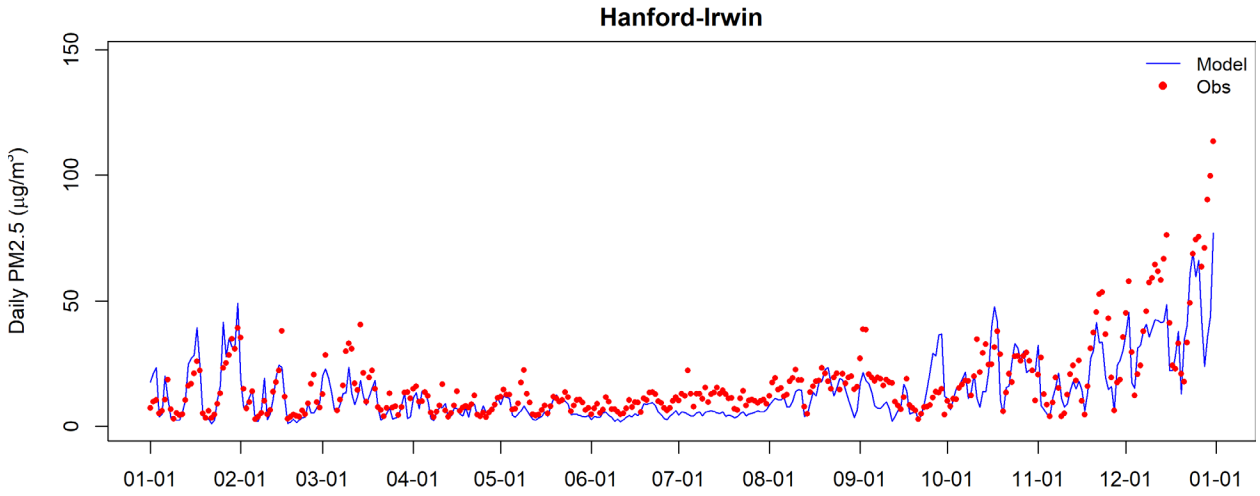

Figure S 33. Observed and modeled 24-hour average $PM_{2.5}$ at Madera.

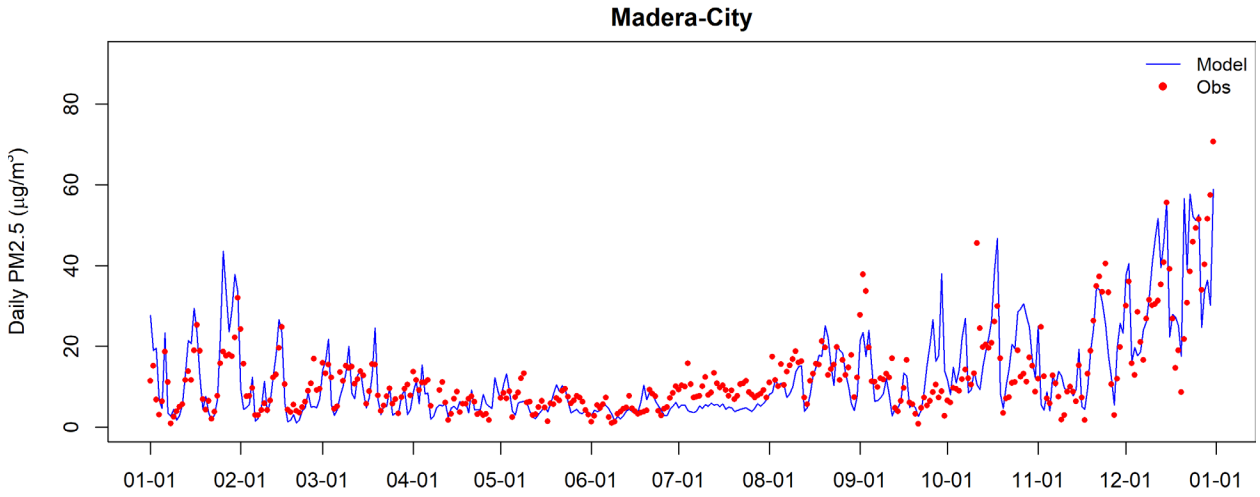

Figure S 34. Observed and modeled 24-hour average $PM_{2.5}$ at Merced.

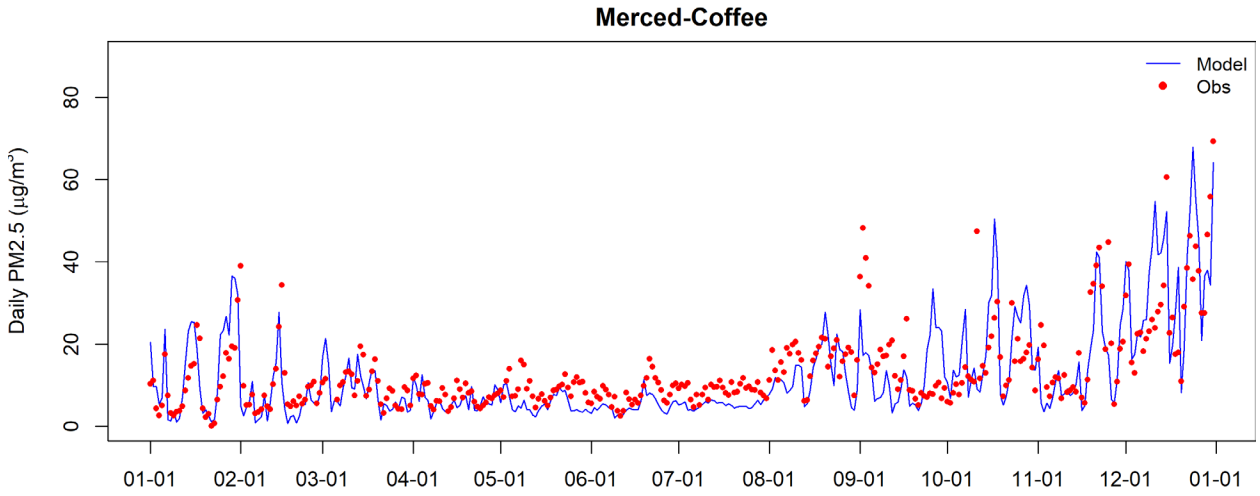

Figure S 35. Observed and modeled 24-hour average $PM_{2.5}$ at Stockton.

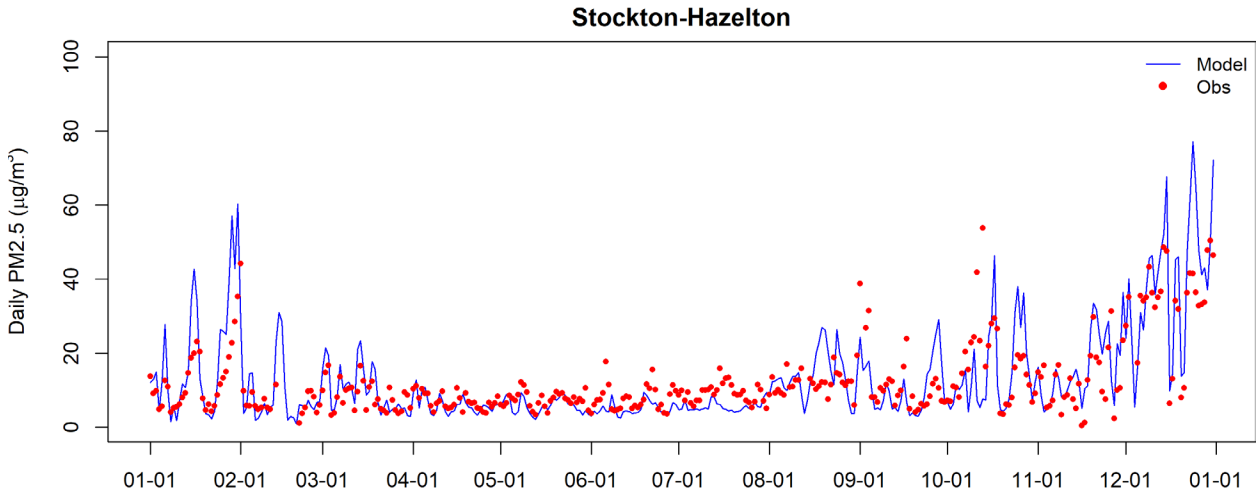

Figure S 36. Observed and modeled 24-hour average $PM_{2.5}$ at Manteca.

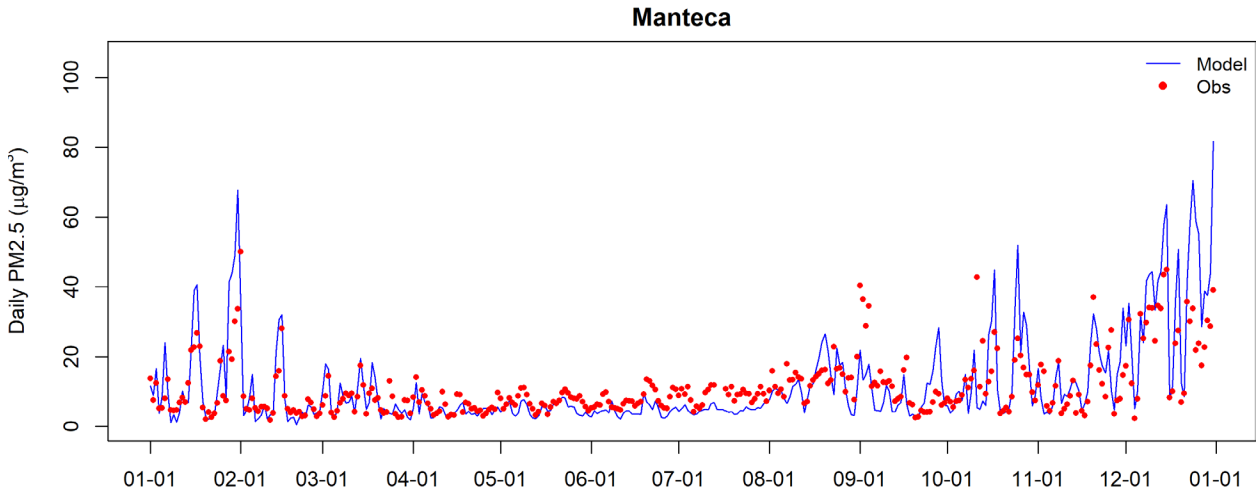

Figure S 37. Observed and modeled 24-hour average $PM_{2.5}$ at Modesto.

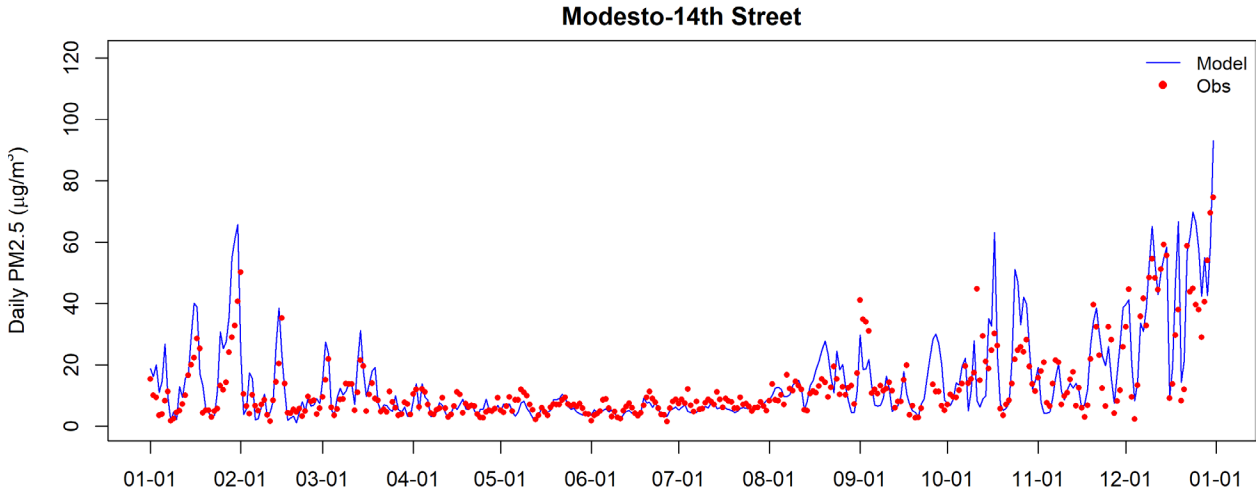

Figure S 38. Observed and modeled 24-hour average $PM_{2.5}$ at Turlock.

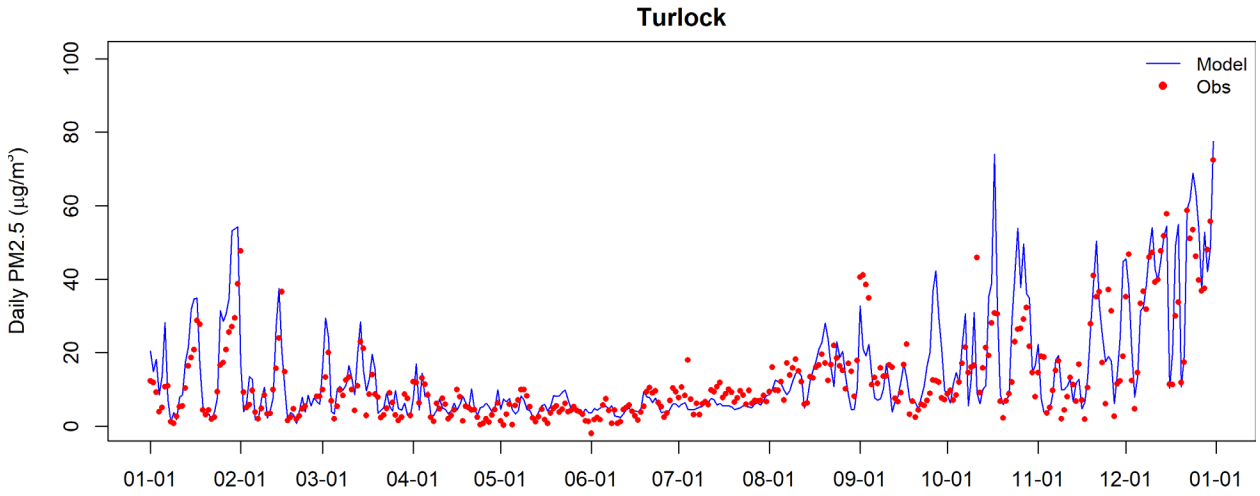

Figure S 39. Scattering plot of observed and modeled 1-hour NO_2 mixing ratio at Fresno – Drummond Street.

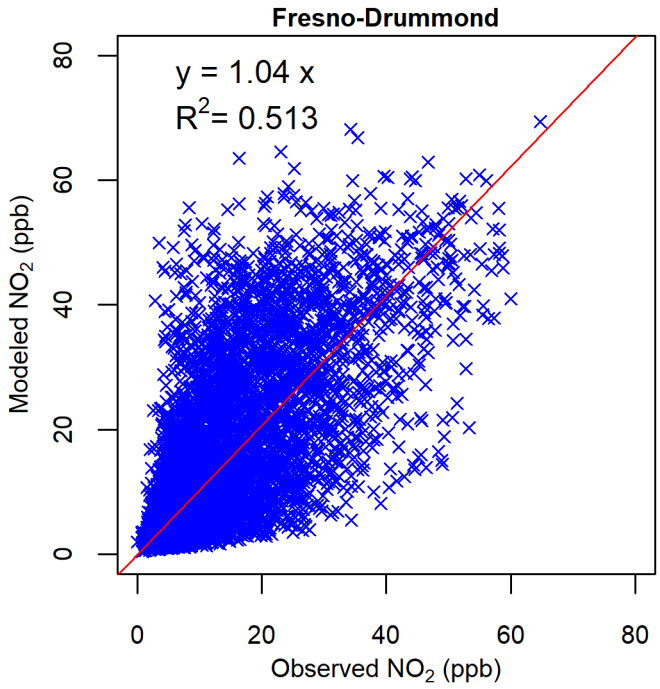

Figure S 40. Scattering plot of observed and modeled 1-hour NO_2 mixing ratio at Visalia.

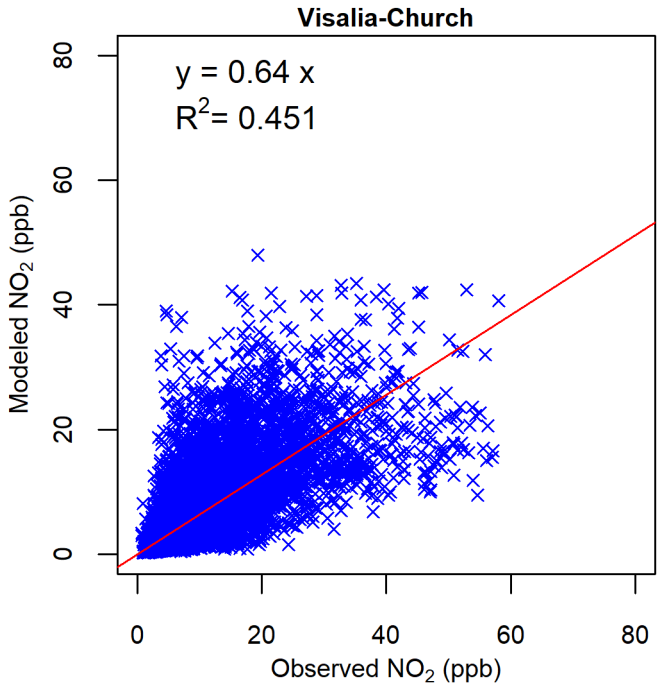

Figure S 41. Scattering plot of observed and modeled 1-hour NO_2 mixing ratio at Stockton.

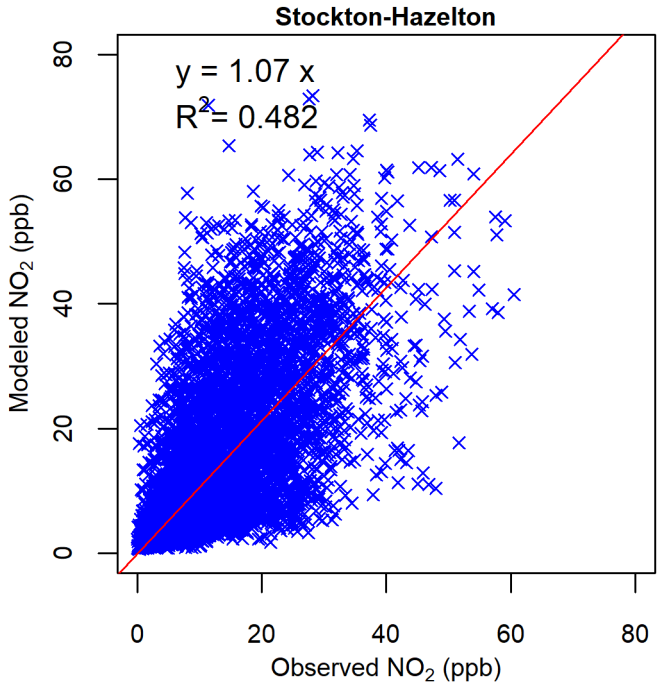

Figure S 42. Scattering plot of observed and modeled 1-hour NO_2 mixing ratio at Parlier.

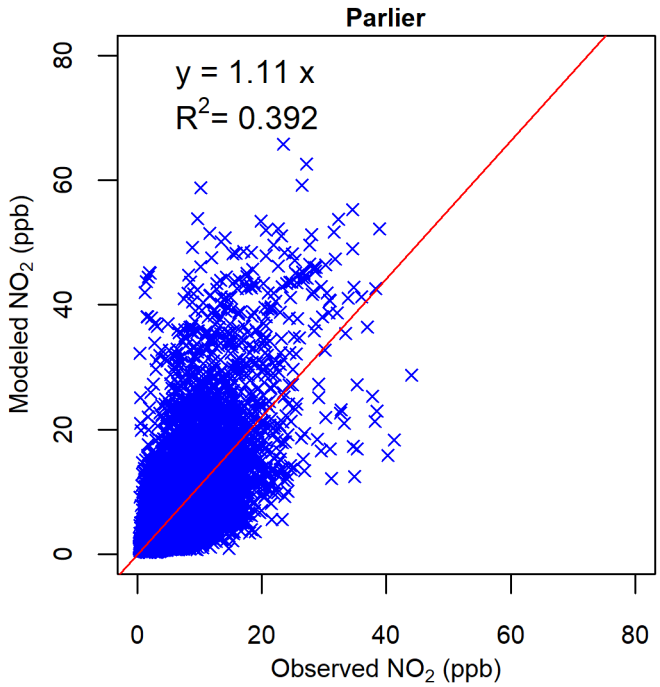

Figure S 43. Scattering plot of observed and modeled 1-hour NO_2 mixing ratio at Edison.

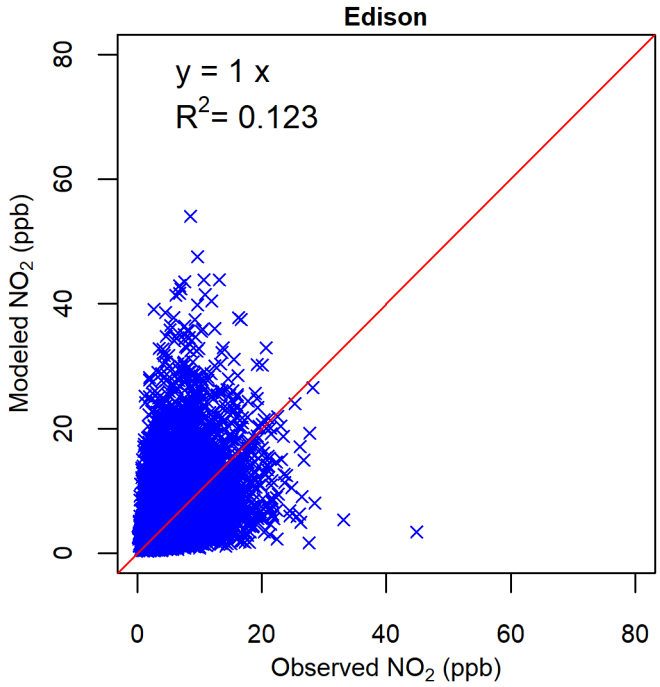

Figure S 44. Scattering plot of observed and modeled 1-hour NO_2 mixing ratio at Fresno – Sierra Sky Park.

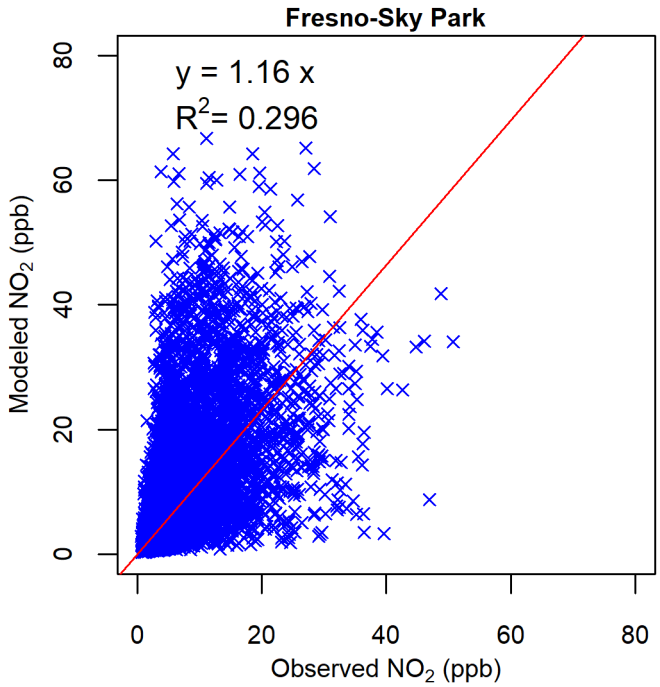

Figure S 45. Scattering plot of observed and modeled 1-hour NO_2 mixing ratio at Shafter.

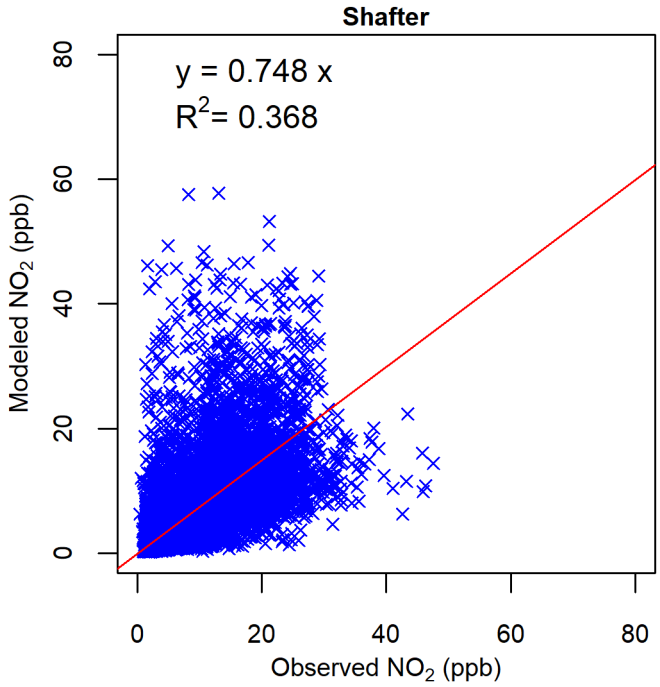

Figure S 46. Scattering plot of observed and modeled 1-hour NO_2 mixing ratio at Turlock

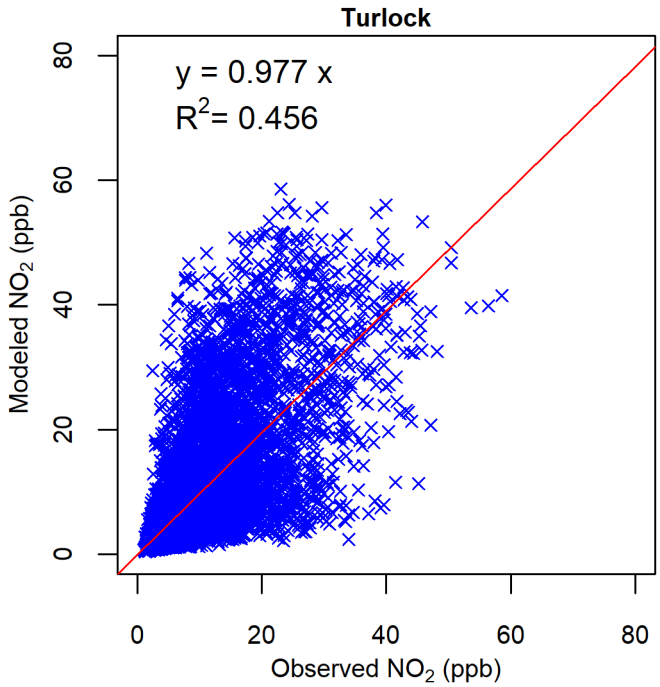

Figure S 47. Scattering plot of observed and modeled 1-hour NO_2 mixing ratio at Merced

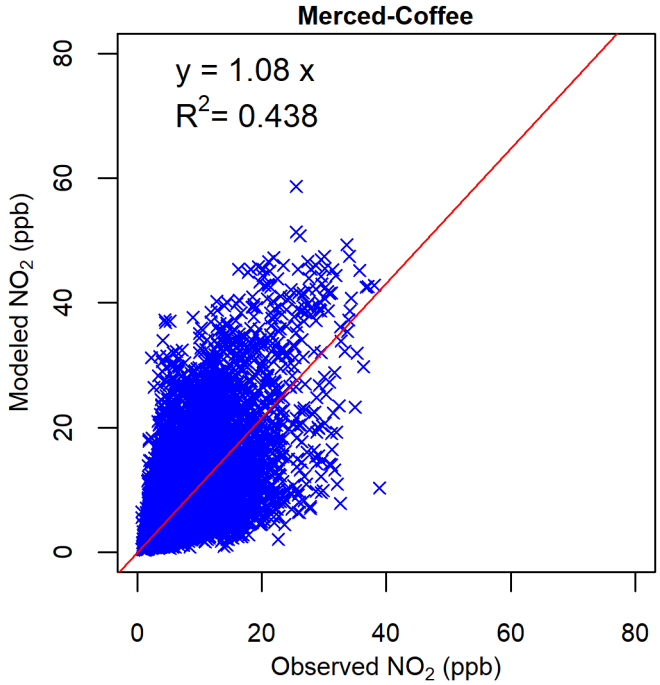

Figure S 48. Scattering plot of observed and modeled 1-hour NO_2 mixing ratio at Clovis.

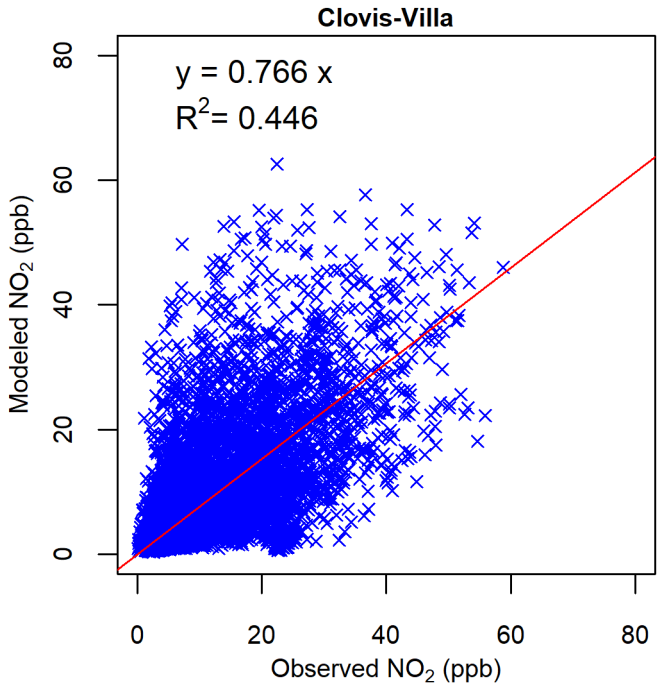

Figure S 49. Scattering plot of observed and modeled 1-hour NO_2 mixing ratio at Bakersfield – California Avenue.

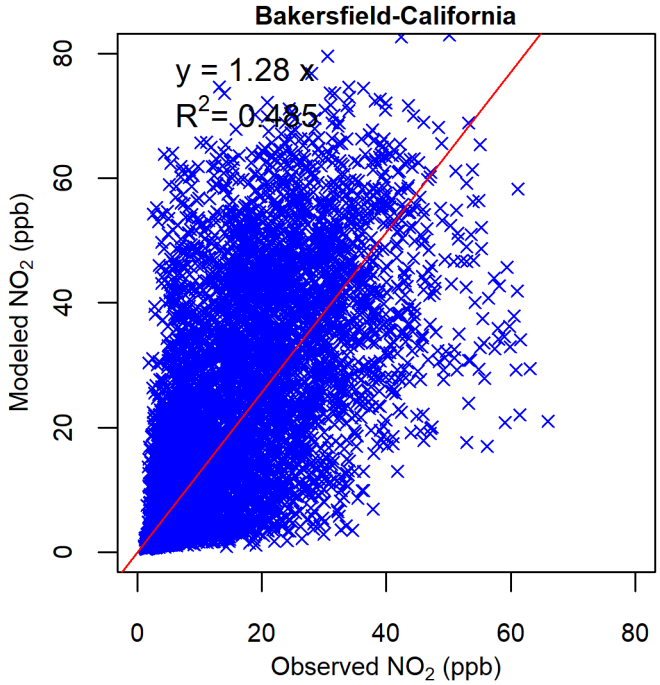

Figure S 50. Scattering plot of observed and modeled 1-hour NO_2 mixing ratio at Madera.

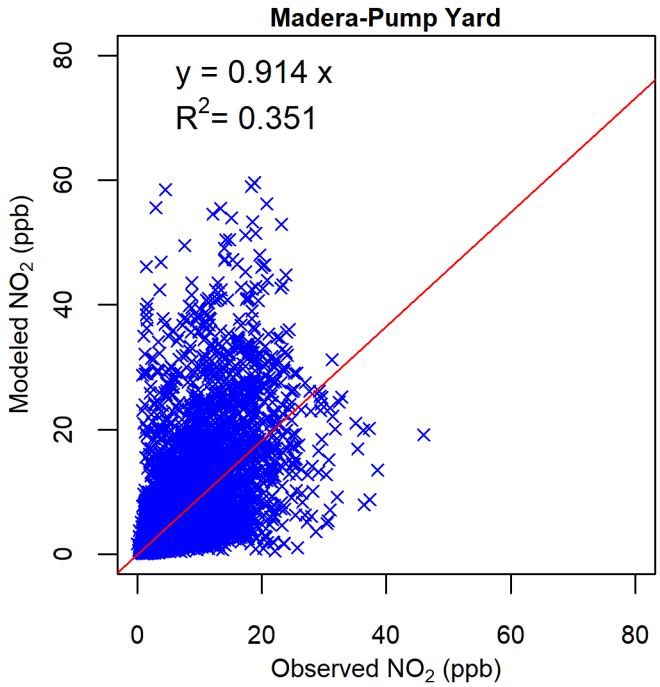

Figure S 51. Scattering plot of observed and modeled 1-hour NO_2 mixing ratio at Tracy.

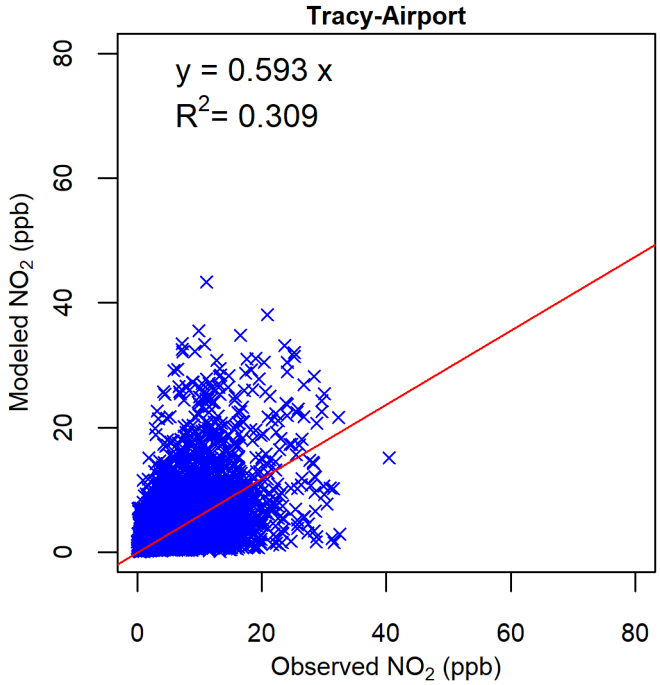

Figure S 52. Scattering plot of observed and modeled 1-hour NO_2 mixing ratio at Fresno – Garland.

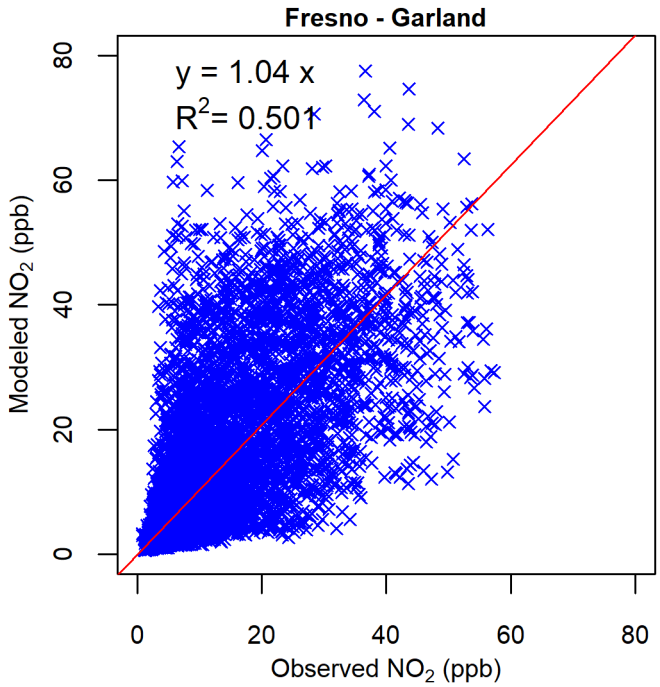

Figure S 53. Scattering plot of observed and modeled 1-hour NO_2 mixing ratio at Bakersfield – Municipal Airport

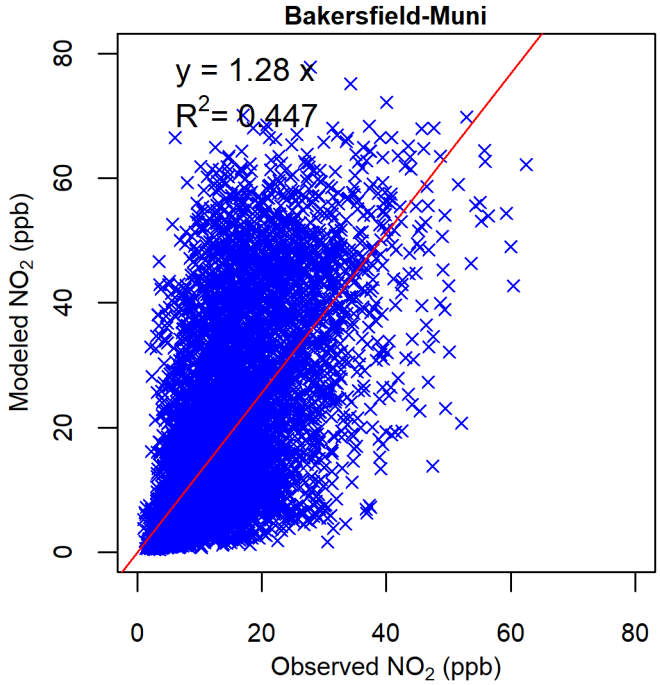

Figure S 54. Scattering plot of observed and modeled 1-hour O_3 mixing ratio at Fresno – Drummond Street.

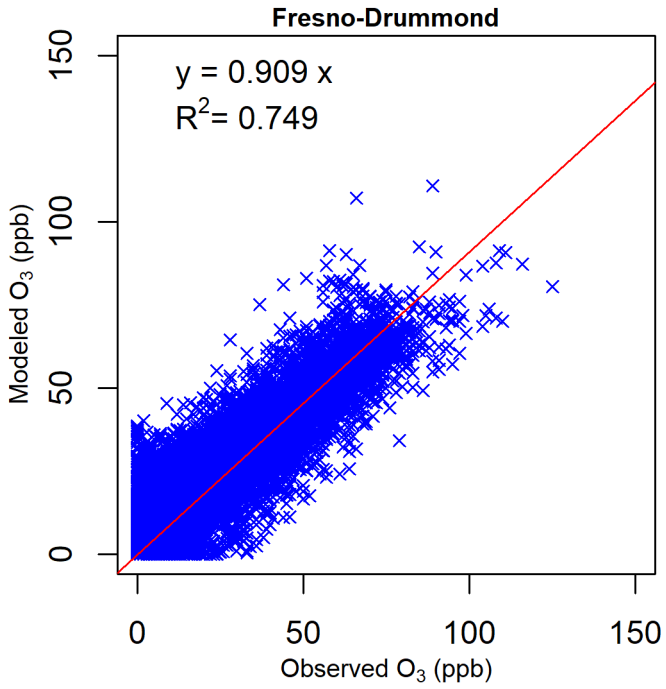

Figure S 55. Scattering plot of observed and modeled 1-hour O_3 mixing ratio at Visalia

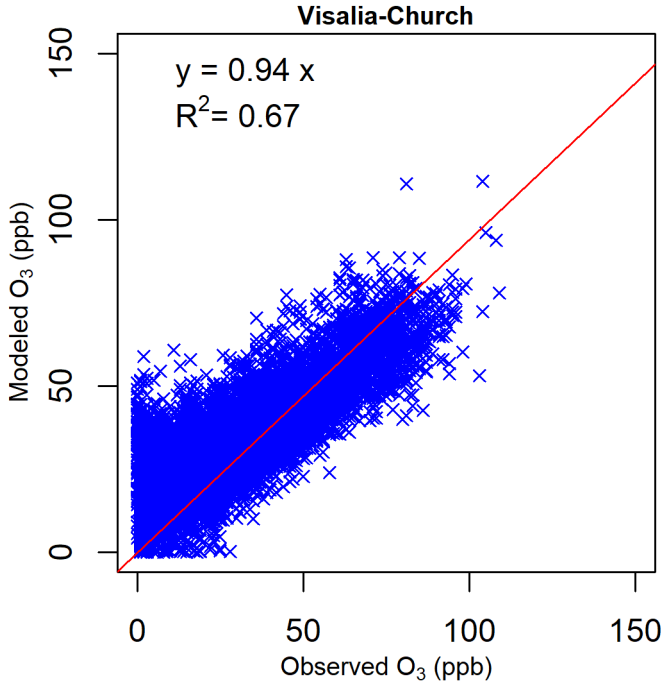

Figure S 56. Scattering plot of observed and modeled 1-hour O_3 mixing ratio at Stockton

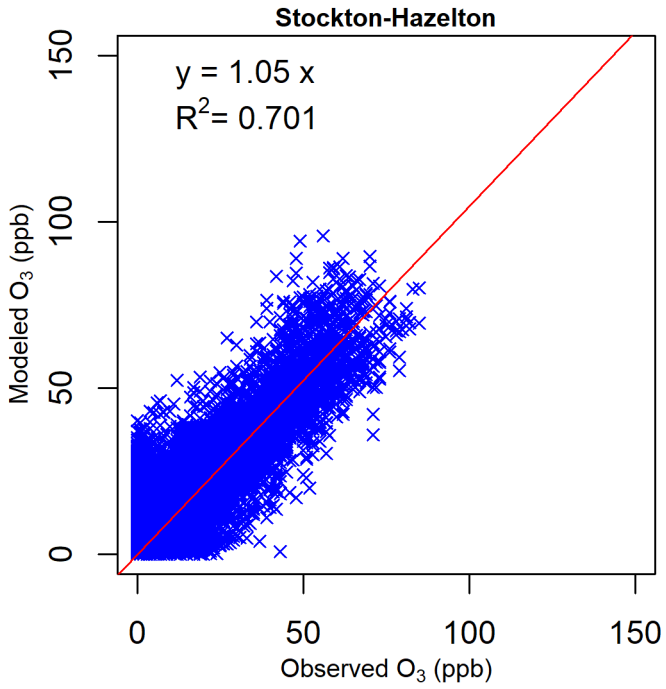

Figure S 57. Scattering plot of observed and modeled 1-hour O_3 mixing ratio at Parlier

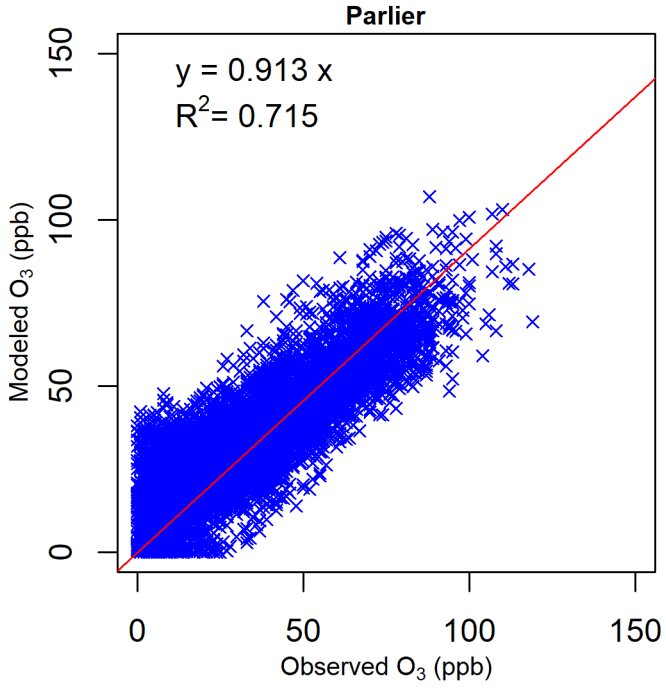

Figure S 58. Scattering plot of observed and modeled 1-hour O_3 mixing ratio at Edison

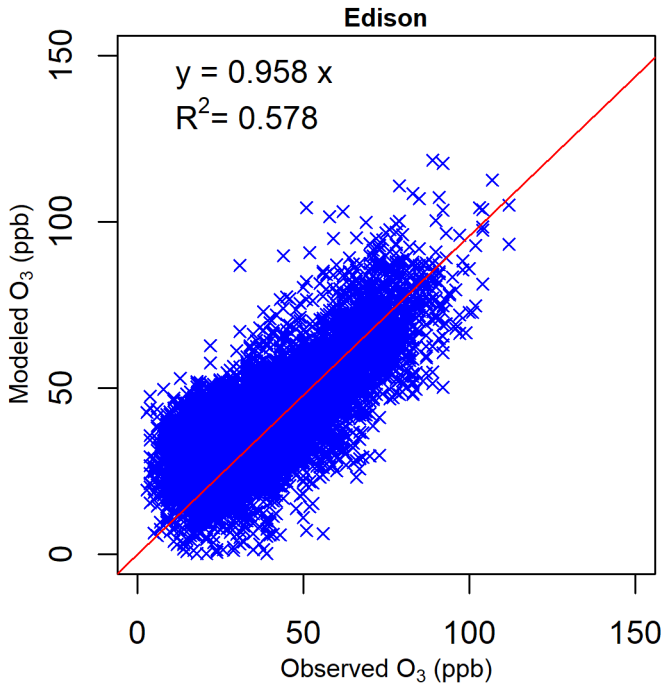

Figure S 59. Scattering plot of observed and modeled 1-hour O_3 mixing ratio at Oildale

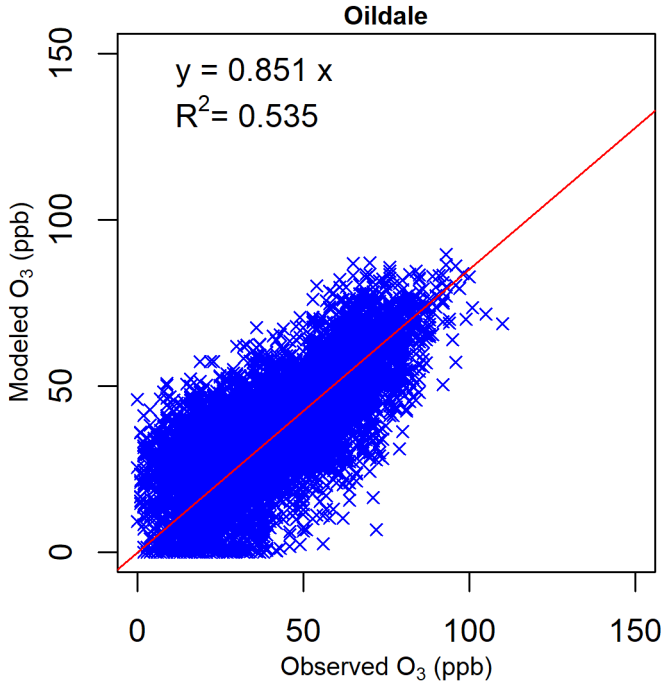

Figure S 60. Scattering plot of observed and modeled 1-hour O_3 mixing ratio at Modesto -14th Street

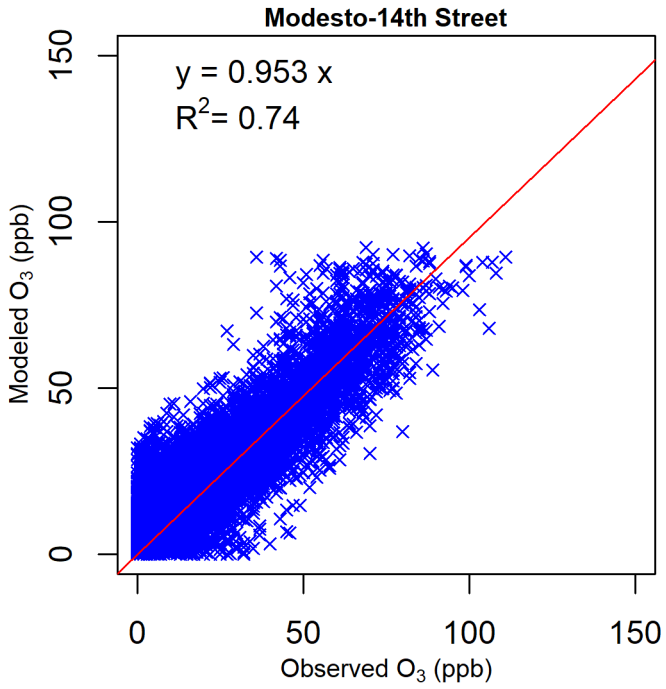

Figure S 61. Scattering plot of observed and modeled 1-hour O_3 mixing ratio at Fresno –Sierra Sky Park

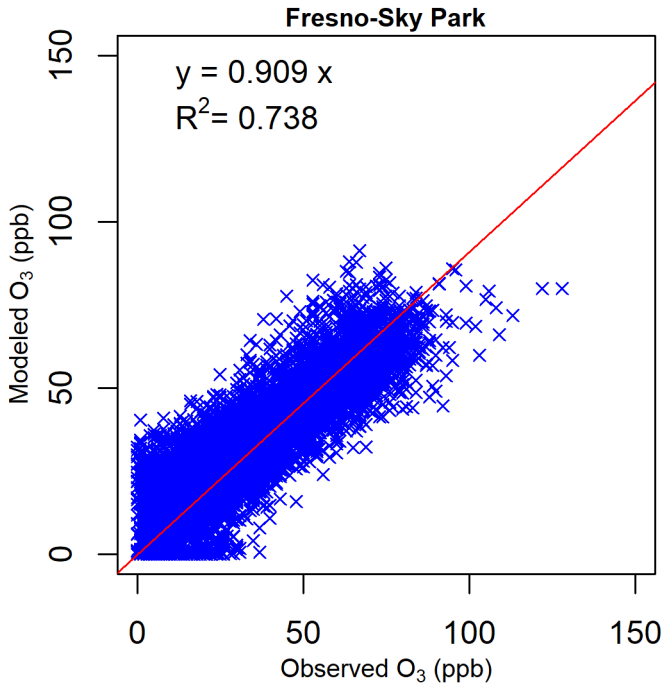

Figure S 62. Scattering plot of observed and modeled 1-hour O_3 mixing ratio at Maricopa

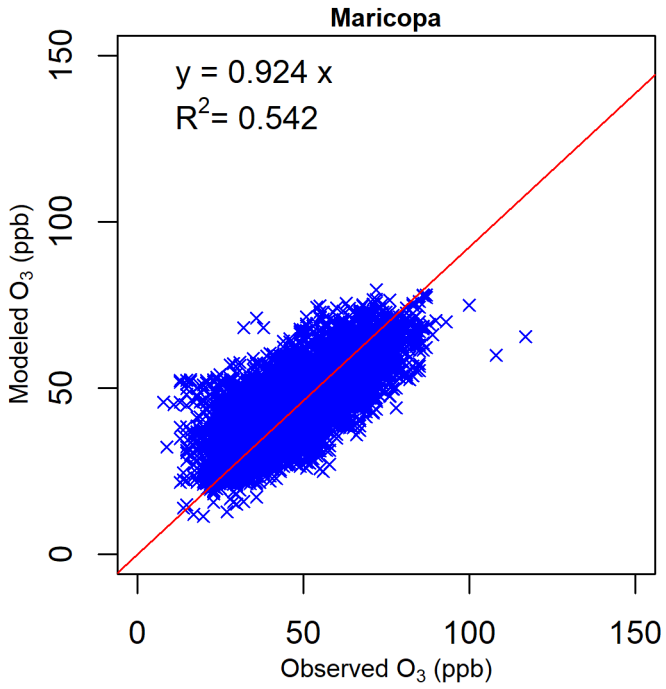

Figure S 63. Scattering plot of observed and modeled 1-hour O_3 mixing ratio at Shafter

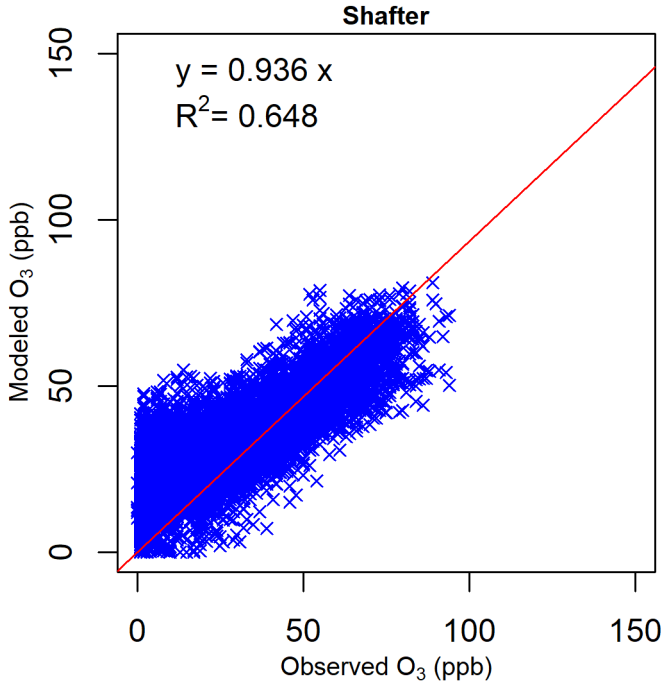

Figure S 64. Scattering plot of observed and modeled 1-hour O_3 mixing ratio at Turlock

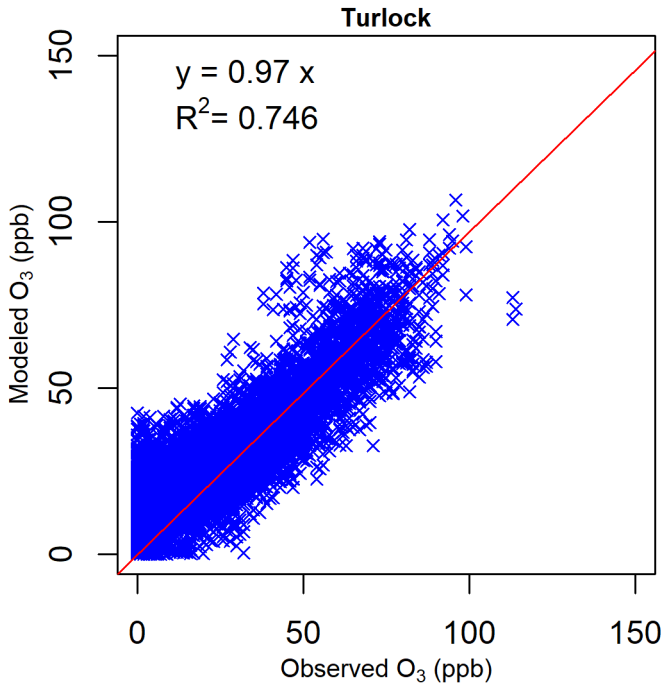

Figure S 65. Scattering plot of observed and modeled 1-hour O_3 mixing ratio at Merced – S Coffee Avenue

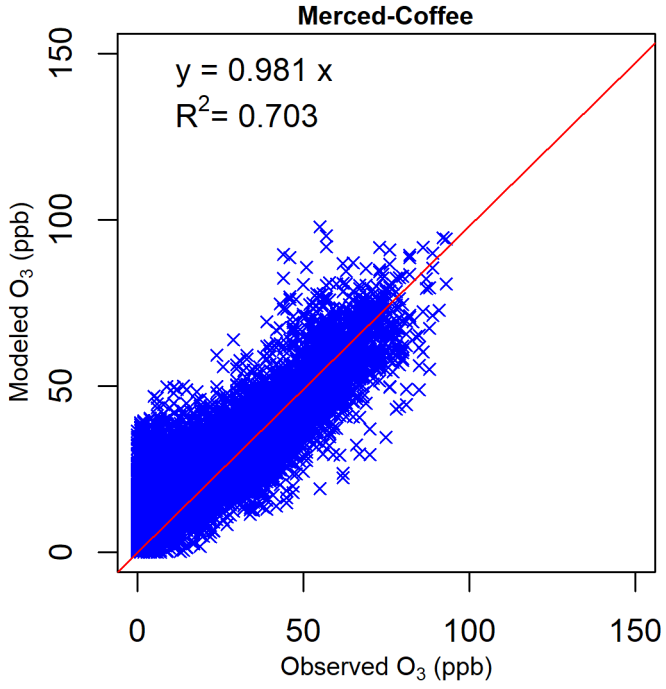

Figure S 66. Scattering plot of observed and modeled 1-hour O_3 mixing ratio at Clovis

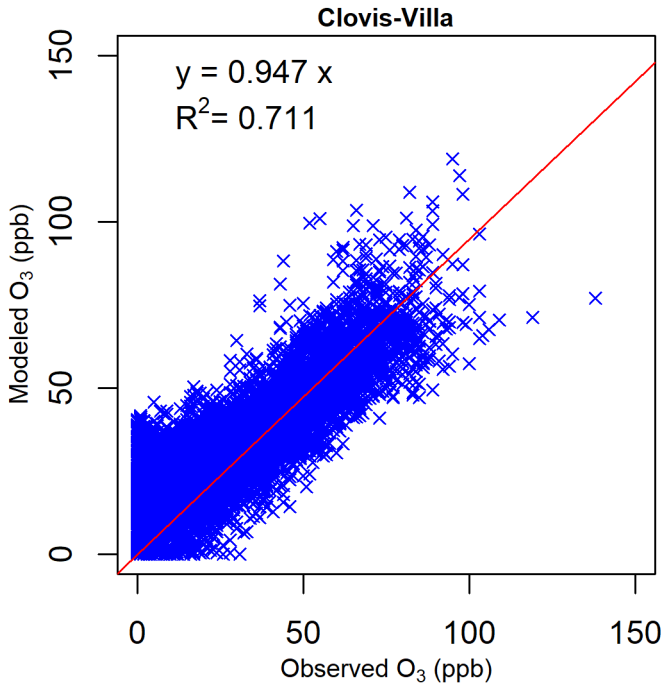

Figure S 67. Scattering plot of observed and modeled 1-hour O_3 mixing ratio at Sequoia National Park

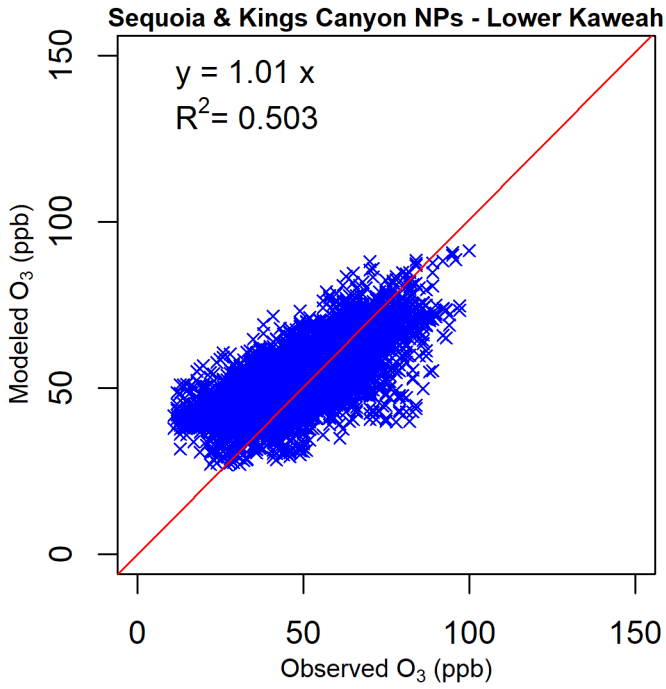

Figure S 68. Scattering plot of observed and modeled 1-hour O_3 mixing ratio at Hanford

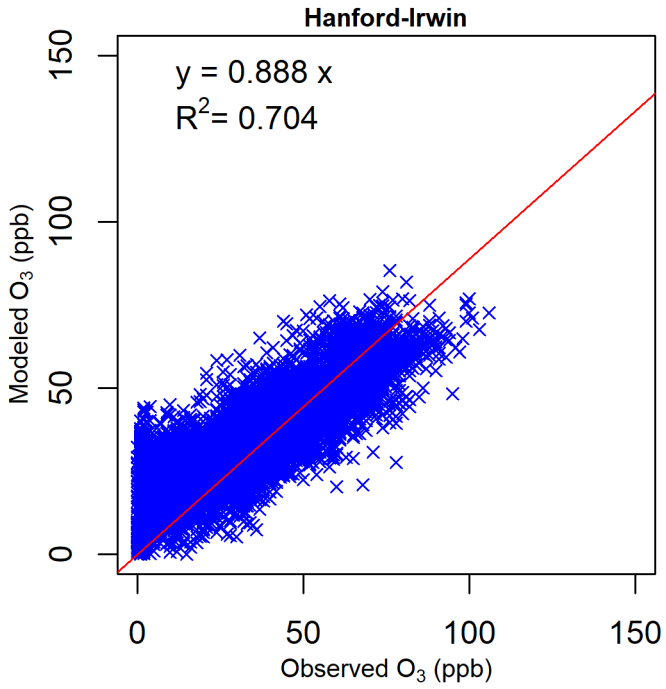

Figure S 69. Scattering plot of observed and modeled 1-hour O_3 mixing ratio at Bakersfield – California Avenue

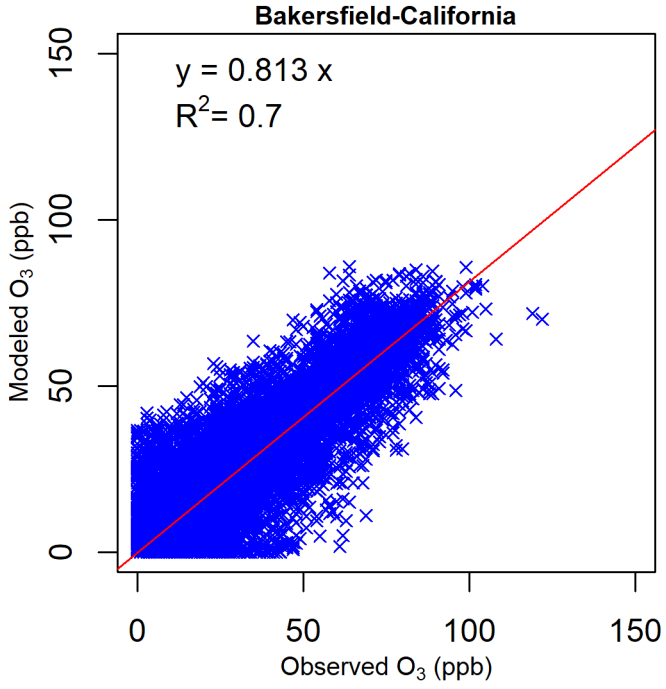

Figure S 70. Scattering plot of observed and modeled 1-hour O_3 mixing ratio at Madera – Pump Yard

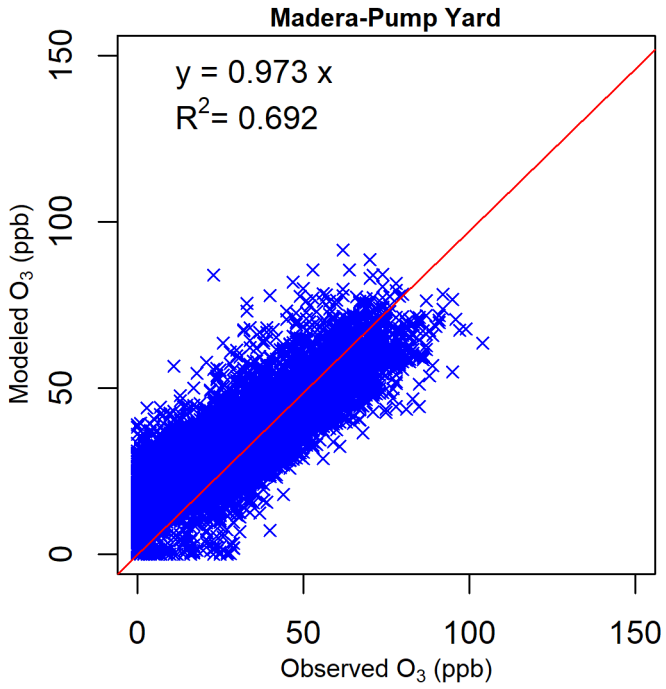

Figure S 71. Scattering plot of observed and modeled 1-hour O_3 mixing ratio at Sequoia and Kings Canyon National Park

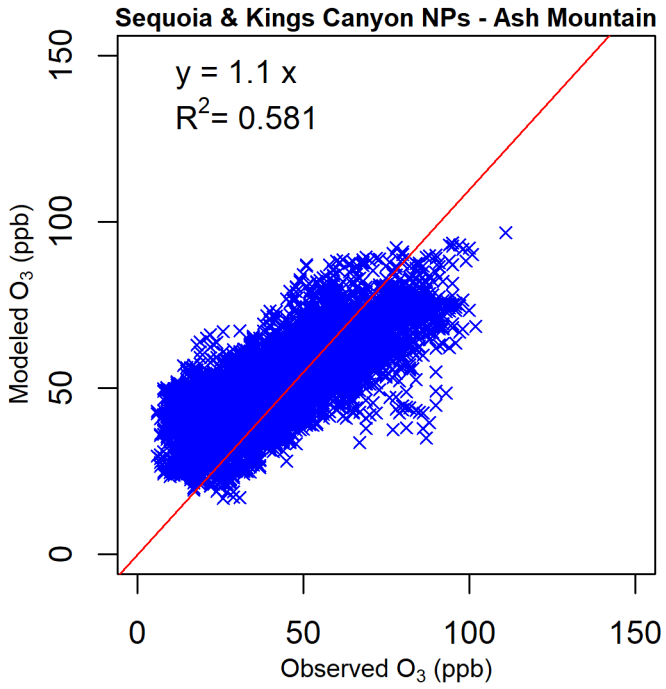

Figure S 72. Scattering plot of observed and modeled 1-hour O_3 mixing ratio at Tracy

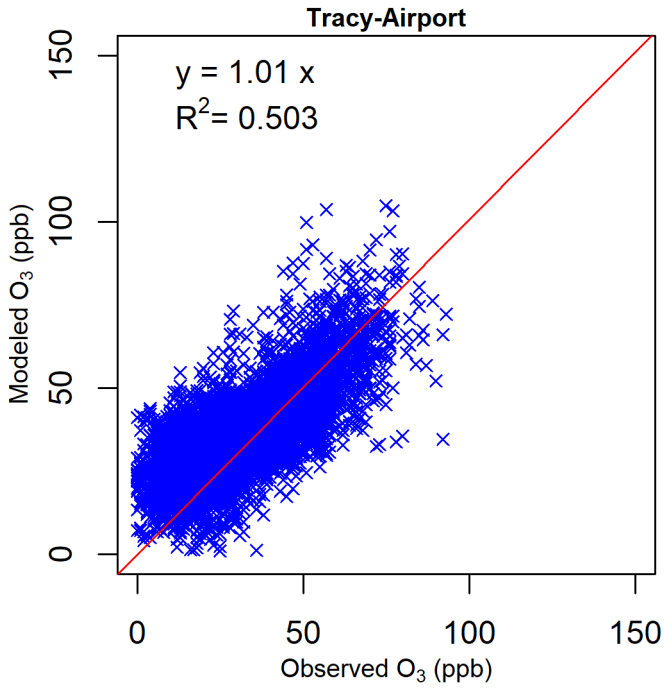

Figure S 73. Scattering plot of observed and modeled 1-hour O_3 mixing ratio at Arvin

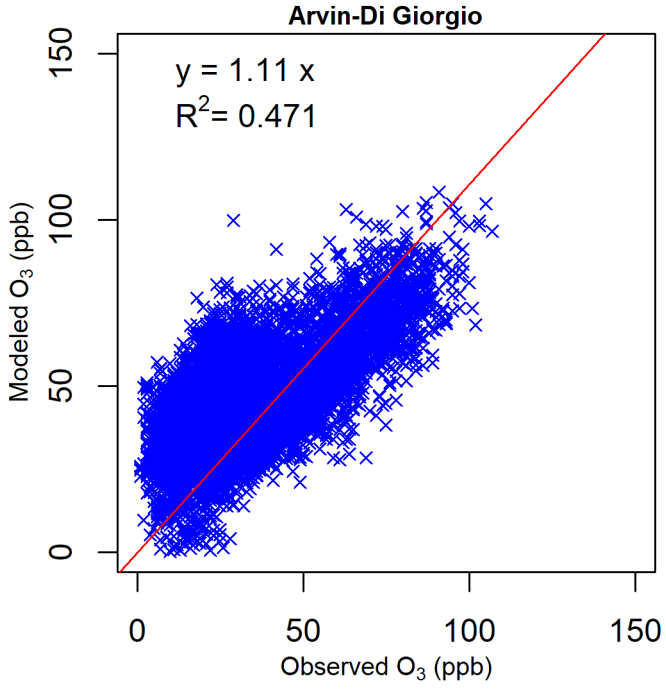

Figure S 74. Scattering plot of observed and modeled 1-hour O_3 mixing ratio at Tranquillity

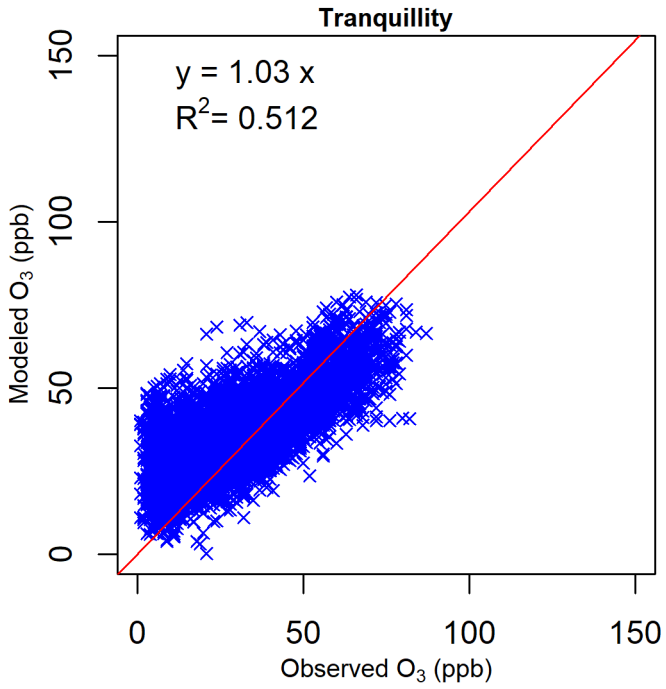

Figure S 75. Scattering plot of observed and modeled 1-hour O_3 mixing ratio at Porterville

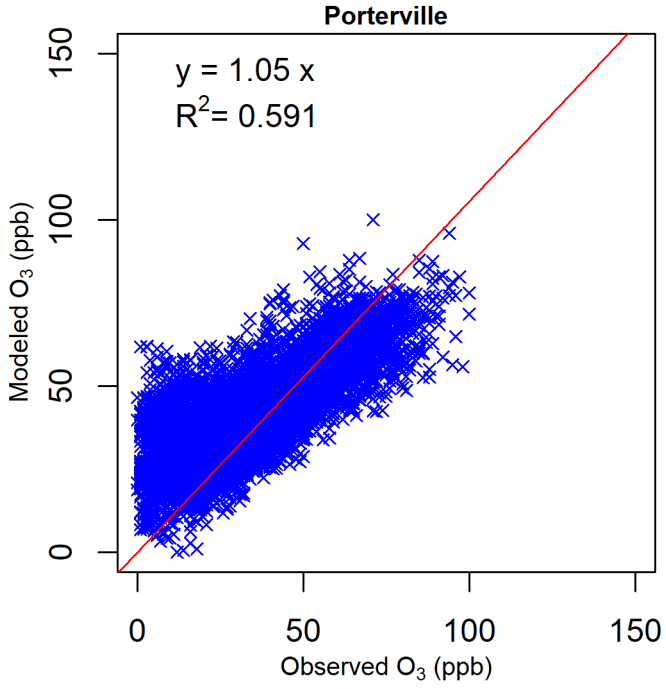

Figure S 76. Scattering plot of observed and modeled 1-hour O_3 mixing ratio at Madera – 28261 Avenue

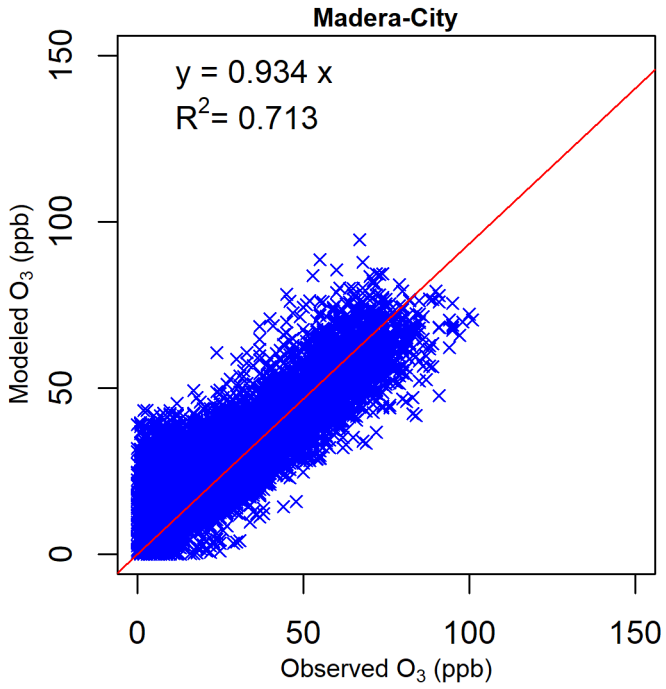

Figure S 77. Scattering plot of observed and modeled 1-hour O_3 mixing ratio at Fresno-Garland

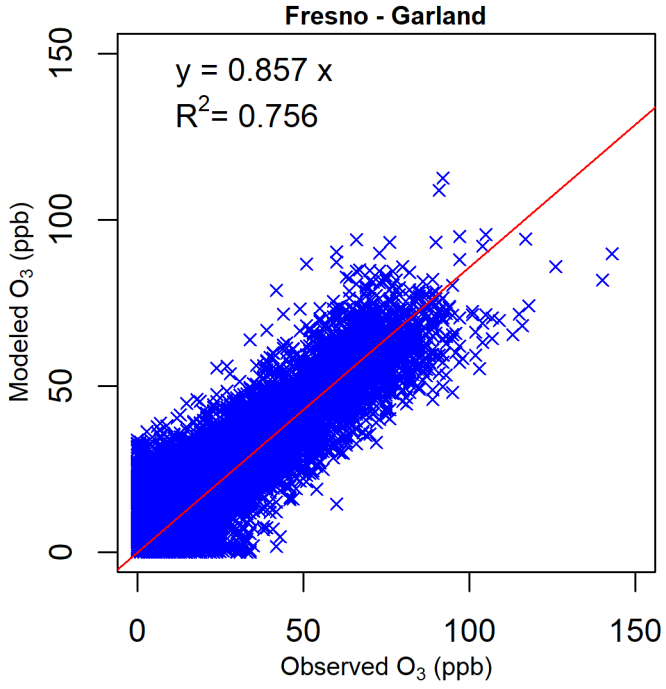

Figure S 78. Scattering plot of observed and modeled 1-hour O_3 mixing ratio at Bakersfield – Municipal airport.

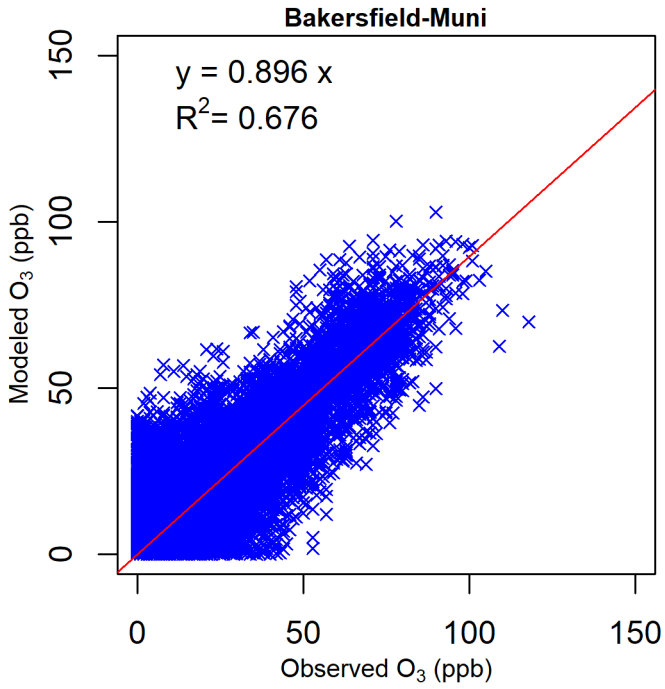

Figure S 79. Comparison of annual average NH3 column from IASI satellite measurements and model simulations.

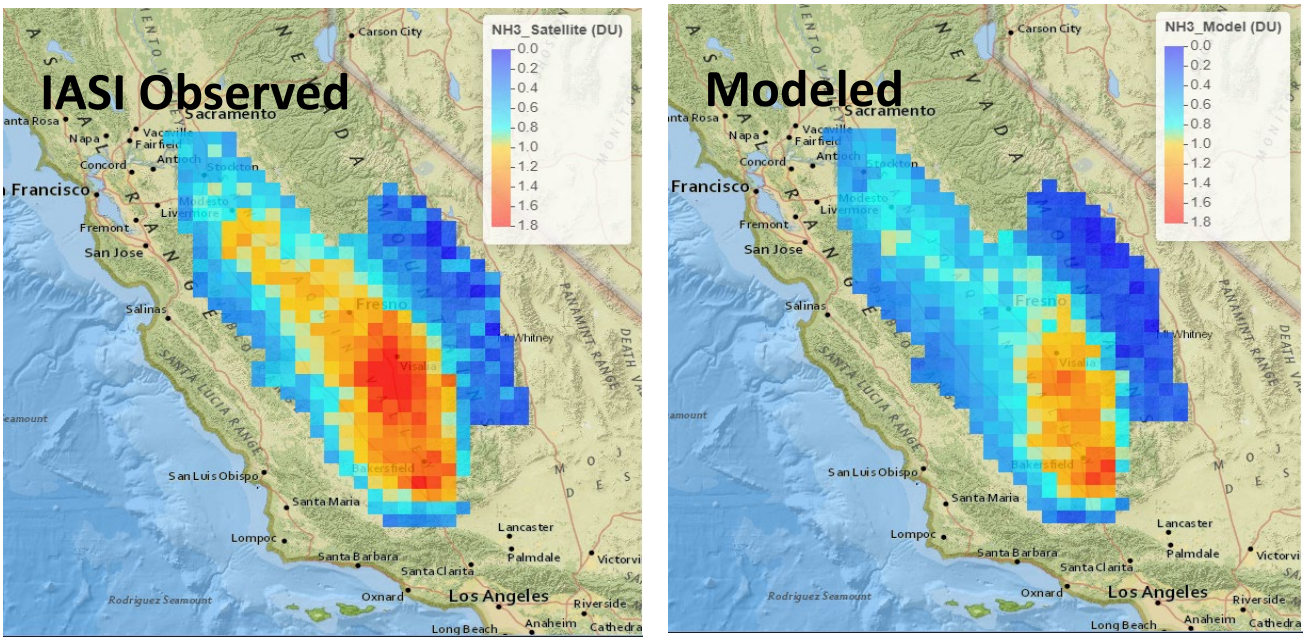

Figure S 80. Observed and modeled (regular: using the default MEGAN soil NOx scheme; BDSNP: using the MEGAN Berkeley Dalhousie soil NOx scheme) $PM_{2.5}$ species at Fresno.

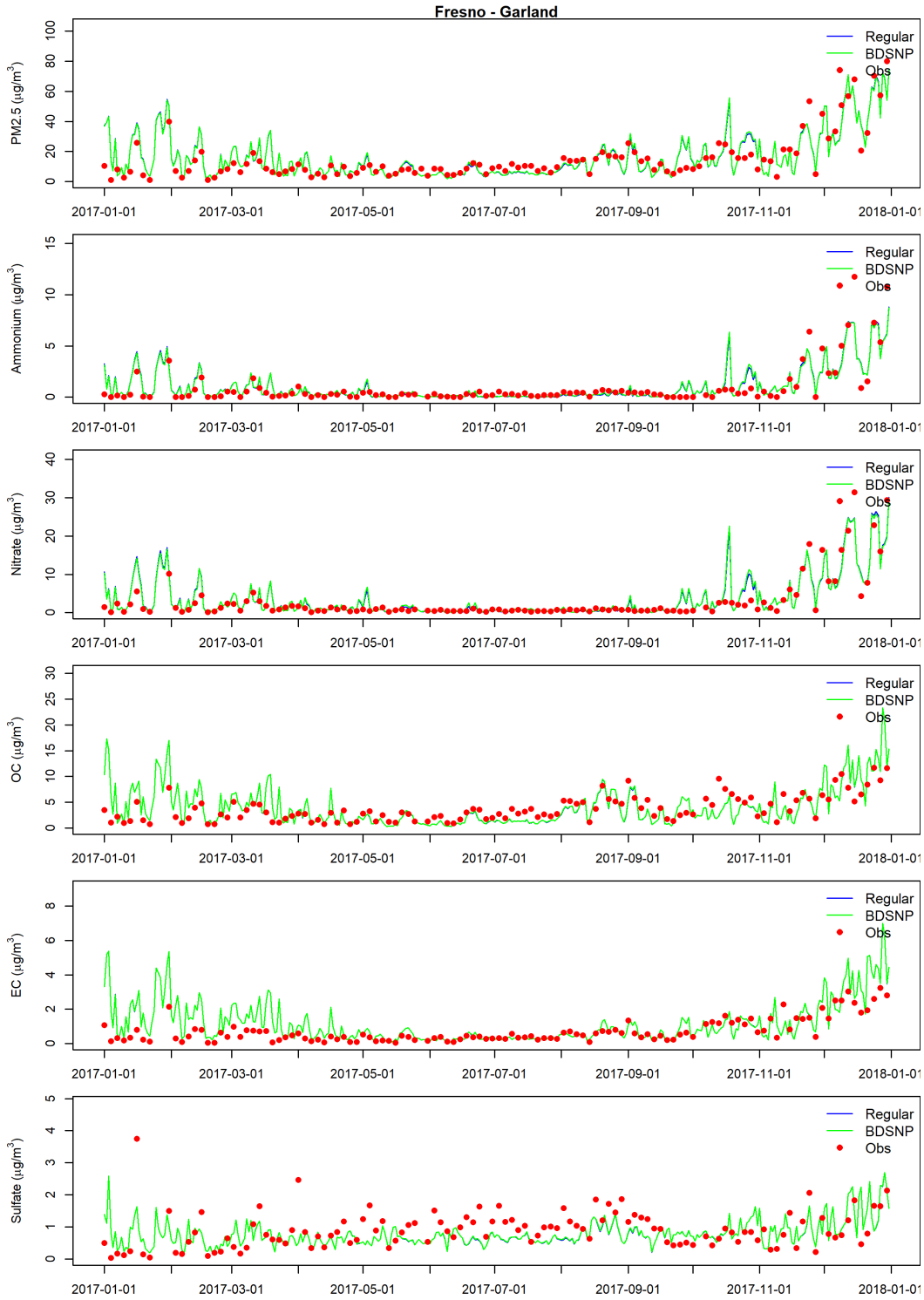

Figure S 81. Observed and modeled (regular: using the default MEGAN soil NOx scheme; BDSNP: using the MEGAN Berkeley Dalhousie soil NOx scheme) $PM_{2.5}$ species at Bakersfield.

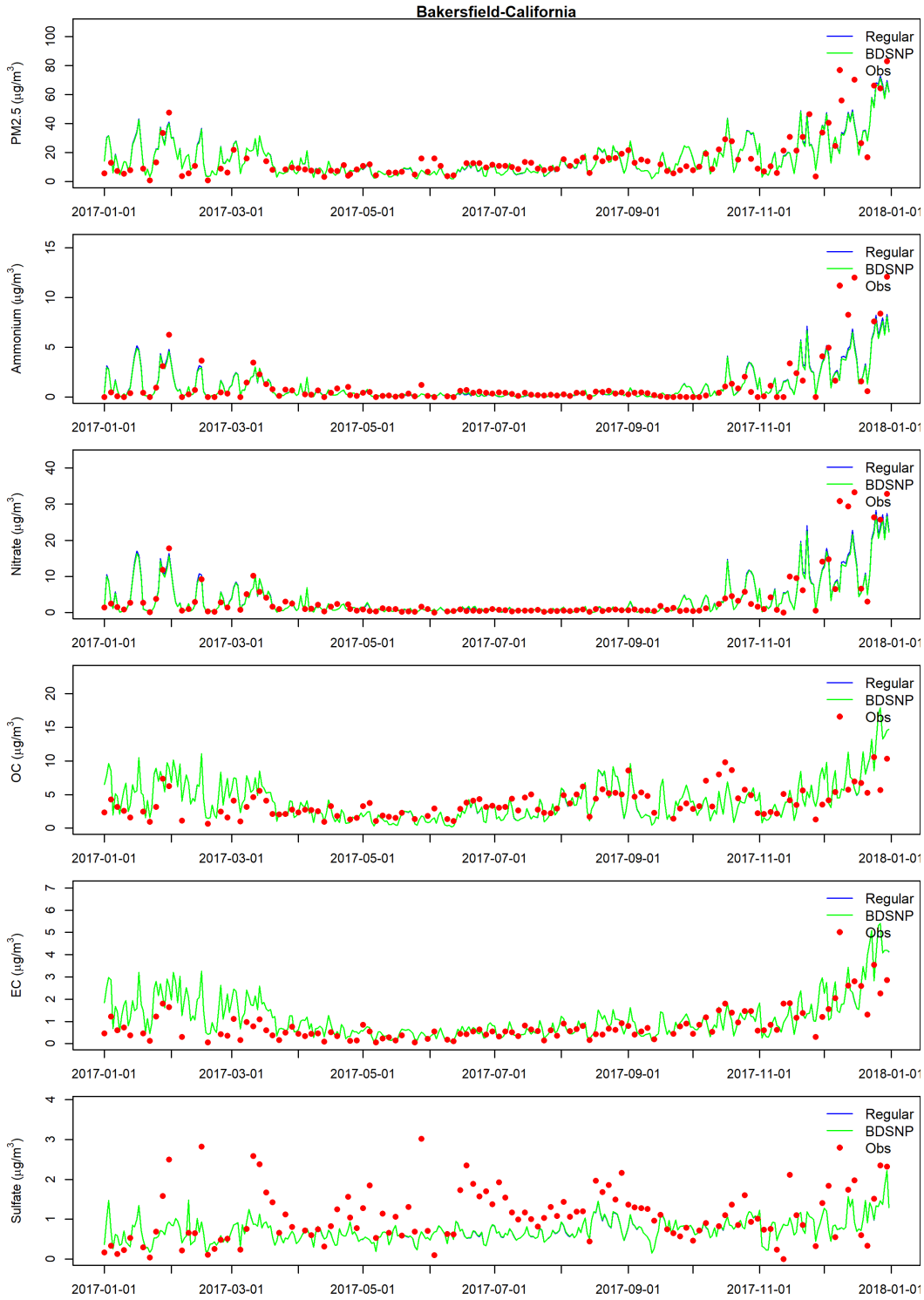

Figure S 82. Observed and modeled (regular: using the default MEGAN soil NOx scheme; BDSNP: using the MEGAN Berkeley Dalhousie soil NOx scheme) $PM_{2.5}$ species at Visalia.

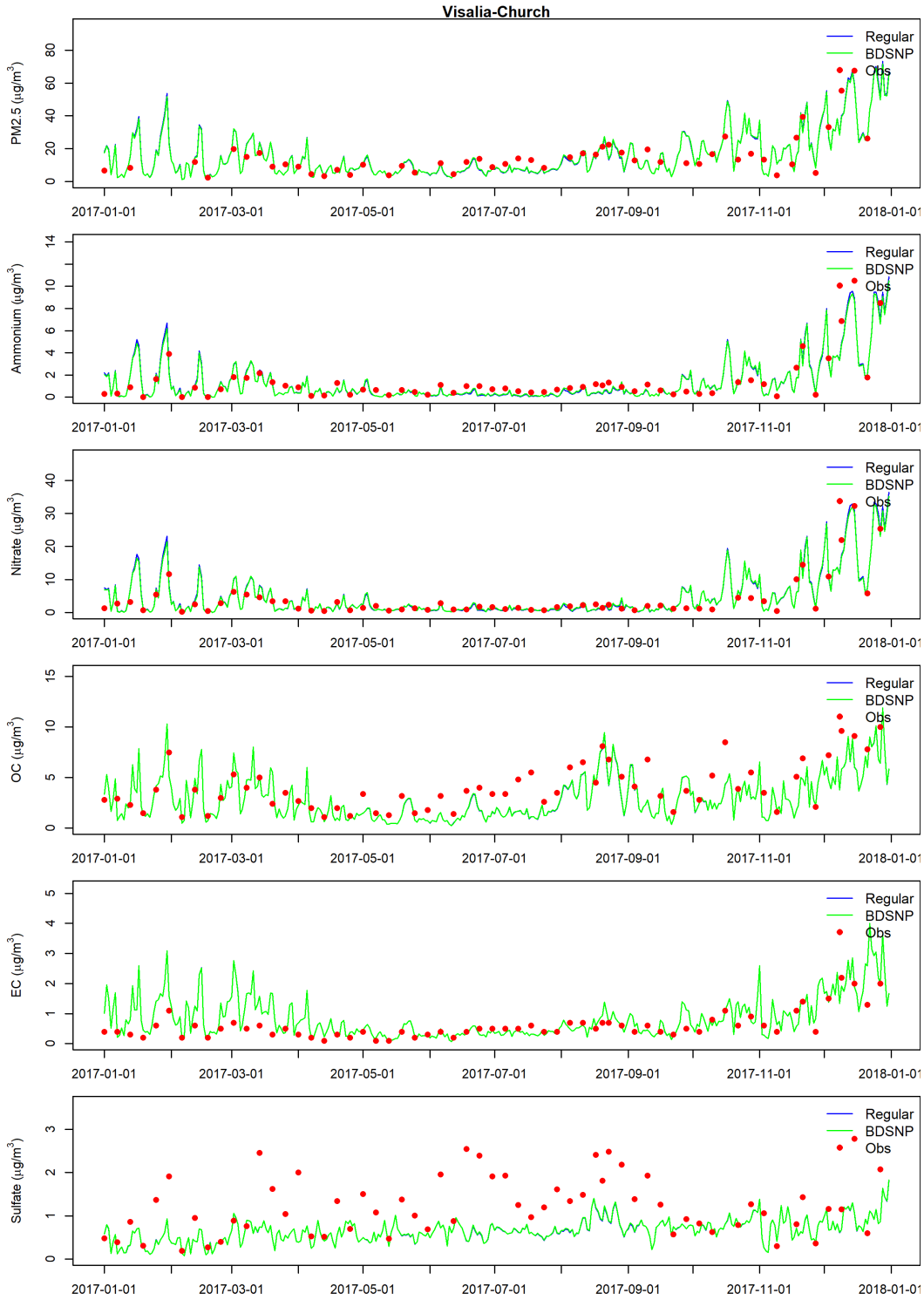

Figure S 83. Observed and modeled (regular: using the default MEGAN soil NOx scheme; BDSNP: using the MEGAN Berkeley Dalhousie soil NOx scheme) $PM_{2.5}$ species at Modesto.